ABSTRACT

GU, JUANJUAN. Numerical Modeling of Ultrasound Wave Propagation. (Under the direction of Dr. Yun Jing).

Numerical modeling of medical ultrasound has advanced significantly in recent years. Numerous algorithms have been developed and applied to study different medical ultrasound applications, including ultrasound imaging, transducer design, transducer acoustic field characterization and treatment planning. An in-depth literature and technical review of recent progress on numerical modeling of medical ultrasound is provided in Chapter 1.

A mixed-domain method (MDM) is presented in Chapter 2 for modeling linear/nonlinear wave propagation in biological tissue with arbitrary heterogeneities, in which speed of sound, density, attenuation coefficients, and nonlinear coefficients are all spatially varying functions. The present method is based on solving an integral equation derived from the Westervelt-like equation. One-dimensional problems are first studied to verify the MDM and to reveal its limitations. It is shown that this method is accurate for cases with small variation of sound speed. A two-dimensional case is further studied with focused ultrasound beams to validate the application of the method in the medical field. Results from the MATLAB toolbox k-Wave are used as the benchmark solutions. It is shown that the MDM is a computationally efficient and accurate method for modeling nonlinear wave propagation in soft tissue.

The wave fields at a certain frequency can be produced by MDM in two ways for linear wave propagation. The first approach is applying the Fourier transform to the transient simulation MDM result (denoted transient MDM, or TMDM). A more computationally efficient approach is to directly calculate the pressure field at the specific frequencies of interest (denoted frequency-specific MDM, or FSMDM). In this dissertation, the FSMDM is extended for modeling the second harmonic ultrasound field in heterogeneous, lossy media for weakly nonlinear cases. Five two-

dimensional cases, including a realistic human tissue map, are studied to systematically verify the FSMDM. Results from the TMDM are used as the benchmark solutions. Comparisons indicate that both methods give similar results for all cases. More importantly, the FSMDM has a crucial advantage over the TMDM in that it can be two orders of magnitude faster.

Phase correction and amplitude compensation are introduced in Chapter 4 to the MDM, which is only accurate for modeling wave propagation in weakly heterogeneous media. Multiple reflections are also incorporated with the one-way model to improve the accuracy. The resulting model is denoted as the modified mixed-domain method (MMDM) and is numerically evaluated for its accuracy and efficiency using two distinct cases: a layered medium and a human skull. It is found that the MMDM is significantly more accurate than the MDM for strongly heterogeneous media, especially when the phase aberrating layer is roughly perpendicular to the acoustic beam. Additionally, convergence study suggests that the second-order reflection is sufficient for wave modeling in lossy biological media.

mSOUND is an open-source toolbox written in MATLAB and it is developed based on the TMDM, FSMDM and MDMM. This toolbox is intended for modeling linear/nonlinear wave propagation with arbitrary heterogeneities. In Chapter 5, a general guideline is given along with three representative examples to illustrate how to set up simulations using mSOUND. TMDM forward projection can be used to compute the pressure waveform. FSMDM forward projection can be used to rapidly obtain the spatial distribution of the pressure directly at the fundamental and second harmonic frequencies, provided that linear or weakly nonlinear wave propagation is considered. The third example demonstrates how to use TMDM backward projection to reconstruct the initial source image in photoacoustic tomography (PAT). mSOUND (https://m-

sound.github.io/mSOUND/) is expected to be useful for a wide range of applications in medical ultrasound including treatment planning, PAT, transducer design and characterization, etc.

Numerical Modeling of Ultrasound Wave Propagation

by
Juanjuan Gu

A dissertation submitted to the Graduate Faculty of
North Carolina State University
in partial fulfillment of the
requirements for the degree of
Doctor of Philosophy

Mechanical Engineering

Raleigh, North Carolina
2019

APPROVED BY:

_____	_____
Dr. Yun Jing Chair of Advisory Committee	Dr. Marie Muller
_____	_____
Dr. Gianmarco Pinton	D r. Fuh-Gwo Yuan

BIOGRAPHY

Juanjuan Gu was born in Yancheng, Jiangsu Province, China. She was raised up in a loving and cosy family. In 2014, she received her B.S. degree in Energy and Power Engineering from Jiangsu University, China. She joined Dr. Yun Jing's group in 2013 when she studied at North Carolina State University as a visiting student for one year. In 2015, she was admitted to the direct doctoral program in Department of Mechanical and Aerospace Engineering at North Carolina State University and worked with Dr. Yun Jing. Her research focuses on numerical modeling of ultrasound wave propagation.

Publications

- **Juanjuan Gu** and Yun Jing, Modeling of wave propagation for medical ultrasound: a review, IEEE Transactions on Ultrasonics, Ferroelectrics and Frequency Control, 62, 1979-1992, 2015.
- Jun Zhang, Yi Zhang, **Juanjuan Gu**, Yun Jing, Rui-min Chen, Mark S. Humayun, K. Kirk Shung, Andrew C. Weitz*, and Qifa Zhou*, Transducer Selection for In Vivo Ultrasonic Retinal Stimulation: A Porcine Eye Model Study, Journal of Ophthalmology and Ophthalmic Surgery, 2 (1): 100112, 2016.
- **Juanjuan Gu** and Yun Jing, Numerical Modeling of Ultrasound Propagation in Weakly Heterogeneous Media Using a Mixed Domain Method, IEEE Transactions on Ultrasonics, Ferroelectrics and Frequency Control, 65, 1258-1267, 2018.
- **Juanjuan Gu** and Yun Jing, Simulation of the second harmonic ultrasound field in heterogeneous soft tissue using a mixed domain method, IEEE Transactions on Ultrasonics, Ferroelectrics and Frequency Control, 66, 669-675, 2019. (Highlighted as the front cover)
- Dingjie Suo, Bala Govind, **Juanjuan Gu**, Paul A. Dayton, and Yun Jing, Dynamic assessment of dual-frequency microbubble-mediated sonothrombolysis in vitro, Journal of Applied Physics, 2019.
- **Juanjuan Gu** and Yun Jing, A modified mixed domain method for modeling acoustic wave propagation in strongly heterogeneous media. (submitted to The Journal of the Acoustical Society of America), 2019.

ACKNOWLEDGMENTS

First and foremost, I would like to thank my advisor, Dr. Yun Jing, for his continuous support and guidance throughout my Ph.D. study. He was always there when I need a discussion. His depth and breadth of technical knowledge in the acoustic field always shed light on my research when I was trapped. Meanwhile, I learned from him that it was very important to be rigorous and serious in doing research. Mechanism is much more important than the good result. His confidence, patience and hard-working towards unknows will always encourage me in my future research work.

Next, I would like to thank other committee members, Dr. Fuh-Gwo Yuan, Dr. Marie Muller, Dr. Gianmarco Pinton and Dr. Omer Oralkan, for their time and input into my research and dissertation. Because of Dr. Fuh-Gwo Yuan's invitation, I got the chance to study at North Carolina State University for one year during my undergraduate study and worked on acoustic research projects with Dr. Yun Jing. I learned the importance of being critical in doing research when took Dr. Marie Muller's class: Applied acoustics (MAE 589). Dr. Gianmarco Pinton provided the data of the human tissue for the evaluation of my numerical model. Dr. Omer Oralkan gave me some invaluable suggestions on scientific writing when I took his class: Special topics in electrical engineering: Micromachined sensors (ECE 592).

I also want to thank my labmates in the Acoustics and Ultrasonics Lab for making my time at this lab enjoyable: Dr. Chen Shen, Dr. Tai-Yun Huang, Dr. Ni Sui, Dr. Dingjie Suo, Dr. Yong Yang, Mr. Sean Maguire, Mr. Bal Govind, Mr. Yuanchen Deng, Mr. Raj Nikhil Gerard Josephraj Kishore, and Mr. Jun Ji.

Last but not the least, I want to thank my family and friends for their support and love during my studies. Especially to my parents, Lingqin Kong and Yuanjun Gu, and my boyfriend,

Fujun Wang, for their unceasing encouragement and love. And to the brothers and sisters in Church in Raleigh, for their care and pray.

Additionally, this project is supported by the National Institute of Health (NIH) under the Grant R01EB025205. From 2015 to 2018, I was also supported by a fellowship award from China Scholarship Council (CSC).

TABLE OF CONTENTS

LIST OF TABLES

LIST OF FIGURES

CHAPTER 1

INTRODUCTON

The work presented in this chapter is published on IEEE Transaction on Ultrasonics, Ferroelectronics, and Frequency Control [1]

In the last two decades, we have witnessed a tremendous amount of development of medical ultrasound in both the imaging and therapy communities. The technologies and equipment associated with medical ultrasound are noninvasive, portable, and relatively inexpensive (particularly for imaging) compared with competing technologies. Consequently, they are increasingly widely used in clinical applications, such as B-mode and tissue harmonic imaging of parts of the human body, and treatment of uterine fibroids [2] and brain tumors [3]. To improve these applications, it is vital to have a fast, accurate, and versatile ultrasound propagation model. For example, numerical simulations can be utilized to shed light on why tissue harmonic imaging (THI) and super-harmonic imaging (SHI) are superior to conventional B-mode imaging under realistic medical diagnostic conditions. Relevant features of these imaging methods, including the lateral beam shape and axial pulse shape, can conveniently be compared by means of numerical simulations [4]. Results from simulations (such as the optimal transmission frequency) can in turn guide the design of phased arrays so as to achieve optimal imaging performance.

This chapter intends for offering an overview on recent developments on numerical modeling of medical ultrasound. A variety of model equations will be first reviewed. Including the Westervelt equation and the Khokhlo-Zabolotskaya-Kuznetsov (KZK) equation. The solution methods for these equations will then be discussed. We will first review methods for solving the linear wave equation, followed by methods for solving the nonlinear wave equation. The

applications of numerical modeling in transducer design and characterization, ultrasound imaging, and treatment planning will be presented. Finally, we will address future challenges of medical ultrasound modeling. Because the majority of ultrasound approaches only involve longitudinal waves, this review will not include shear wave modeling [5]-[7].

1.1. Model Equations

1.1.1. Westervelt Equation

The Westervelt equation recently emerged as a very popular method model equation for ultrasound modeling because of its high accuracy. The generalized Westervelt equation reads [8], [9]

$$\rho\nabla\cdot\left(\frac{1}{\rho}\nabla p\right)-\frac{1}{c^2}\frac{\partial^2 p}{\partial t^2}+\frac{\delta}{c^4}\frac{\partial^3 p}{\partial t^3}+\frac{\beta}{\rho c^4}\frac{\partial^2 p^2}{\partial t^2}=0, \tag{1.1}$$

where ρ is the sound pressure, c is the speed of sound, δ is the sound diffusivity, β is the coefficient of nonlinearity, and ρ is the ambient density. All parameters can be spatially varying functions. Note that Eq. (1.1) is different from the original Westervelt equation used to study parametric arrays [10], which does not take the medium heterogeneity into account. In Eq. (1.1), the first term takes diffraction into account. The third term accounts for attenuation. The last term introduces the quadratic nonlinearity. Several simplified versions can be derived from Eq. (1.1). For instance, the one-way Westervelt equation with retarded time can be found in [11]. By using constants for all acoustic parameters, the Westervelt equation for homogeneous media can be recovered [12]

$$\nabla^2 p-\frac{1}{c_0^2}\frac{\partial^2 p}{\partial t^2}+\frac{\delta_0}{c_0^4}\frac{\partial^3 p}{\partial t^3}+\frac{\beta_0}{\rho_0 c_0^4}\frac{\partial^2 p^2}{\partial t^2}=0, \tag{1.2}$$

where c_0, ρ_0, δ_0 and β_0 are the acoustic parameters for the background medium. for axis-symmetrical problems, the Laplace operator can be rewritten in cylindrical coordinates [13]. The linear acoustic wave equation can be derived by setting β_0 to 0. So that

$$\nabla^2 p - \frac{1}{c_0^2}\frac{\partial^2 p}{\partial t^2} + \frac{\delta_0}{c_0^4}\frac{\partial^3 p}{\partial t^3} = 0. \quad (1.3)$$

We do not intend to devote a separate section to the linear wave equation model [14]. It will be discussed within the Westervelt equation section. Eqs. (1.2) and (1.3) are useful for studies on characterizing acoustic fields of transducers and comparing them with experimental data obtained from underwater measurement [15]. They are sometimes also used for approximately estimating the acoustic field in biological tissues [16] which are sometimes considered weakly heterogeneous. Eq. (1.3) is used when medium heterogeneity must be considered, e.g., studying the propagation of ultrasound beams through the skull [8], [17]. On the other hand, nonlinear Eqs. (1.1) and (1.2) must be sued when high-pressure ultrasound is present, e.g., lithotripsy [18], histotripsy [19], and tissue harmonic imaging (THI) [20]. Some studies have suggested that using the linear acoustic approximation could underestimate the temperature elevation in tissue [16]. Soneson and Myers examined the problem of determining the thresholds at which nonlinear effects become important [21]. The choice of using the nonlinear or linear wave equation also depends on the available computational resources. In general, solving the nonlinear or linear wave equation also depends on the available computational resources. In general, solving the nonlinear wave equation calls for considerably more refined spatial and temporal resolutions because the presence of higher harmonics, especially when high-pressure wave fields are simulated, as in the context of HIFU.

The Westervelt equation can be considered as a simplification of the Kuznetsov equation [22]. It is considered an appropriate approximation when local effects can be ignored, which is generally true when the propagation distance is much greater than a wavelength or sound beams are highly directional (e.g., quasi-plane waves) [23]. A recent study suggested that the Westervelt equation is accurate even for highly focused transducers (aperture angle at 80°) [24]. All in all, there seems to be a general consensus that the Westervelt equation is not only suitable for

numerical modeling but could also provide very accurate solutions to acoustic wave propagation for problems of interest in the medical ultrasound community. The suitability of the Westervelt equation for numerical modeling, however, still depends on the available computational and implementation resources.

One variation of Eqs. (1.1) – (1.3) occurs when considering arbitrary frequency-dependent absorption laws and dispersion. Although it is straightforward to consider there two phenomena in the frequency domain, it is intrinsically different to implement in the time domain. Eqs. (1.1) and (1.2) only consider the thermoviscous absorption, in which $\delta_0 = 2\alpha_0 c_0^3/\omega^2$ (α_0 is the absorption coefficient and ω is the angular frequency) and therefore the absorption is proportional to frequency squared. Dispersion is also not accounted for. To consider absorption following arbitrary power laws and dispersion due to thermal relaxation in tissue, a variety of approaches have been proposed [9], [25]-[30]. For example, Szabo derived a causal convolution operator that accounts for both power law absorption and dispersion [27]. This approach was later verified numerically [31] and modified by Chen and Holm [26]. Ochmann and Makarov used fractional derivative to account for the power law absorption [32]. Kelly and McGough proposed a hierarchical fractal network model to describe the power law absorption [29]. Treeby and Cox used a fractional Laplacian to model power law absorption and dispersion [25]. An alternative wave equation for homogeneous media was derived and reads

$$\nabla^2 p - \frac{1}{c_0^2}\frac{\partial^2 p}{\partial t^2} + \left\{\tau_0 \frac{\partial}{\partial t}(-\nabla^2)^{y/2} + \eta_0(-\nabla^2)^{(y+1)/2}\right\} p + \frac{\beta_0}{\rho_0 c_0^4}\frac{\partial^2 p^2}{\partial t^2} = 0, \tag{1.4}$$

where τ_0 and η_0 are two proportionality coefficients and y is the power law exponent. This term yields a dispersion relation of the form

$$\tilde{k}^2 = \frac{\omega^2}{c_0^2} + \frac{2i\alpha_0\omega^{y+1}}{c_0} + \frac{2\alpha_0 \tan(\pi y/2)\omega^{y+1}}{c_0}, \tag{1.5}$$

where $\tilde{k}$ is the complex wave number. Note that (1.4) is slightly different from [24, Eq. (28)], where the nonlinearity is not considered.

1.1.2. Khokhlov-Zabolotskaya-Kuznetsov (KZK) Equation

Although the numerical ultrasound community has gradually gravitated toward the Westervelt equation in recent years, the KZK equation has been the most widely used equation because it is the simplest model which include diffraction, absorption, and nonlinear effects. The KZK equation accounting for energy losses was first published in 1971 [33] and there has been a tremendous amount of numerical investigation sine then. The KZK equaiton can be viewed as the parabolic approximation of the Westervelt equation, and therefore it is less accurate in the near field and at a position off the main axis. In other words, wide-angled or steered beams [34] cannot be accurately modeled by the KZK equation. For a focused transducer, the KZK equation is in theory valid for wavs traveling within 15° to 16° of the nominal axis of the beam (typically in the z-axis) [35], [36]. This is roughly equivalent to a f-number >1.5. In practice, however, it was found that the KZK equation can be relatively accurate in the frequency domain for f-number at 1.0 (about 25° off the nominal axis) [37]. The parabolic form of the wave which is the main advantage of the KZK equation. The KZK equation is an equation of evolution type and has the first-order derivative with respect to the propagation main axis, and it therefore inherently describes one-way wave propagation. The KZK equation for homogeneous, thermoviscous media can be written as [23]

$$\frac{\partial^2 p}{\partial z \partial t'} - \frac{c_0}{2}\nabla_\perp^2 p - \frac{\delta_0}{2c_0^3}\frac{\partial^3 p}{\partial t'^3} - \frac{\beta_0}{2\rho_0 c_0^3}\frac{\partial^2 p^2}{\partial t'^2} = 0, \tag{1.6}$$

where t' is the retarded time ($t' = t - z/c_0$), and $\nabla_\perp^2 = (\partial^2/\partial x^2) + (\partial^2/\partial y^2)$ is the transverse Laplacian. In cylindrical coordinates, the transverse Laplacian is $\nabla_\perp^2 = (\partial^2/\partial r^2) + (1/r)(\partial/\partial r)$, [38]. By dropping $\nabla_\perp^2$(i.e., diffraction), the KZK equation reduces to the Burgers equation. Eq.

(1.6), however, is rarely directly solved. Other forms of the KZK equation exits. For instance, by integrating both sides (1.6) with regard to time and taking arbitrary absorption and dispersion into account, we arrive at an extended KZK equation [39]

$$\frac{\partial p}{\partial z} = \frac{c_0}{2}\int_{-\infty}^{t'} \nabla_\perp^2 p dt'' + \frac{\delta_0}{2c_0^3}\frac{\partial^2 p}{\partial t'^2} + \frac{\beta_0 p}{\rho_0 c_0^3}\frac{\partial^2 p}{\partial t'} + \sum_v \frac{c_v'}{c_0^2}\int_{-\infty}^{t'} \frac{\partial^2 p}{\partial t''^2} e^{-(t'-t'')/t_v} dt'' = 0, \qquad (1.7)$$

where t_v is the relaxation time and c_v is the small-signal speed of sound increment for each relaxation process v ($v = 1,2,...$). Eq. (1.6) can be transformed into nondimensional form for simplification. For example, in Cartesian coordinates, (1.7) can be transformed into

$$\frac{\partial p}{\partial \sigma} = \frac{1}{4}\int_{-\infty}^{t'} \left(\frac{1}{G_x}\frac{\partial^2 P}{\partial X^2} + \frac{1}{G_y}\frac{\partial^2 P}{\partial Y^2}\right) d\tau' + A\frac{\partial^2 P}{\partial \tau^2} + NP\frac{\partial P}{\partial \tau} + \sum_v D_v \int_{-\infty}^{\tau} \frac{\partial^2 p}{\partial \tau'^2} e^{-(\tau-\tau'')/\theta_v} d\tau'' = 0, \quad (1.8)$$

for rectangular transducers [39], where

$P = p/p_0, \quad \tau = \omega_0 t'$, $X = x/a$, $Y = y/b$, $\sigma = z/d$, $G_x = k_0 a^2/2d$, $G_y = k_0 b^2/2d$, $N = d/\bar{z}, A = \alpha_0 d, D_v = k_0 d c_v'/c_0, \theta_v = \omega_0 t_v$.

p_0 is a characteristic pressure, ω_0 is a characteristic angular frequency, a and b are the characteristic lengths in the x- and y-directions, d is a characteristic length in the propagation direction, $k_0 = \omega_0/c_0$, $\bar{z}$ is the plane wave shock formation distance [$= 1/(\beta\varepsilon k)$, where ε is the peak particle velocity Mach number], and α_0 is the thermoviscous absorption coefficient at the characteristic frequency. The dimensionless KZK equation in cylindrical coordinates can be found in [38] and [40], which is useful for axis-symmetrical problems, e.g., acoustic fields of circular apertures. Augmented KZK equations for heterogeneous media were derived by Jing and Cleveland [41] and Varslot and Taraldsen [42]. The KZK equation was validated by comparing it to the Westervelt equation both numerically and experimentally [13]. The error introduced by the parabolic approximation was examined in [35], [43], [44]. It was found that, for small-f-numbers (f-number = 1.5), the lateral beam-plot could exhibit 2 to 3 dB errors.

1.1.3. Other Equations

Although the Westervelt and KZK equation are the two most widely used equations for medical ultrasound modeling, other model equations also exist and will be briefly reviewed here. The Kuznetsov equation, which is considered to be a more accurate equation than the Westervelt equation for nondirectional beams and in the near field, can be written as [33]

$$\frac{\partial^2\phi}{\partial t^2} - c_0^2\nabla^2\phi = \frac{\partial}{\partial t}\left[\frac{1}{\rho_0}\left(\mu_B + \frac{4}{3}\mu\right)\nabla^2\phi + (\nabla\phi)^2 + \frac{\beta-1}{c_0^2}\left(\frac{\partial\phi}{\partial t}\right)^2\right], \tag{1.9}$$

where ϕ is the velocity potential, μ_B is the coefficient of bulk viscosity, and μ is the coefficient of shear viscosity. There is a direct relation between the diffusivity and the two coefficients [23]. Roughly on the same order of accuracy, an equation in terms of the acoustic pressure yields

$$\nabla^2 p - \frac{1}{c_0^2}\frac{\partial^2 p}{\partial t^2} + \frac{\delta_0}{c_0^4}\frac{\partial^3 p}{\partial t^3} + \frac{\beta_0}{\rho_0 c_0^4}\frac{\partial^2 p^2}{\partial t^2} + \left(\nabla^2 + \frac{1}{c_0^2}\frac{\partial^2}{\partial t^2}\right)L = 0, \tag{1.10}$$

where L is the Lagrangian density of acoustical energy [23], [24]. By dropping L, Eq. (1.10) reduces to the Westervelt equation. Note that for plane progressive waves, L is exactly equal to zero. Directly solving Eq. (1.9) or (1.10) is extremely challenging and they have not been shown to be considerably more accurate than the Westervelt equation for medical ultrasound problems; therefore, they are rarely used in the medical ultrasound community. However, under the weakly nonlinear assumption, numerical studies using (1.9) and (1.10) were carried out. For example, the lossless, perturbed Kuznetsov's equations were solved by the finite element method and the solutions were compared with those of the KZK equation [43]. Equation (1.10) under the weakly nonlinear assumption was solved by the angular spectrum approach and was compared with the Westervelt equation for focused transducers [24]. It was found that the Westervelt equation is accurate even for highly focused transducers (aperture angle at 80°).

Another model equation is the spheroidal beam equation (SBE) [45]-[47]. Similar to the KZK equation, SBE is also a parabolic equation. It is, however, more suitable for focused

transducers due to the use of the oblate spheroidal coordinates. In addition, linear and nonlinear acoustic simulations showed that the SBE equation is more accurate than the KZK equation for focused transducers and is valid for an aperture half-angle up to 40° [45]. It should be pointed out that the SBE contains two different equations: one for the spherical wave region and the other for the focus region.

Furthermore, Kamakura *et al*. derived a wide-angle one-way wave equation using the split-step Padé approximation [48]. It was shown to be valid for an aperture half-angle up to 40°. Treeby *et al*. [49] and Tabei *et al*. [50] studied first-order wave equations and solved them using the k-space method. One advantage of using first-order wave equations is that the perfectly matched layer (PML) can be more easily incorporated [50], [51]. A PML is an artificial absorbing layer that is commonly used to minimize reflection from artificial boundaries of the computational domain. The first-order wave equations are particularly suited to be solved by time-domain methods, such as the finite-difference time-domain (FDTD) method [52]. The nonlinear first-order wave equations read

$$\begin{aligned} \frac{\partial \mathbf{u}}{\partial t} &= -\frac{1}{\rho}\nabla p \\ \frac{\partial \rho'}{\partial t} &= -(2\rho' + \rho)\nabla \cdot \mathbf{u} \\ p &= c^2\left(\rho' + \frac{B}{2A}\frac{\rho'^2}{\rho} - \hat{\boldsymbol{L}}\rho'\right) \end{aligned} \quad , \tag{1.11}$$

where $\mathbf{u}$ is the velocity vector, ρ' is the acoustic density, B/A is the nonlinearity parameter, and $\hat{\boldsymbol{L}}$ is a power-law absorption operator. For linear acoustics, it is sufficient to only consider two coupled equations (pressure-velocity formulation) [51]. An asymptotic model that extends parabolic approximation for acoustic fields of strongly focusing transducers was developed in [53].

Finally, while it is typically sufficient to consider only the quadratic nonlinearity term, it was argued that for some applications (e.g., extra-corporeal shock wave lithotripsy) where the

pressure is extremely high (> 100 MPa), cubic nonlinearity should also be taken into account. Wave equations with higher orders can be found in [54]-[57].

1.2.Solution Methods

This section will review solution methods for solving the above-mentioned linear wave equations, Westervelt equation, and KZK equation. Since analytical solutions only exist for few circumstances [43], [58]-[60], the focus of this section is purely numerical methods for two- and three-dimensional wave propagation. We will emphasize the methods used in the medical ultrasound community. There are some different developments in other areas, such as room-acoustics and geophysics. They will not be discussed in this dissertation, though. A recent review of this topic (solution methods) can be also found in [61].

1.2.1. Linear Wave Equation

Among the three equations, the linear wave equation [e.g., (1.3)] is the easiest to solve because the nonlinearity term vanishes. For linear wave equation in homogeneous media, several approaches are available for time-harmonic solutions and they include the Rayleigh-Sommerfeld integral [60], [62], fast near-field method (FNM) [63]-[65], and angular spectrum approach (ASA) [66]-[69]. Although the first approach is rather time-consuming, particularly in the near-field, the second approach specifically addresses this problem by using one-dimensional integrals. In particular, FNM removes the singularity in the integrand, resulting in a smooth integral which is evaluated using quadrature methods with spectral accuracy. The ASA is emerging as a widely used approach in medical ultrasound modeling because of its high accuracy and efficiency as it utilizes the 2D fast Fourier transform (FFT). In this approach, computing the acoustic field on a desired plane from a known plane requires only a single operation. For circularly symmetrical problems, the 2D Fourier transform can be reduced to the Hankel transform [70], although it is still not as

efficient as the 1D FFT. The errors of ASA due to discrete Fourier transform (DFT) and discretization as well as spatial aliasing are discussed in [71] and [72]. The spatial aliasing can be overcome by using the so-called "spatial propagator" as opposed to the "spectral propagator". Alternatively, this error can be reduced by using an absorption layer [73]. Attenuation can be conveniently accounted for by considering a complex wave number [74]. Most recently, Koskela *et al*. [75] introduced a novel stochastic ray-tracing method to predict the HIFU fields. They verified the model using experiments on *ex vivo* tissue.

For transient solution, the spatial impulse response approach [76], [77] and ASA [70], [78] have been used. Although the spatial impulse response approach excels in computing the acoustic field at an arbitrary point, the ASA is more suited when the acoustic field on a certain plane is desired. The ASA is also capable of backward propagating the acoustic field: if the field on a plane away from the source is known, the field on another plane closer to the source can be extrapolated [66], [79]. Although the Rayleigh-Sommerfeld integral and spatial impulse response approaches can be applied to nonplanar/focused transducers, the ASA is more often used for planar transducers and the focusing can be achieved assuming phased arrays. Nevertheless, there have been some recent developments that extend the ASA to curved transducers [80], [81]. For example, in a hybrid method, the Rayleigh-Sommerfeld integral can be used first to calculate the acoustic field on a certain plane (an acoustic hologram), and then ASA method can be used to calculate the field on any plane parallel to that initial plane. The inclusion of attenuation and dispersion in these two approaches was discussed in [12], [82]. As ASA employs a frequency-domain formulation, it allows straightforward implementations of general dispersions [12].

For heterogeneous media, different approaches are typically required for solving the wave equation [e.g., Eq. (1.1) without the nonlinearity term]. One exception is layered structures with weak

contrast, where the ASA method can still be conveniently used [69], [83] with reasonable accuracy. A very recent paper developed a new, hybrid ASA method to deal with linear, heterogeneous media, although only up to the first order reflections were considered [84]. Three most commonly used approaches for solving the heterogeneous media wave equation in the medical ultrasound community are the FDTD method [85]-[88], pseudo-spectral time-domain method (PSTD) [89]-[96], and k-space time-domain (KSTD) method [50], [97]-[103], although they can also be used to study wave propagation in homogeneous media [52]. Although FDTD uses finite different to approximate the spatial derivative in the wave equation, the other two spectral approaches use the Fourier transform to compute the spatial derivative and are considerably more accurate with low numerical dispersion errors (not to be confused with the true physical dispersion due to the acoustic media). It must be emphasized that this is only the case when spectral methods are used to approximate smooth functions. When used to approximate fields with steep gradients or discontinuities (like shocked fields as well as some source functions), they could be less efficient than low-order methods. In general, the most commonly used FDTD scheme (fourth order in space and second order in time) requires 8 to 10 grid points per wavelength to achieve reasonably accurate results, whereas the other two approaches theoretically only need 2 grid points per wavelength for smooth fields [101]. The k-space method is considered more accurate or efficient than the pseudo-spectral method as it uses a semi-analytical time-stepping scheme [97], whereas the pseudo-spectral method uses finite-difference approximation. Consequently, the k-space method allows for a larger time-step and is less time-consuming [101]. Both of these two spectral methods have the so-called wrap-around problem, because the use of FFT implies that the acoustic field is periodic. The PML or absorption layer can be used to minimize this artifact [8], [50]. One drawback of the spectral methods is that their errors grow as the contrast (heterogeneity) becomes

greater [101]. This is, however, not a significant concern for problems encountered in medical ultrasound as the contrast is in general relatively small.

All three approaches can be applied to either the second-order wave equation or the first-order wave equations. When applied to the first-order wave equations, it is common to use staggered grids [50] for better accuracy. When applied to the second order wave equation and when heterogeneity of the density exists, it is common to define a normalized wave field $f = p/\sqrt{\rho}$ to remove the first-order derivative term in the wave equation [101]. For instance, (1.1), without the nonlinearity term, can be transformed into

$$\nabla^2 f - \frac{1}{c_0^2}\frac{\partial^2 f}{\partial t^2} = f\sqrt{\rho}\nabla^2\frac{1}{\sqrt{\rho}} + \frac{1}{c_0^2}\left(\frac{c_0^2}{c^2} - 1\right)\frac{\partial^2 f}{\partial t^2} - \frac{\delta}{c^4}\frac{\partial^3 f}{\partial t^3} = 0, \tag{1.12}$$

The transformed equation with the nonlinearity term can be found in [8]. In some problems, a hybrid approach seems to be more efficient. For instance, Qiao *et al.* [104] used the Rayleigh-Sommerfeld integral first to compute the field on the posterior surface of the rib cage. The k-space was then used to estimate the field through the rib cage. In the last step, the ASA was used to simulate the field behind the rib. Finally, finite-difference frequency-domain methods and finite element methods (FEM) also exist [105], [106], but are not frequently used for medical ultrasound modeling.

1.2.2. Westervelt and KZK Equations

For homogeneous media, currently existing approaches for solving the nonlinear wave equation often use an operator-splitting scheme. In this scheme, the effects of diffraction, nonlinearity, and attenuation are computed separately using specialized numerical algorithms. Because these three effects are in fact interdependent, the operator-splitting scheme will inevitably introduce errors. However, these errors are reasonably small as long as small steps are taken [107]. Cleveland *et al*. [40, Appendix A] showed that as the step size approaches zero, the splitting

scheme exactly solves the original equation. Christopher and Parker used a scheme equivalent to a first-order operator-splitting scheme for nonlinear wave modeling [108]. Tavakkoli *et al*. applied a second-order operator-splitting (Strang splitting) scheme which allows for a larger step size [109] and has been widely used thereafter. Some mixed time-domain/frequency-domain methods use the operator splitting and FFT to take advantage of frequency-domain linear methods and superior time-domain nonlinear methods [107]. This section intends to focus on methods for solving the diffraction and nonlinearity. For the absorption, briefly, it can be solved either in the frequency-domain [110] or the time domain [38].

For the diffraction part, the solution methods used for solving the linear acoustic wave equation can be used. For instance, Tavakkoli *et al.* [109] and Khokhlova *et al.* [110] used the Rayleigh integral for solving the full diffraction field. Christopher and Parker used an exact formulation based on the Kirchhoff-Helmholtz integral to model full diffraction from axisymmetric transducers [108]. Zemp *et al.* used the ASA and addressed the sampling and aliasing issues [107]. It was found to be more computationally efficient than the Rayleigh integral. Similarly, Yuldashev and Khokhlova made use of the ASA for solving the diffraction term in the Westervelt equation [11]. Spatial filtering and artificial absorption were used to minimize numerical errors. They studied the acoustic field from a multi-element HIFU transducer. Berntsen, Lee and Hamilton used an implicit backward difference method in the near field and the Crank-Nicolson method beyond the near field for solving the diffraction term in the KZK equation [38], [111]. Their algorithm targets axisymmetric problems. This finite-difference approach was later adopted in [112], [113] for studying focused transducers and was improved by using the alternating direction implicit method and extended to non-axisymmetric problems [39], [114]. Very recently,

Hasani *et al.* further improved the accuracy of this finite-difference method using a five-point scheme [115].

For the nonlinearity part, solution methods can be divided into two groups: time-domain methods and frequency-domain methods. In general, frequency-domain methods are more suited to problems with weak nonlinearity whereas time-domain methods are advantageous for strongly nonlinear waves. This is because the computation time approximately increases as M^2 (where M is the number of harmonics) for the frequency-domain methods. On the other hand, the computation time is proportional to M for time-domain methods [38].

The first exclusively frequency-domain method was developed by Aanonsen *et al.* [116]. This method and its modified version were popular in the 1980s [117], [118] and 1990s [119]. In this approach, a Fourier series expansion of the pressure is substituted into the KZK equation and the resulting system of equations is solved using an implicit backward difference scheme. Later, Christopher and Parker used the frequency-domain solution to the Burgers' equation to account for nonlinearity [108]. Khokhlova *et al*. developed a frequency-domain method that uses the fourth-order Runge–Kutta method [110]. To reduce the computational burden, the number of harmonics included in the solution gradually grew as the propagation distance increased. In their paper, the frequency-domain method was also compared with a time-domain method for its accuracy. An asymptotic spectral algorithm that enables modeling strongly nonlinear waves with shock fronts using a few number of harmonics (~30) was developed and used to study both plane wave propagation [120] and enhanced thermal effects in focused beams [121].

Time-domain methods were first introduced by Lee and Hamilton [38]. Implicit analytical solution (the Poisson solution) was used to solve for the nonlinear term [109], [122]. Varslot and Taraldsen used the method of characteristics to solve the nonlinearity term [42]. To achieve good

results, 10 to 15 samples per wavelength at the highest harmonic frequency were needed. To model highly nonlinear shock waves in the time-domain, Pinton and Trahey investigated the validity of Godunov's method and the monotonic up wind scheme [18]. It was found that they are significantly more efficient than the implicit solution-based method. Yuldashev and Khokhlova used a hybrid method to model nonlinearity [11]. The frequency-domain method was used in the near field and the Godunov-type method [123] was used when the steepness of the wave profile exceeded a certain quantity.

Other approaches not using the splitting scheme are also reviewed here for completeness. Hallaj and his co-workers performed FDTD on the Westervelt equation using the cylindrical coordinates [16], [124]. Doinikov *et al.* implemented three-dimensional FDTD and compared numerical results with experimental data from a phased array [125]. Other demonstrations of FDTD for solving the full nonlinear wave equation can be found in [13], [126] and [127]. A modified ASA was introduced by Jing *et al.* to solve the Westervelt equation [12]. Similar to the ASA for solving the linear wave equation, this approach is capable of backward projection, which could extrapolate fields very close to the source plane (i.e., transient nonlinear acoustical holography) [128]. A recent paper proposed two improved stepping schemes for the modified ASA, which were shown to be considerably more efficient and accurate [129]. Under weakly nonlinear conditions, the modified ASA can be simplified to allow an arbitrary step size for rapid field estimation [130]. Huijssen and Verweij developed an iterative nonlinear contrast source (INCS) method for solving the Westervelt equation [131]. They treated the nonlinear term as a contrast source and used a filtered convolution method to minimize the computation [132]. When strong contrast sources are present (e.g., strong and inhomogeneous attenuation), the nonlinear contrast source can be linearized in order to resolve the convergence problem [133]. This approach

relies on the four-dimensional Fourier transform and therefore could require a large memory size for large scale problems. Unlike many other approaches which assume the main nonlinear distortion is in the direction normal to the transducer surface [42], [107]. both methods (modified ASA and INCS methods) are free of any assumed wave-field directionality [12], [131]. This is considered more accurate, particularly for highly focused transducers and steered beams. Other researchers have used FEMs, although they are in general computationally less efficient [43], [134], [135].

Several numerical methods have been used to solve the nonlinear wave equation for heterogeneous media. For example, Pinton *et al.* implemented a FDTD algorithm that accounts for nonlinearity, heterogeneity, and frequency-dependent attenuation [9]. They used the algorithm to study ultrasound pulse propagating through a human abdominal wall. Jing *et al.* developed a k-space method based on the Westervelt equation [8]. They showed that the k-space method is superior to the FDTD method because it requires fewer grid points per wavelength. Only thermoviscous absorption was considered, however. Treeby *et al.* [49] developed the k-space method based on the first order nonlinear wave equation [i.e., Eq. (1.11)]. Treeby later improved this k-space method for strongly nonlinear problems by using non-uniform grids [136]. One-dimensional problems were demonstrated to validate the algorithm. The INCS method is intrinsically suited to modeling heterogeneous media [132], [137]. For example, Demi *et al.* studied nonlinear wave propagation in media with spatially inhomogeneous attenuation [138] Varray *et al.* [139] extended the ASA to modeling inhomogeneous nonlinearity coefficient and used their algorithm to generate B-mode images [140]. Jing and Cleveland derived a modified KZK equation for heterogeneous media [41]. They dealt with the spatial variation in the sound speed and nonlinearity using the Poisson solution. The term that accounts for the density

fluctuations was solved using a first-order finite difference scheme. Varslot and Taraldsen used an implicit Euler scheme to find the numerical solution for both the diffraction and the scattering [42]. The method of both Jing and Cleveland [41] and Varslot and Taraldsen [42] assume one-way propagation, and therefore ignore the high-order scattering. Albin *et al.* [141] solved the nonlinear acoustics Navier-Stokes equations using the Fourier continuation (FC) method. An array of rigid cylinders were considered as scatterers and the FC method was found to be highly efficient.

To close this section, a table (Table 1.1) is provided here to summarize and recap a selected group of modern ultrasound modeling algorithms. Studies comparing different algorithms can be found in [142]-[144]. Although it is difficult to assess exactly the computational load of each algorithm because they are highly problem-dependent, in general, spectral, one-way models are more computationally efficient than finite-difference or finite element based, full-wave models.

Table 1.1. A summary of modern ultrasound modeling algorithms

Authors	Governing equation	Solution method	Remarks
Christopher and Parker [69]	Linear wave equation, axisymmetric	ASA	Hankel transform was used. Valid for homogeneous/layered media with frequency dependent attenuation.
Christopher and Parker [108]*	Equivalent to the Westervelt equation, axisymmetric	Operator-splitting	A follow-up paper of [69]. Used ASA for the diffraction and solved the nonlinear part in the frequency-domain.
Lee and Hamilton [38]*	KZK equation, axisymmetric	Operator-splitting	Solved the diffraction using finite-difference schemes and nonlinear part in the time-domain. Valid for thermoviscous, homogenous media.

Table 1.1. (continued).

Cleveland *et al*. [40]*	KZK equation, axisymmetric	Operator-splitting	A follow-up paper of [38]. A time-domain relaxation algorithm was demonstrated.
Tavakkoli *et al*. [109]*	KZK equation, axisymmetric	Operator-splitting	First paper that used a 2nd order operator-splitting scheme in nonlinear wave modeling. Valid for homogeneous media with frequency-dependent absorption and dispersion.
Liu [90]+	Linearized, coupled first-order acoustic equations	PSTD	Valid for linear, heterogeneous, dispersionless media.
Hallaj and Cleveland [16]*	Westervelt equation	FDTD	Valid for thermoviscous, homogeneous media.
Yuan *et al*. [52]+	Linearized, coupled first-order acoustic equations	FDTD	Valid for linear, heterogeneous media with relaxation dominated attenuation.
Kamakura *et al*. [45]*	SBE	Frequency-domain, finite difference	Valid for thermoviscous, homogeneous media. Considered geometrically focused transducers.
Mast *et al*. [101]+	Linear wave equation	KSTD	Valid for heterogeneous media. Nonlinearity and absorption were not considered.

Table 1.1. (continued).

Khokhlova *et al.*[110], Filonenko and Khokhlova [145]*	KZK equation, axisymmetric	Operator-splitting	Solves both diffraction and nonlinear part in the frequency-domain, variable number of harmonics and spatial windows to optimize modeling shock wave propagation; power law of absorption with dispersion in [145].
Tabei *et al*. [50]$^{+}$	Linearized, coupled first-order acoustic equations	KSTD	Valid for heterogeneous media with relaxation absorption. Nonlinearity was not considered.
Clement and Hynynen [83]	Linear wave equation	ASA	Valid for homogeneous/layered media with frequency dependent attenuation and dispersion.
Zemp *et al*. [107]*	Equivalent to the Westervelt equation	Operator-splitting	An extension of [108]. Solved the diffraction using ASA and nonlinear part in the frequency-domain. Attenuation is combined with the nonlinear substep. Valid for homogeneous media with frequency dependent attenuation.
Varslot and Taraldsen [42]*	Modified KZK and Westervelt equations	Operator-splitting	Solved the diffraction using either a finite difference scheme or a pseudo-differential model. The nonlinear part was solved using the method of characteristics. Power-law absorption was considered. Heterogeneities were considered but multiple scatterings were not taken into account.

Table 1.1. (continued).

Varslot and Taraldsen [42]*	Modified KZK and Westervelt equations	Operator-splitting	Solved the diffraction using either a finite difference scheme or a pseudo-differential model. The nonlinear part was solved using the method of characteristics. Power-law absorption was considered. Heterogeneities were considered but multiple scatterings were not taken into account.
Khokhlova *et al.* [114]*	KZK equation, 3D	Operator-splitting	Solves nonlinear part in the time-domain; diffraction, absorption, and dispersion part in the frequency-domain; power law of absorption with dispersion for short pulses.
Canney *et al*. [37], Bessonova *et al*. [146]*	KZK equation, axisymmetric	Operator-splitting	Combined frequency and time-domain for the nonlinear term, Godunov-type algorithm is used for modeling shock wave propagation; boundary condition set based on measurement in [37].
Huijssen and Verweij [131]*$^{+}$	Westervelt equation	INCS	Valid for heterogeneous media with frequency-dependent absorption and dispersion.
Yuldashev and Khokhlova [11], Kreider *et al*. [15]*	Westervelt equation	Operator-splitting	Diffraction in k-space and frequency domain; nonlinear term both in frequency and time-domains; Godunov-type algorithm for modeling shock wave propagation; boundary condition obtained from acoustic holography measurements in [15].

Table 1.1. (continued).

Jing *et al*. [129], [12]*	Westervelt equation	Modified ASA	Valid for homogeneous media with arbitrary absorption and dispersion.
Treeby *et al*. [49] and Jing *et al*. [8]*+	Westervelt equation [8] or coupled nonlinear wave equations [49]	KSTD	Both valid for heterogeneous media. Jing *et al*. [8] only considered thermoviscous media while Treeby *et al*. [49] considered power law absorption.

* the corresponding method models nonlinear wave propagation

+ the corresponding method is a full-wave method: no parabolic approximation; considers multiple scattering

1.3. Applications

Numerical modeling of medical ultrasound has a wide range of applications for both ultrasound imaging and therapeutic ultrasound. This section discusses its applications in four main categories.

1.3.1. Transducer Design

Numerical modeling greatly facilitates transducer design. A series of iterative modeling steps can be performed to obtain the optimal transducer design and shed light on how a certain variable (e.g., frequency, focal length, etc.) affects the acoustic field. For example, Al-Bataineh *et al.* [147] used the k-space method to design transducer arrays for prostate cancer treatment. The design was validated by using MRI thermometry. Pajek and Hynynen [148] designed semi-spherical arrays for stroke treatment using numerical simulations. It was found that extremely high powers are needed to achieve inertial cavitation transcranially above 1 MHz. Zeng *et al*. [149] utilized a waveform-diversity-based approach for optimizing three-dimensional power depositions generated by ultrasound phased arrays. Heat volume within the tumor was increased with simultaneously decreased normal tissue heating. Baron *et al.* [150] used the FDTD method to

study intracranial acoustic fields in clinical trials of sonothrombolysis. Their model has been proven useful for transducer design for sonothrombolysis. They concluded that the hemorrhages observed in the TRUMBI study are possibly due to standing waves formed in the brain at a low frequency. Newer therapeutic applications such as histotripsy that rely on very high pressure levels and the presence of shock fronts at the focus require transducers specifically designed for these applications. Recently a method to determine parameters of transducers to achieve shock formation regimes and certain shock amplitudes at the focus was developed based on the multi-parametric modeling of the KZK equation [151]. Other studies on this topic can be found in [152]-[158].

1.3.2. Transducer Acoustic Field Characterization

Exact knowledge of the acoustic field including side lobes and focal dimensions of the field produced by a transducer is critically important in evaluating its efficacy and safety. Accurate measurement of the four-dimensional field (x, y, z, and time t) could be challenging and unrealistically time-consuming, particularly at high frequencies. For highly nonlinear fields, the hydrophone could also be readily damaged by cavitation. Numerical modeling has been used as an important adjunct for transducer characterization. In this case, a numerical model including both a governing wave equation and a boundary condition that corresponds to a certain ultrasound transducer will be used. Setting a realistic boundary condition to the Westervelt or KZK models is an important and nontrivial problem for obtaining a correct solution that corresponds to the experiment. Acoustic holography or back-projection method has been developed and validated for single-element transducers operating in both continuous wave (CW) [159] and transient [160] cases and for transducer arrays [15] to obtain realistic distribution of vibrational velocity or acoustic pressure at the transducer surface. Clement and Hynynen [66] used the ASA to implement forward and backward projection and to characterize phased array transducers. For nonlinear

fields, Jing and coworkers [128], [129] demonstrated that a transient nonlinear acoustical holography could be used to characterize HIFU transducers. This type of approach has been recognized to be the most accurate, and the IEC standard for characterizing high-intensity fields includes a normative annex on acoustic holography (back-projection) methods [161]. Simpler methods of varying parameters of a boundary condition, typically, the aperture and acoustic pressure of a single-element source, to match experimentally measured beam scans on the axis and in the focal plane, can be also used. It has been shown that the KZK equation with the boundary condition set in this way provides accurate results for nonlinear pressure fields in the focal region of the beam for transducers with up 80° focusing angle [37]. Similar approaches were adopted by Bessonova and Wilkens [162] and Chen *et al*. [163] to examine focused transducers. Chen *et al*., however, chose the SBE as the governing equation. A method of setting a boundary condition by direct measurement of acoustic field close to the source has been used to characterize the field of a clinical shockwave therapy device [164].

KZK equation for wave propagation in water written in dimensionless form contains only two parameters that are combinations of the transducer and propagation medium parameters. For practical applications, besides developing new codes, already existing data of multi-parametric modeling of the KZK equation for a focused piston source can be useful for evaluation of the degree of nonlinear effects and corresponding outputs for quasilinear propagation condition, shock formation, and saturation regimes in water [146]. Again, the parameters of the equivalent single-element source for the KZK model can be determined by matching beam scans measured at low power level to the linear solution of the KZK equation. More relevant literatures on transducer characterization can be found in [11], [15], [160], [165], and [166].

1.3.3. Ultrasound Imaging

Numerical modeling helps researchers better understand the limitation of ultrasound imaging and validate or improve methodologies [167]-[175]. It also facilitates imaging approaches such as the full waveform tomography (FWT) and photo-acoustic tomography (PAT). For example, Li and Zagzebski [176], Treeby *et al*. [177] investigated B-mode and tissue harmonic imaging using numerically acquired pulse echoes. Pinton *et al*. [20] used an FDTD algorithm to study sources of image degradation in fundamental and harmonic ultrasound imaging. Van Neer *et al*. [4] numerically studied and compared fundamental, second harmonic, and super-harmonic echocardiography at their optimal transmission frequencies. Several papers studied the phase aberration in tissue and discussed its effect on imaging [87], [178], [179]. In FWT, ultrasound modeling plays an indispensable role. FWT is an iterative approach for generating quantitative images of sound speed and attenuation. Each iteration involves at least two full wave propagation problems (forward and backward propagation). FWT is emerging as a powerful imaging approach and has been recently applied to breast imaging [180]-[182]. Another area that heavily utilizes ultrasound modeling is PAT, particularly when the time-reversal approach is adopted. Treeby *et al*. [183] used the k-space method and demonstrated how received photo-acoustic signals can be numerically back-propagated to generate PAT images in absorptive media. Treeby and other researchers have followed along this line and applied PAT to areas such as brain imaging [184]-[186]. In PAT, linear acoustics is typically assumed because of the low pressure involved.

1.3.4. Treatment Planning

HIFU treatment planning relies on numerical modeling to predict the pressure distribution and temperature elevation in a patient's body. In return, it provides guidance on the needed phase delays and "dose" for the treatment and optimizes the outcome of the therapy. In general, a

patient's CT or MRI images are used as input for the numerical modeling. Treatment planning is especially important for brain therapy (e.g., treating essential tremor, stoke, brain tumor, etc.), because the phase distortion due to the skull has to be compensated. Clement and Hynynen [187] used a modified ASA to estimate the required phased delay on each element to focus ultrasound beams through skulls. CT images of the skulls are used as the input to provide the density and speed of sound. This approach has been successfully applied to clinical studies [3]. Aubry *et al*. [188] and Jing *et al*. [189] used time-domain, full scattering methods to estimate the phase delay. Although more time-consuming than the ASA method, their approaches could be more accurate at megahertz range. A similar topic is transcostal beam focusing and relevant studies can be found in [104], [190]. Solovchuk *et al*. [191] studied the importance of nonlinear wave propagation on treatment planning. They found that the temperature rise can be strongly enhanced by nonlinear waves. Wu *et al*. [192] developed an integrated tool for HIFU treatment planning that includes ultrasound simulation and interactive visualization. For other research on this topic, the readers are referred to [17], [193]-[196]. It is worth mentioning that, ultrasound modeling models will only perform as well as they are trusted to produce reliable outcomes. This trust should be understood by evaluating uncertainties that could affect the algorithms. Sinden and Haar discussed three types of uncertainties in treatment planning and their impact [197]: errors in segmentation of images and acoustic and thermal parameters of tissue; image registration errors, and artifacts due to organ motion and deformation. Vaughan and Hynynen specifically looked at the effects of parameter errors (speed of sound and CT data errors) in the simulation of transcranial focused ultrasound [198]. It was found that the predicted pressure can change a few percent because of the parameter errors they considered.

1.4.Discussion

There has been a tremendous amount of development in medical ultrasound modeling over the past twenty years. In addition, there is a trend of making ultrasound modeling algorithms freely available by the developers. Seven types of popular open-source softwares on medical ultrasound modeling are listed in Table 1.2, although in fact there are more than seven types of software packages available in the public domain. The open source software packages have generated a strong, positive impact and moved medical ultrasound forward. For instance, the k-Wave software [199] (based on the k-space method), released in 2010, was quickly adopted by the medical ultrasound community and used widely to study PAT and ultrasound imaging [184]-[186], [200]. While being optimistic overall, we must point out that several challenges still exist for ultrasound modeling. Computational speed is still a concern even though current computers are much more powerful than twenty years ago and modeling algorithms have been improved. This is particularly a problem for shock wave modeling (e.g., histotripsy and boiling histotripsy), which calls for both extremely fine spatial and temporal resolutions. There are some methods that could help reduce the temporal resolution, such as the Godunov's method [11], Gagenbauer reconstructions [201], and a modified spectral method [120]. Nevertheless, there are no efficient ways to deal with the discontinuity in the spatial domain caused by shock waves. Even for linear wave modeling, a dramatic speed-up could be beneficial. For example, real-time or quasi-real-time treatment planning could reduce both the waiting time for the patients and the cost [189]. The most efficient approaches (ASA or k-space) used in medical ultrasound still require at least 2 grid points per smallest wavelength simulated. An algorithm that breaks this limit while remains accurate could be a breakthrough. The ultra-weak variational formulation (UWVF) seems to meet this requirement [202]. This approach, however, could have stability problems and has not been widely

used. Other than further improving modeling algorithms, researchers have also investigated the use of parallel computing [102], [105] and graphic processing units (GPU) [8], [177], [199], [203]-[206] for faster modeling. For example, almost one order of magnitude speed-up using single GPUs was reported in [8]. As a final remark, realistic modeling of ultrasound interacting with biological tissue is always desired, but may be quite challenging because of the complex nature of the *in vivo* environment. In addition, when cavitation and/or boiling occurs, the widely varying stochastic nature of cavitation strongly limits the applicability of existing computer models to treatment planning scenarios. Articles addressing these problems are scarce [207]-[209] and clearly more extensive studies are warranted. For example, the wave equation could be coupled with the acoustic streaming hydrodynamic equations or bubble dynamics equations to study their effects on tissue heating [210].

Table 1.2. A summary of currently existing open-source software for ultrasound modeling

Software	Nonlinearity	Heterogeneity	GPU support
Field II [211]	No	No	No
FOCUS [63]	KZK-based	Layered structures	No
Abersim [212]	Westervelt/KZK-based	Random phase layer	No
KZK Texas/Bergen code [38], [111]	KZK-based	No	No
K-WAVE [199]	Westervelt-based	Arbitrary heterogeneity	Yes
HIFU simulator [213]	KZK-based	Layered structures	No
CREANUIS [140]	Westervelt-based	Inhomogeneous nonlinearity coefficients	Yes

CHAPTER 2

TRIENT MIXED DOMAIN METHOD

The work presented in this chapter is in published in IEEE Transaction on Ultrasonics, Ferroelectronics, and Frequency Control [223].

A mixed domain method (MDM) is presented in this chapter for modeling one-way linear/nonlinear wave propagation in biological tissue with arbitrary heterogeneities, in which sound speed, density, attenuation coefficients and nonlinear coefficients are all spatially varying functions. The present method is based on solving an integral equation derived from a Westervelt-like equation. One-dimensional problems are first studied to verify the MDM and to reveal its limitations. It is shown that this method is accurate for cases with small variation of sound speed. A two-dimensional case is further studied with focused ultrasound beams to validate the application of the method in the medical field. Results from the MATLAB toolbox k-Wave are used as the benchmark. Normalized root-mean-square (RMS) error estimated at the focus of the transducer is 0.0133 when the coarsest mesh (1/3 of the wavelength) is used in the MDM. Fundamental and second-harmonic fields throughout the considered computational domains are compared and good agreement is observed. In overall, the MDM is demonstrated to be a computationally efficient and accurate method when used to model wave propagation in biological tissue with relatively weak heterogeneities.

2.1.Introduction

HIFU has received a great deal of attention in recent years due to its non-invasive characteristic. HIFU has been applied to treating a variety of diseases such as uterine fibroids [214], breast cancer [215], [216], brain tumor [217], stroke [218], pancreatic cancer [219], [220],

among others. One challenge to the expansion of HIFU technology is the need to fully understand and compensate for the potential of excessive heating and unwanted cavitation to damage healthy tissue. Fast, accurate characterization of the waveform and pressure distribution is crucial for both scientific investigation and clinical translation of HIFU techniques. Direct measurement of acoustic wave pressure and temperature fields inside tissue is extremely difficult and suffers from various types of hydrophone measurement errors and viscous heating artifacts when using thermocouples. Numerical acoustic wave propagation models can be utilized as an alternative or adjunctive approach to study the safety and effectiveness of HIFU devices under a broader range of conditions than can be investigated experimentally. Another advantage of numerical modeling is that it could facilitate treatment planning [189], [192], [221] and transducer design [148], [149] with reduced cost when compared to experimental testing using real transducers.

During the last two decades, many studies have focused on numerical modeling of ultrasound propagation in tissue-like media. A time-domain numerical model is presented in [109] for studying HIFU in homogeneous media. Diffraction, nonlinearity and absorption effects are treated independently using the method of fractional steps with a second-order operator-splitting algorithm. To investigate the pressure and temperature distribution from focused ultrasound, researchers have used a FDTD method to model the propagation of a finite-amplitude sound in homogeneous thermos-viscous fluids [16]. Though the finite difference method is a powerful technique for modeling wave propagation, it can be time-consuming as very fine spatial and temporal resolutions may be required. Clement and Hynynen [66] investigated the forward and backward projection of linear acoustic fields in homogeneous media with the ASA. A modified ASA was proposed and evaluated in [12], [129] for homogeneous media with nonlinearity considered. However, these methods are not sufficient because they assume homogeneous media,

but the biological tissue is heterogeneous and may have complicated geometries. This is confounded by the fact that the larger the transducer aperture is (to achieve a sharper focusing), the stronger the defocusing is, since heterogeneities distort the wave front. The ability to capture the defocusing in a numerical model is critically important for HIFU safety evaluation.

A wide spectrum of wave solvers have been developed for modeling wave propagation in heterogeneous media. An INCS method was developed [138] to model wave propagation in heterogeneous media. Liu [90] proposed a pseudo-spectral time-domain algorithm to solve large-scale problems for acoustic waves in multidimensional, heterogeneous, absorptive media. Varslot and Taraldsen [42] derived a one-way wave equation which permits smooth variation in all acoustically important variables. Both finite difference and angular spectrum methods are applied for numerical implementation. A second-order wave equation describing nonlinear wave propagation in heterogeneous, attenuating media is solved numerically with the FDTD method by Pinton *et al*. [9]. An algorithm for modeling shock wave propagation in weakly heterogeneous and lossless media was proposed in [222]. A k-space time-domain method for modeling of wave propagation in heterogeneous media was investigated by Mast *et al.* [101] and was later extended to take nonlinear wave propagation into account [8], [49]. Clement and Hynynen [83] combined the ASA with ray theory to describe the propagation of ultrasound through randomly oriented, dissipative, layered media. Vyas and Christensen [84] modified the traditional ASA for simulating linear wave propagation in inhomogeneous media. For a more extensive literature review, the readers are referred to chapter 1 or a recent reviewer paper [1].

The MDM is presented in this chapter for modeling linear/nonlinear wave propagation in dissipative, weakly heterogeneous media, which are considered good approximations for soft tissue. The methodology of MDM is presented in section 2.2. This method is based on solving a

Westervelt-like equation and it utilizes an implicit analytical solution derived by Jing *et al*. [129], [12]. The implicit analytical solution calculates results in the frequency domain and is able to model one-way wave propagation in soft tissue with variations in sound speed, density, attenuation coefficient, and nonlinearity coefficient. Two sets of problems are studied in this chapter and are described in section 2.3. The first set of problems are one-dimensional (1D) problems. Four separate cases are studied: media with inhomogeneous speed of sound; media with inhomogeneous density; media with inhomogeneous attenuation; and media with inhomogeneous nonlinearity. Analytical solutions are used as benchmarks for the first two cases. Simulation results obtained from toolbox k-Wave [199] are used as the benchmark for the last two cases. The second set of problems are two-dimensional (2D) with focused ultrasound beams and involve a more realistic medium. k-Wave results are used as the benchmark. To fully validate the accuracy of the MDM, we consider heterogeneities in the speed of sound, density, attenuation coefficient, and nonlinearity coefficient in a progressive manner. Results are compared in the time-domain as well as in the frequency-domain. Discussion and conclusion can be found in sections 2.4 and 2.5.

2.2.Governing Equation and Method

A Westervelt-like equation is first employed to describe the wave propagation in heterogeneous media [23]:

$$\rho\nabla\cdot\left(\frac{1}{\rho}\nabla p\right)-\frac{1}{c^2}\frac{\partial^2 p}{\partial t^2}+\frac{\delta}{c^4}\frac{\partial^3 p}{\partial t^3}+\frac{\beta}{\rho c^4}\frac{\partial^2 p^2}{\partial t^2}=0, \tag{2.1}$$

where p is the acoustic pressure; ρ is the ambient density; c is the speed of sound; δ is the sound diffusivity and $\delta = 2\alpha_{NP}c^3/\omega^2$, where α_{NP} is the attenuation coefficient with unit Np/m, ω is the angular frequency; β is the nonlinearity coefficient. All material parameters are spatially varying functions, providing great flexibility to the model. It was also demonstrated that the Westervelt equation is accurate for strongly focused transducers [24]. By applying the normalized wave field

$p = f \times \sqrt{\rho}$, Eq. (2.1) becomes

$$\nabla^2 f - \frac{1}{c^2}\frac{\partial^2 f}{\partial t^2} = f\sqrt{\rho}\nabla^2 \frac{1}{\sqrt{\rho}} - \frac{\delta}{c^4}\frac{\partial^3 f}{\partial t^3} - \frac{\beta}{\sqrt{\rho}c^4}\frac{\partial^2 f^2}{\partial t^2}. \tag{2.2}$$

By performing the Fourier transform with respect to time t, Eq. (2.2) becomes

$$\nabla^2 F_t(f) + \tilde{k}^2 F_t(f) = \sqrt{\rho}\nabla^2 \frac{1}{\sqrt{\rho}} F_t(f) + \frac{i\delta\omega^3}{c^4} F_t(f) + \frac{\beta\omega^2}{\sqrt{\rho}c^4} F_t(f^2), \tag{2.3}$$

where F_t is the Fourier transform operator in the time domain and $\tilde{k}^2 = \omega^2/c^2$. To satisfy both the power law attenuation and Kramers-Kronig dispersion relation [224]-[226], we have [227]

$$\tilde{k} = \frac{\omega}{c} - \frac{\alpha(-i)^{y+1}\omega^y}{\cos(\cos(\pi y/2))}, \tag{2.4}$$

where y is the power law exponent. By neglecting the second-order attenuation terms and recognizing that $(-i)^y = \cos(\pi y/2) - i\sin(\pi y/2)$, the following equation can be obtained [25]

$$\tilde{k}^2 = \frac{\omega^2}{c^2} + \frac{2i\alpha\omega^{y+1}}{c} + \frac{2\alpha\tan(\pi y/2)\omega^{y+1}}{c}. \tag{2.5}$$

The imaginary part of Eq. (2.5) corresponds to the dispersion and the third term accounts for the attenuation. We drop the imaginary part in Eq. (2.5) as attenuation has already been considered in Eq. (2.1) or Eq. (2.2). Now Eq. (2.5) is simplified to

$$\tilde{k}^2 = \frac{\omega^2}{c^2} + \frac{2\alpha\tan(\pi y/2)\omega^{y+1}}{c}. \tag{2.6}$$

Replacing $\tilde{k}^2$ in Eq. (2.3) with Eq. (2.6) yields

$$\nabla^2 F_t(f) + \left(\frac{\omega^2}{c^2} + \frac{2\alpha\tan(\pi y/2)\omega^{y+1}}{c}\right) F_t(f) = \sqrt{\rho}\nabla^2 \frac{1}{\sqrt{\rho}} F_t(f) + \frac{i\delta\omega^3}{c^4} F_t(f) + \frac{\beta\omega^2}{\sqrt{\rho}c^4} F_t(f^2). \tag{2.7}$$

By performing an inverse temporal Fourier transform to Eq. (2.7), a wave equation satisfying Kramers-Kronig dispersion relation is given [227]

$$\nabla^2 f - \frac{1}{c^2}\frac{\partial^2 f}{\partial t^2} = f\sqrt{\rho}\nabla^2 \frac{1}{\sqrt{\rho}} + \frac{2\alpha\tan(\pi y/2)}{c}\frac{\partial^{y+1} f}{\partial t^{y+1}} - \frac{\delta}{c^4}\frac{\partial^3 f}{\partial t^3} - \frac{\beta}{\sqrt{\rho}c^4}\frac{\partial^2 f^2}{\partial t^2}. \tag{2.8}$$

Alternatively, the Kramers-Kronig dispersion relation can be applied to Eq. (2.1) directly by

replacing the speed of sound c with c_p and $c_p = \left(\frac{1}{c} + \alpha_0 \tan(\pi y/2)\, \omega^{y-1}\right)^{-1}$, where $\alpha_0 = \alpha_{NP}\omega^{-y}$. Other models for dispersion and absorption are discussed in [26], [27], [30], [106], [227] and [228]. By performing Fourier transform to Eq. (2.8) with respect to x, y and t, we have

$$\frac{\partial^2}{\partial z^2}\tilde{F} + K^2\tilde{F} = F_{xy}\left\{\left[\sqrt{\rho}\nabla^2\frac{1}{\sqrt{\rho}} - \frac{\omega^2}{c_0^2}\left(\frac{c_0^2}{c^2} - 1\right) - \frac{2\alpha\tan(\pi y/2)\omega^{y+1}}{c} + \frac{i\delta\omega^3}{c^4}\right]F_t(f)\right\} + F_{xy}\left(\frac{\beta\omega^2}{\sqrt{\rho}c^4}F_t(f^2)\right), \quad (2.9)$$

where $\tilde{F}$ is the Fourier transform of f in x, y and t; F_{xy} is the Fourier transform operator in x- and y- dimensions; c_0 is the background sound speed and

$$K^2 = \frac{\omega^2}{c_0^2} - k_x^2 - k_y^2, \quad (2.10)$$

where k_x and k_y are wavenumbers in x and y dimensions. For forward one-way propagation, the solution to Eq. (2.9) can be derived from the one-dimensional Green's function in an integral form [12], such that

$$\tilde{F}(z) = \tilde{F}(0)e^{iKz} + \frac{e^{iKz}}{2iK}\int_0^z e^{-iKz'}M\big(f(z')\big)dz', \quad (2.11)$$

where

$$M = F_{xy}\left\{\left[\sqrt{\rho}\nabla^2\frac{1}{\sqrt{\rho}} - \frac{\omega^2}{c_0^2}\left(\frac{c_0^2}{c^2} - 1\right) - \frac{2\alpha\tan(\pi y/2)\omega^{y+1}}{c} + \frac{i\delta\omega^3}{c^4}\right]F_t(f)\right\} + F_{xy}\left(\frac{\beta\omega^2}{\sqrt{\rho}c^4}F_t(f^2)\right). \quad (2.12)$$

By applying the inverse Fourier Transform to $\tilde{F}(z)$ in Eq. (2.11), the acoustic pressure p can be recovered by $f \times \sqrt{\rho}$. This method is a mixed domain method because Eq. (2.11) indicates that operations are needed in both the real physical domain (x and y) and the wave-vector domain (k_x and k_y). The term $\sqrt{\rho}\nabla^2(1/\sqrt{\rho})$ in Eq. (2.12) accounts for the variation of density, followed by the terms that account for the variation of sound speed, attenuation, and dispersion. The last term in Eq. (2.12) outside the brace considers the variation of nonlinearity. Equation (2.11) can be

solved with a Simpson-like integral [129], which is implemented in this study. In this way, the acoustic fields on planes parallel to the x-y plane can be extrapolated with a step size dz. One limitation of the proposed method is that, when modeling media with inhomogeneous speed of sound, it is only accurate for weak heterogeneities (Appendix).

2.3.Simulation Results

2.3.1. One-dimensional Simulation Results

We first investigate a set of one-dimensional problems. Four separate cases are studied: media with inhomogeneous speed of sound; media with inhomogeneous density; media with inhomogeneous attenuation; and media with inhomogeneous nonlinearity. We use analytical solutions as benchmark solutions for the first two cases and k-Wave results as the benchmark for the last two cases. k-Wave is a software package for simulating linear/nonlinear wave propagation using the k-space time-domain method [199]. A Gaussian modulated pulse is used and is expressed as

$$p_{source} = p_0 \exp(-t^2 f_c^2/2)\sin(2\pi f_c t), \tag{2.13}$$

where $p_0 = 1$ Pa is the magnitude of the pulse; the center frequency of the pulse f_c is 1 MHz. For a two-step stair-like medium with speed c_{m1} in the first half of the domain and c_{m2} in the second half, and with a total propagation distance of z, the analytical solution is [230]

$$p_{speed} = T_c p_0 \exp(-t_c^2 f_c^2/2)\sin(2\pi f_c t_c), \tag{2.14}$$

where $t_c = z/2c_{m1} + z/2c_{m2}$ and $T_c = 2c_{m2}/(c_{m1} + c_{m2})$. For a two-step stair-like medium with density ρ_{m1} in the first half of the domain and ρ_{m2} in the second half, sound speed of c, and a total propagation distance of z, the analytical solution is [230]

$$p_{density} = T_\rho p_0 \exp(-t_\rho^2 f_c^2/2)\sin(2\pi f_c t_\rho), \tag{2.15}$$

where $t_\rho = z/c$ and $T_\rho = 2\rho_{m2}/(\rho_{m1} + \rho_{m2})$. The accuracy of the model is quantified by

calculating the normalized root mean square (RMS) error which is defined as [84]

$$\Delta_{nrms} = \sqrt{\frac{\sum_{i=1}^{N} |P_{MDM}(i) - P_{benchmark}(i)|^2}{N}}, \tag{2.16}$$

where $p_{MDM}(i)$ and $p_{benchmark}(i)$ are normalized pressures calculated with the MDM and the benchmark method, respectively. N is the number of sampling points. In this 1D case, results are obtained at a certain receiver location (21 mm away from the source) and the points are sampled in the time-domain. Step size dz does not significantly affect the result for this special case with only one interface and it is chosen as $1/27\lambda$.

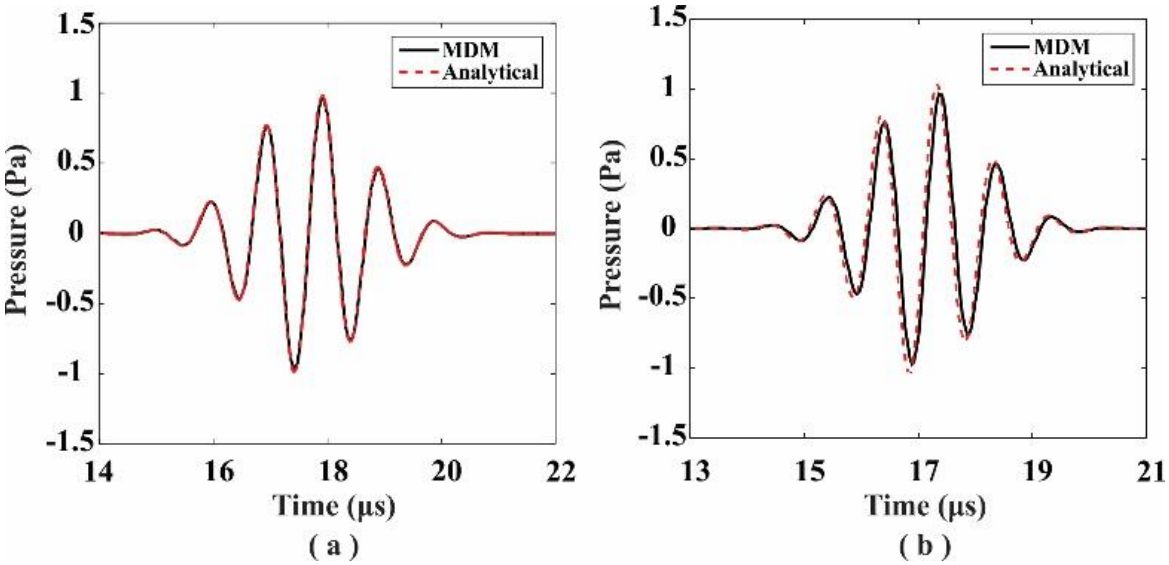

Figure 2.1 Comparison between the MDM and analytical solution for the 1D case with (a) a weak sound speed contrast and (b) a stronger sound speed contrast.

Figure 2.1 illustrates the results for the wave propagation in a 1D inhomogeneous medium with sound speed variation only. The total computational domain is 21 mm long. The received signal is recorded at the end of the computational domain. In Fig. 2.1(a), the sound speed for the first half of the computational domain is 1500 m/s, while it is 1575 m/s for the second half, indicating a relatively small contrast ratio of 1.05. In Fig. 2.1(b), the sound speed within the second half of the computational domain is increased to 1725 m/s, indicating a stronger contrast ratio of

1.15. Analytical solution for these two cases is Eq. (2.14). When wave propagates in the weakly heterogeneous medium, simulation results from the MDM are very close to the analytical results. More appreciable phase difference and amplitude difference can be observed in Fig. 2.1(b). In fact, the amplitude of the pulse remains almost unchanged for the MDM. These observations are consistent with the expectation that the MDM works better for weakly heterogeneous media and the transmission coefficient due to speed of sound variation is not considered (Appendix). On the other hand, the MDM does take the phase change into account, though the accuracy also depends on the contrast of the heterogeneity. The RMS errors are 0.0135 and 0.1465 for the two cases, respectively. The proof that MDM currently works the best for weakly heterogeneous media (in speed of sound) is presented in the Appendix. It demonstrates that the MDM does not take the transmission coefficient due to sound speed variation into account, and the phase change is modeled most accurately when the sound speed contrast is low.

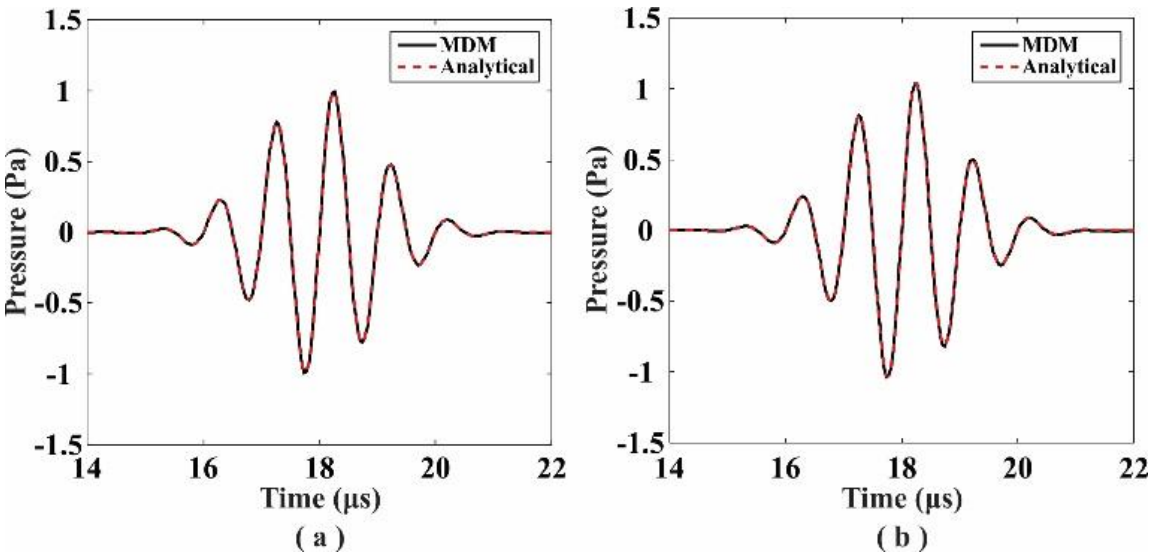

Figure 2.2 Comparison between the MDM and analytical solution for the 1D case with (a) weak density contrast and (b) stronger density contrast.

Figure 2.2 records signals for the wave propagation in a 1D inhomogeneous medium with density variation only. In Fig. 2.2(a), the density for the first half of the computational domain is

1000 kg/m^3, while at the second half is 1050 kg/m^3, indicating a relatively small contrast ratio of 1.05. In Fig. 2.2(b), the density within the second half of the computational domain is increased to 1150 kg/m^3, indicating a stronger contrast ratio of 1.15. Analytical solution for the two cases is Eq. (2.15). The RMS errors for the cases with weak and stronger contrast are 0.0005 and 0.0052, respectively. Amplitudes of the main waveforms for the MDM and k-Wave results agree well for both weak and stronger contrast cases, indicating that the MDM does take the transmission coefficient into account in this case. The analytically predicted transmission coefficients for the two cases are 1.0243 and 1.0698, whereas the numerically estimated transmission coefficients are 1.0247 and 1.0636.

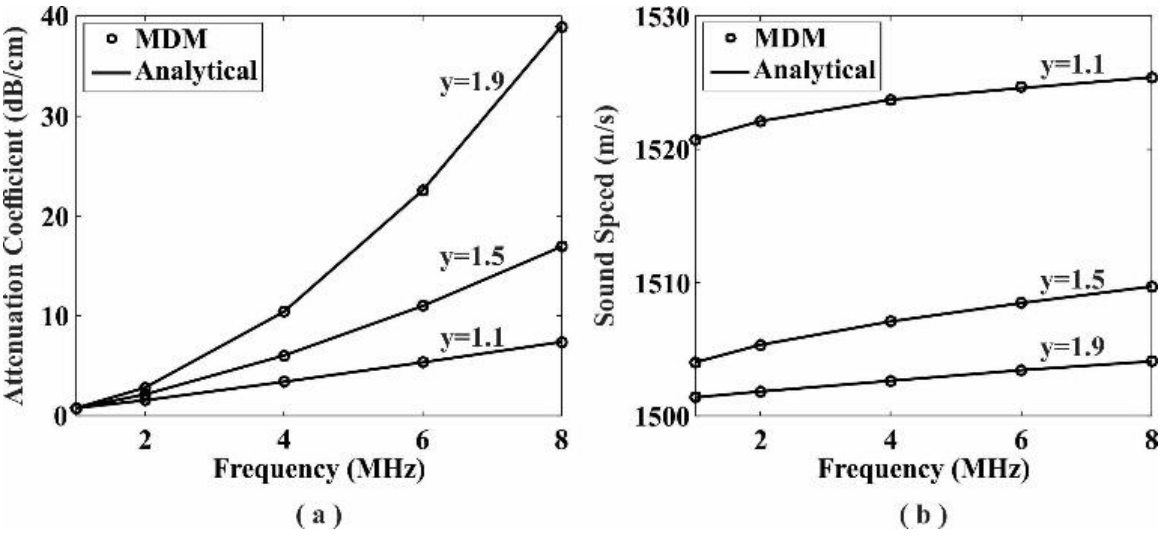

Figure 2.3 (a) Attenuation coefficients and (b) frequency-dependent sound speed are obtained with the MDM at different frequencies for power law exponents of 1.1, 1.5 and 1.9. Analytical values are presented for comparisons.

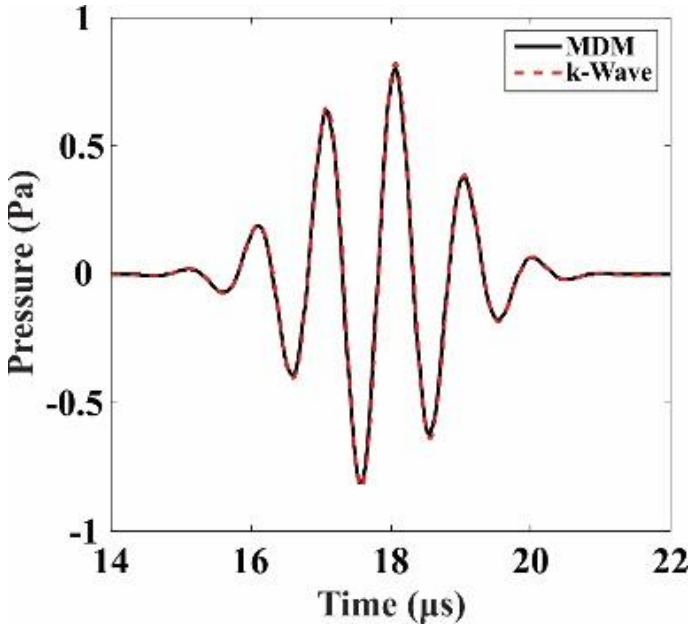

Figure 2.4 Comparison between the MDM and k-Wave method for the 1D case with attenuation coefficient variation.

Attenuation and dispersion play very important roles in ultrasound propagation. While attenuation limits the depth that ultrasound can reach in tissues, dispersion can distort the waveform of ultrasound. The MDM considers both power law attenuation and Kramers-Kronig dispersion relation and can be readily used for modeling arbitrary dispersion and arbitrarily frequency-dependent attenuation as the algorithm operates in the frequency-domain. To demonstrate the ability of the MDM to correctly model power law absorption and dispersion, the propagation of the Gaussian modulated wave through 1D homogeneous absorbing media with different central frequencies ranging from 1 MHz to 8 MHz is studied. In the simulation, the reference speed of sound is 1500 $\mathrm{m/s}$ and density is 1000 $\mathrm{kg/m^3}$. The attenuation coefficient is chosen as 0.75 $\mathrm{dB \cdot MHz^{-y} \cdot cm^{-1}}$ for the whole domain. Attenuation coefficients and frequency-dependent sound speed are extracted from the time series recorded at two positions using the relations [25]

$$\alpha_{dB} = -\frac{20\log_{10}(A_2/A_1)}{100d}, \tag{2.17}$$

$$c_p = -\frac{\omega d}{\phi_2 - \phi_1}, \tag{2.18}$$

where α_{dB} is the attenuation coefficient in unit of $\mathrm{dB/cm}$, $A_{1,2}$ and $\phi_{1,2}$ are the single-sided amplitudes and phase spectra, d is the propagation distance in meters and it is 0.005 m. Analytical values of the attenuation coefficient is calculated with $\alpha_{dB} = \alpha f^y$, where α is in unit $\mathrm{dB \cdot MHz^{-y} \cdot cm^{-1}}$; frequency-dependent sound speed is calculated with $\frac{1}{c_p} = \frac{1}{c_{\omega_0}} + \alpha_0 \tan(\pi y/2)(\omega^{y-1} - \omega_0^{y-1})$, where ω_0 is chosen to be 1 MHz and the corresponding c_{ω_0} is extracted from the simulated data. Fig. 2.3(a) and Fig. 2.3(b) illustrate the attenuation coefficient and the sound speed as a function of frequency for power law exponents of 1.1, 1.5 and 1.9. Simulation and analytical results match very well. Results for the wave propagating in a 1D medium with heterogeneity of attenuation coefficient are shown in Fig. 2.4. Attenuation coefficient at the first half domain is zero and is 1.5 $\mathrm{dB \cdot MHz^{-y} \cdot cm^{-1}}$ for the second half. The power law exponent *y* is 1.1. The normalized RMS error is 0.0185, suggesting that both the loss and dispersion are accurately modeled.

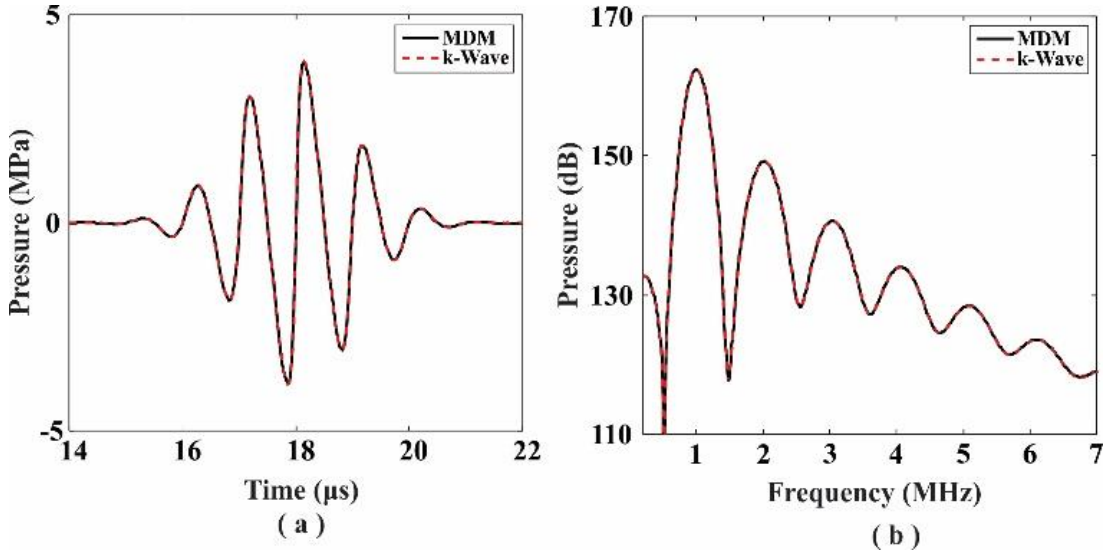

Figure 2.5 Comparison between the MDM and k-Wave method for the 1D case with nonlinearity coefficient variation. (a) Time-domain results; (b) frequency-domain results.

The nonlinearity coefficient plays an important role in the distortion of waveform and the emergence of harmonics as the wave propagates. Media with nonlinearity parameter variation exhibit different nonlinear behaviors and it provides a potential route for ultrasound imaging [140]. Variation of nonlinearity coefficient has also been considered in our study and results are presented in Fig. 2.5. The pressure magnitude is increased to 4 MPa. The nonlinearity coefficient for the first half domain is 3.5 and is 5.0 for the second half. The normalized RMS error is 0.0008. One additional simulation is carried out for MDM which considers a constant nonlinearity coefficient 3.5 for the whole domain. When compared with k-Wave with inhomogeneous nonlinearity coefficients, MDM with constant nonlinearity coefficient has a larger normalized RMS error and is 0.019. This suggests that the ability to model inhomogeneous nonlinearity coefficients does improve the accuracy of the simulation. Further details about nonlinear wave propagation are not discussed here since many studies on this topic have been carried out [11], [15], [107], [139], [231].

2.3.2. Two-dimensional Simulation Results

A 2D problem that is more realistic is further studied to verify the MDM. The same Gaussian modulated pulse is used. Pressure magnitude p_0 is 1 Pa when nonlinearity is not considered and is increased to 2 MPa when the nonlinear effect is investigated. The center frequency f_c is again 1 MHz. A planar phased array is used to model a focused beam. In both MDM and k-Wave, we define a phased array with phase delays in the source plane [12], [199], and we treat each cell in the source plane as a sound source with its individual phase delay. The geometrical focus is around 21 mm and the aperture size is 22 mm. This configuration has variations in speed of sound, density, attenuation coefficient, and nonlinearity coefficient. It is used as a model to study the wave propagation from water to fat with tumors. Acoustic properties

used in this model are listed in Table 2.1. The power law exponent y is 1.1 throughout the computational domain. In theory, the power law exponent is 2 in water. However, k-Wave, which is used to generate benchmark solutions, cannot model problems that contain multiple values of power law exponent. Fig. 2.6(a) illustrates the geometry of the 2D problem. The transverse dimension of the computational domain is 72.5 mm and it is sufficiently large to reduce the wrap-around error [68]. It should be pointed out that absorption layers can be incorporated into the MDM to reduce the computational domain size [73]. Ultrasound wave propagates in the water (light blue) first and then penetrates the fat (dark blue). Tumors are represented with three cylinders and their diameters are 3.5 mm, 3.0 mm, and 1.0 mm respectively. Two of them have overlapped area. The reason why we choose simple geometries here is because later on we can easily vary the spatial resolution without changing the geometry of the problem. Both spatial step size and temporal step size used in the k-Wave are fine enough to obtain well-converged results. Spatial step sizes in the x and y directions are both $1/27\lambda$ (λ is the wavelength in fat and it is 1.48 mm at 1 MHz); the time step size is 4.6×10^{-4} μs. The corresponding Courant–Friedrichs–Lewy (CFL) number is 0.0123. The reason we choose such a small CFL number here is because a solution that is as accurate as possible is desired for benchmark. Additionally, a convergence study is carried out on k-Wave and some slight phase errors at larger CFL numbers are observed and we want to minimize these errors. We investigate the accuracy of the MDM by varying the spatial step size dz. Additionally, for simplicity, it is assumed that $dx = dz$, though in theory they could be different. For the MDM, three spatial step sizes are selected and they are $1/3\lambda$, $1/9\lambda$, and $1/27\lambda$. The temporal resolution dt is fixed at 0.037 μs and additional simulations show that different dt does not significantly affect the result once the Nyquist sampling rate is well satisfied. The temporal domain size (end time) is 44 μs for all cases.

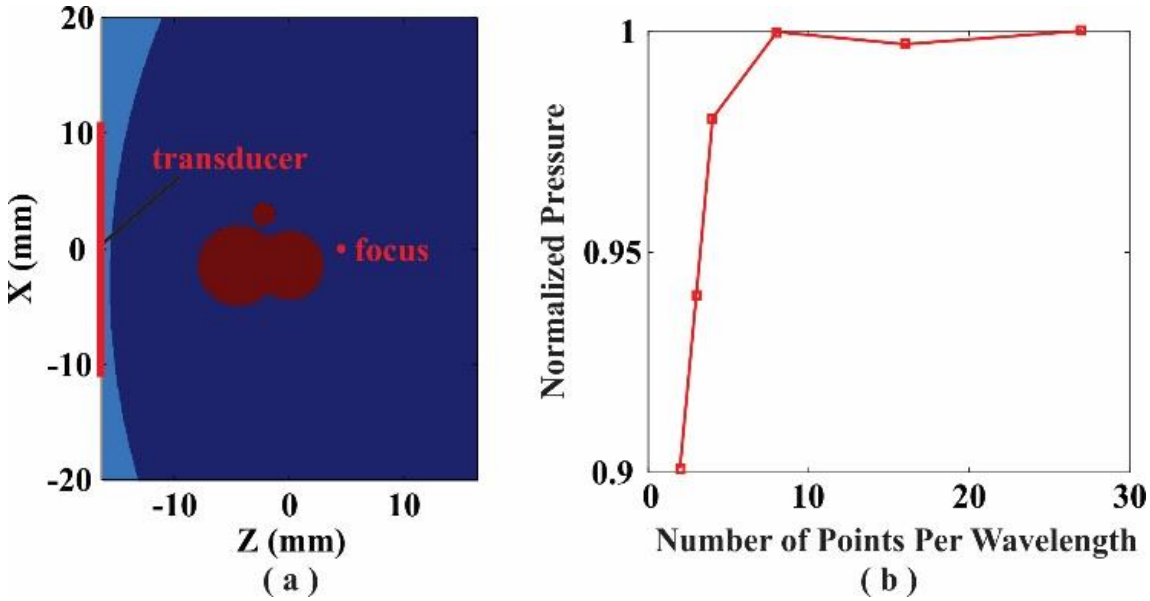

Figure 2.6 (a) Geometry of the 2D case. The computational domain shown here is cropped from the original domain for illustration purposes. The acoustical properties for different parts are listed in Table 2.1. The light blue part is water; dark blue part represents the fat; three cylinders represent the tumors. The red line on the left indicates the array position. The red dot is the geometrical focus. (b) Convergence test for the MDM in the 2D linear inhomogeneous medium with speed and density variations. The pressures at different spatial resolutions are recorded at the geometrical focus of the transducer and are normalized.

Table 2.1. Tissue acoustical properties

	Speed of Sound m/s	Density kg/m^3	Attenuation coefficient $dB \cdot MHz^{-y} \cdot cm^{-1}$	Nonlinearity coefficient
water	1500	1000	0.005	3.6
fat	1480	937	0.40	5.8
tumor	1563	1070	0.57	4.5

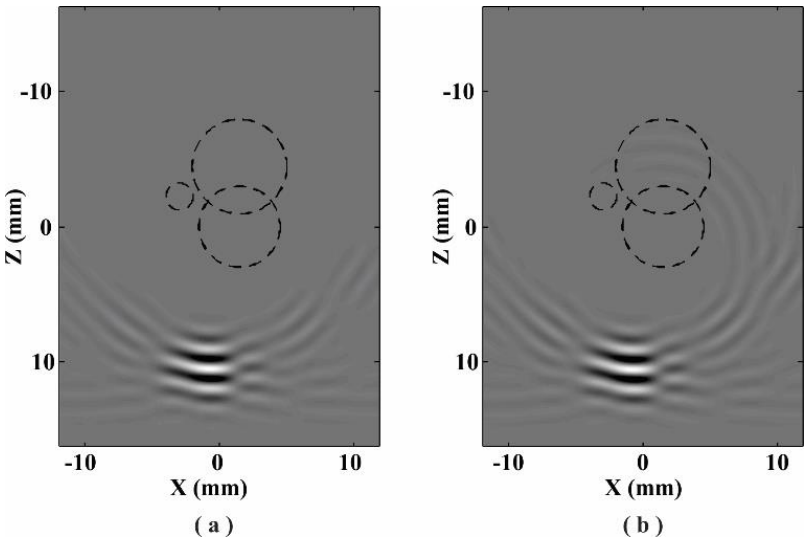

Figure 2.7 Snapshots of the acoustic fields for the case with speed and density variations at $t = 22$ μs. The focused beam is simulated with (a) the MDM and (b) the k-Wave. Dashed lines show the positions of the tumors.

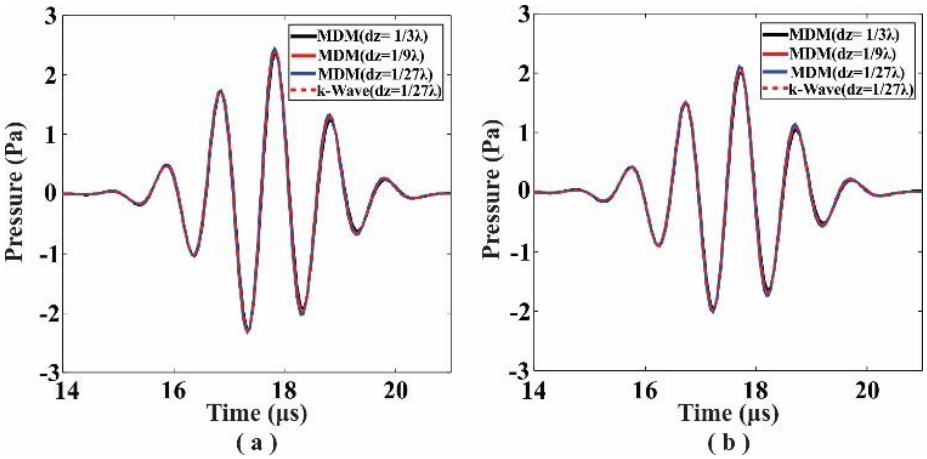

Figure 2.8 Comparison between the MDM and k-Wave simulation results in the 2D linear inhomogeneous medium with speed and density variations and (a) without attenuation and dispersion; and (b) with attenuation and dispersion. Receiver location is at the geometrical focus of the transducer.

We first compare the results with speed and density variations only. A convergence test is conducted for this 2D case at the geometrical focus of the transducer and the result is shown in Fig. 2.6(b). The normalized pressure $P_{normalized}$ [232] is calculated with the formula

$P_{normalized} = P_f/P_{27}$, where P_f is the pressure at the focus of the transducer with different numbers of points per wavelength, and P_{27} is the pressure at the same point when $dx = dz = 1/27\lambda$. Reasonably accurate results can be found starting at $1/4\lambda$. Acoustic fields for this case at $t = 22$ μs are shown in Fig. 2.7. It is noted that the MDM result does not contain reflections due to the one-way approximation. However, the amplitude of the reflection is relatively small compared to transmission in soft biological tissue [42]. The waveforms at the focus are plotted in Fig. 2.8(a) for further comparison. From the comparison for the 1D case (shown in Fig. 2.2(b)), we know that the MDM can predict accurate results even with relatively strong density variation. Thus, the amplitude and phase differences in Fig. 2.8(a) are mainly from the variation of speed of sound.

Next, attenuation and dispersion effects are added to the medium. The results are displayed in Fig. 2.8(b) and the phase and amplitude of the received signal are changed compared to the lossless case. The amplitude is evidently smaller due to the attenuation. Figure 2.9 exhibits the frequency domain results at 1 MHz. Spatial step size for MDM in Fig. 2.9 is $1/3\lambda$. For comparison, the results for the homogeneous case (water only) are also included. Even for the homogeneous case, some near-field discrepancy between the MDM and k-Wave can be observed, which is possibly due to the different boundary conditions used in these two methods: the MDM uses the pressure release surface whereas the k-Wave uses the Kirchhoff (or free field) boundary condition. However, differences from the boundary conditions in the far-field are negligible. For the heterogeneous case, some "ripples" are visible in the tumors in Fig. 2.9(d), which are not observed in Fig. 2.9(c). These features are due to the multiple scattering/reflection which is not considered in the present MDM. Nevertheless, the beam distortion looks very similar between the MDM and k-Wave results.

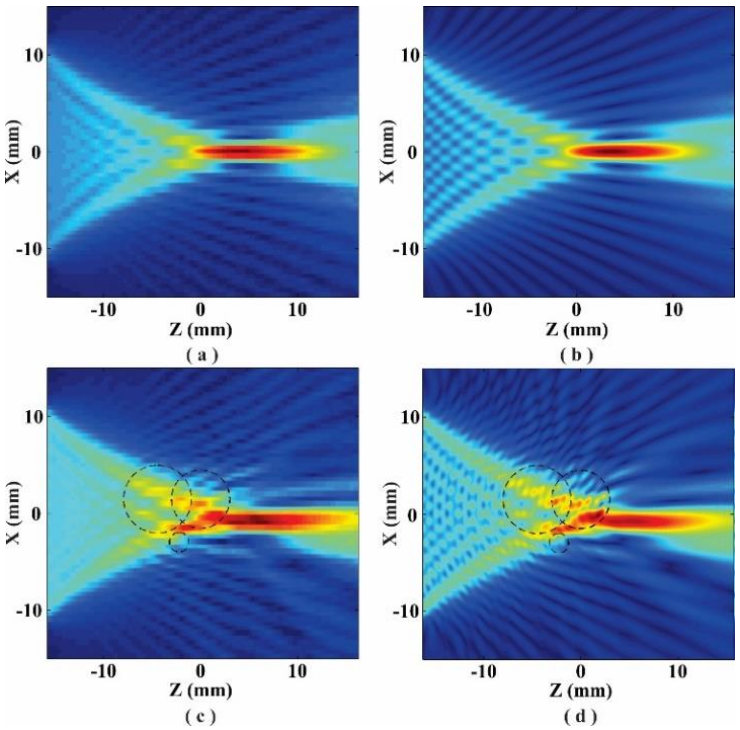

Figure 2.9 Frequency domain results for the fundamental frequency (1MHz) in the homogeneous medium with (a) the MDM and (b) k-Wave. Frequency domain results for the fundamental frequency in the heterogeneous medium with (c) the MDM and (d) k-Wave with speed of sound, density, attenuation and dispersion variations. The MDM results shown here are with the spatial step size of $1/3\lambda$.

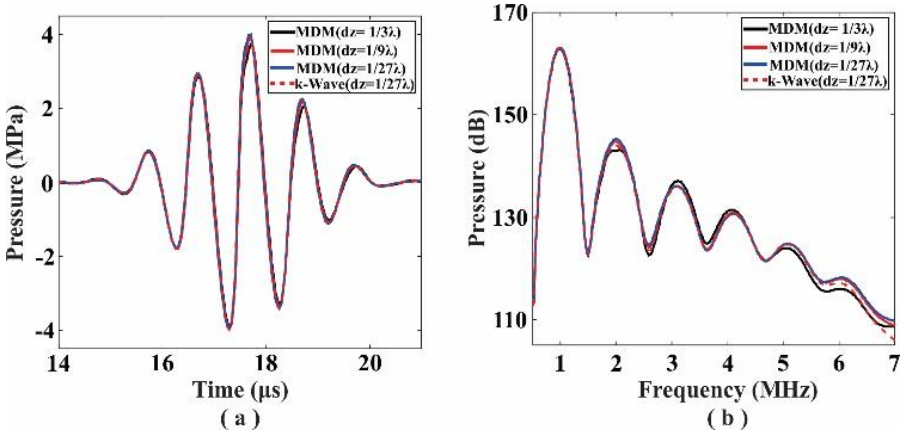

Figure 2.10 Comparison between the MDM and k-Wave in a 2D nonlinear lossy medium with speed and density variations in the (a) time domain and (b) frequency domain. Receiver location is at the geometrical focus of the transducer.

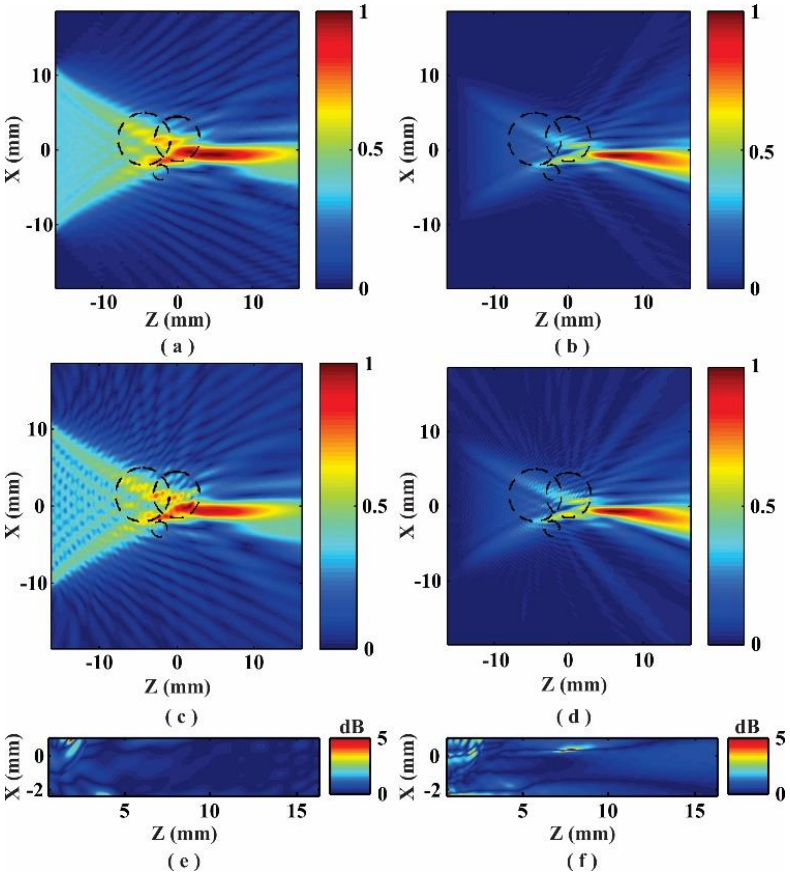

Figure 2.11 Pressure for the (a) fundamental and (b) second-harmonic field simulated by the MDM. Pressure for the (c) fundamental and (d) second-harmonic field simulated by k-Wave. Difference from the fundamental and second-harmonic components between the two methods around the transducer focal region are shown in (e) and (f). The MDM results shown here are with the spatial step size of $1/27\lambda$.

Table 2.2. Normalized RMS errors

Spatial step size	1/3λ	1/9λ	1/27λ
Lossless medium	0.0109	0.0041	0.0040
Lossy medium	0.0111	0.0052	0.0036
Lossy medium with nonlinearity	0.0133	0.0073	0.0062

Afterwards, nonlinearity is considered. The nonlinearity coefficient is directly responsible for the increase of the harmonics in wave propagation. Results are compared in the time domain

(Fig. 2.10(a)) and frequency domain (Fig. 2.10(b)). Normalized RMS errors evaluated at the geometrical focus are listed in Table 2.2 for all spatial resolutions trialed and the errors in general reduce (though not significantly) as the spatial resolution becomes finer. Note that the entire time-domain signal is used for computing the error although Figs. 2.8 and 2.10(a) only show the primary waveform (i.e., first-order transmission). Comparisons for the fundamental and second-harmonic frequency fields are shown in Fig. 2.11. The acoustic pressure fields in Fig. 2.11 are normalized. Figs. 2.11(e) and (f) show the differences for the fundamental and second-harmonic components between the MDM and k-Wave in the focal region in unit dB. Normalized RMS errors in the focal region are 0.0280 for the fundamental frequency field and 0.0149 for the second-harmonic field at the spatial resolution of $1/27\lambda$.

2.4.Discussion

Results from k-Wave are used as the benchmark solution in this study and the accuracy of k-Wave has been well-documented in many papers [25], [49], [232]. The difference between MDM and k-Wave is expected to be due to a combination of different factors, including 1) numerical errors of each method; 2) different model equations; and 3) different boundary conditions. Since very fine spatial and temporal resolutions are used, numerical errors from k-Wave should be minimized. While the MDM solves a second order partial differential equation (PDE), the k-Wave solves a set of coupled first order PDEs. For lossless cases though, it was shown that the second order PDE can be derived from the coupled PDEs [49]. When considering loss, there is a slight difference in our method and k-Wave for the attenuation part. This error should be relatively small as evidenced by Fig. 2.4. There is also a difference in terms of setting up the boundary condition in k-Wave and our model, which has been briefly discussed. This difference mainly exists in the near-field. The MDM has an intrinsic error of not including the

reflection (due to one-way propagation), which should be the main contribution to the difference between the two methods. Reflections can be added into the MDM to improve the accuracy. One possible approach is to use the method proposed in [84]. Although the method in [84] only applies to linear waves, it should be sufficient since reflection in soft tissue has relatively low amplitude and therefore the nonlinear effect is weak.

To fully validate the MDM, two cases are studied. In the 1D case, we investigate the accuracy of the MDM by considering the variations of sound speed, density, and attenuation separately. Results from the 1D case show that this algorithm can predict accurate results in weakly heterogeneous medium. Afterwards, a set of 2D problems are further studied. Variations of sound speed, density, attenuation, and nonlinearity are added step by step. Density variation and sound speed variation are first considered together. It is found that more accurate results can be obtained when the spatial resolution is finer. This is because a smaller step size (dx and dz) will reduce the error from stair-stepped surfaces [233] caused by discrete meshes. Stair-casing errors occur when representing complex geometries (like circular/spherical) with rectilinear grids. Reference [232] specifically studied this error for k-Wave and it is shown to be the most serious error when modeling transcranial ultrasound. The truncation error introduced by the numerical integration [234] will also be reduced if a smaller step size (dz) is used. However, even with a very coarse spatial resolution (i.e., $1/3\lambda$), the error of the MDM can still be kept small (on the order of 0.01). This is a great advantage when compared with the most commonly used FDTD scheme which requires 8 to 10 grid points per wavelength to achieve reasonably accurate results. Besides, spatial aliasing error due to finite domain size is also a possible source of error in the MDM. We have used sufficiently large x-axis range to minimize the spatial aliasing error.

The numerical implementation throughout this study is based on MATLAB 2015b (The

MathWorks Inc., Natick, MA) on a 64-bit operating system with a quad-core 3.60-GHz Intel Xeon 5687 CPU (Intel Corp., Santa Clara, CA) processors and 192 GB of RAM. For the linear 2D case, the MDM with spatial step size $1/3\lambda$ takes 0.013 s to obtain the frequency domain result shown in Fig. 2.9(c). With the same spatial step size and computational domain and a CFL number of 0.11, the k-Wave simulation needs 8.81 s, indicating a 677-fold computation speed difference. This computational difference is expected to be highly problem-dependent though and should not be generalized. The drastically different computation times are due to the fact that for k-Wave simulations, the time-domain simulation needs to be carried out first and the Fourier transform is performed to obtain the results at the frequency of interest. On the other hand, the MDM directly operates in the frequency-domain and therefore can be considerably more efficient in producing frequency-domain results. This is particularly useful for modeling thermal-based HIFU problems since in many cases the frequency-domain results are of utmost importance.

2.5.Conclusion

A mixed domain method is presented in this chapter. The MDM solves the Westervelt-like equation with appropriate assumptions and it is accurate for weakly heterogeneous media. Since the theory is presented for the general 3D case, the algorithm, though only demonstrated in 1D and 2D, can be readily extended to modeling 3D problems. In this study, we have shown that the MDM is an efficient and accurate algorithm for modeling medical ultrasound propagating in soft tissue. There are many foreseeable applications for numerical modeling of ultrasound using the MDM. For example, it can assist HIFU device sponsors in preparing reliable pre-clinical testing data generated from computational modeling or facilitate HIFU treatment planning. Furthermore, ultrasound computed tomography (USCT) is an emerging imaging modality to reconstruct the sound speed, density and attenuation of soft tissue for diagnosis though transmission signals [235]-

[237]. However, computation time is one of the most critical issues for USCT. The computationally efficient MDM, therefore, can be proven to be a promising approach for frequency-domain USCT.

CHAPTER 3

FREQUENCY-SPECIFIC MIXED DOMAIN METHOD

The work presented in this chapter is in published in IEEE Transaction on Ultrasonics, Ferroelectronics, and Frequency Control [229]

A mixed-domain method dubbed frequency-specific mixed domain method is introduced for the simulation of the second harmonic ultrasound field in weakly heterogeneous media. The governing equation for the second harmonics is derived based on the quasilinear theory. The fundamental frequency pressure field is first solved by the frequency-specific mixed domain method, and it is subsequently used as the source term for the second harmonics equation. This equation can be again solved by the frequency-specific mixed domain method to rapidly obtain the second harmonic pressure field. Five two-dimensional cases, including one with a realistic human tissue map, are studied to systematically verify the proposed method. Results from the previously developed transient mixed domain method are used as the benchmark solutions. Comparisons show that the two methods give similar results for all cases. More importantly, the frequency-specific mixed domain method has a crucial advantage over the transient mixed domain method in that it can be two orders of magnitude faster.

3.1.Introduction

Nonlinear ultrasound, a branch of nonlinear acoustics, is of great importance in biomedical ultrasound for both diagnostic and therapeutic applications [23]. For instance, the presence of acoustic nonlinearity could improve B-mode imaging because the harmonic beams are narrower and they have lower sidelobes than those of the fundamental frequency [238]. The combination of the fundamental frequency and its harmonics can enhance the image quality and help better

visualize tissue structures [239]. Nonlinear parameter diffraction-based tomography can help better distinguish diseased tissues from healthy ones compared to ultrasound imaging purely based on linear parameters [240], [241]. On the other hand, when high intensity focused ultrasound (HIFU) is used for therapeutic applications, the nonlinear effect can be pronounced, though its extent very much depends on factors such as *F*-number [242], frequency, propagation medium [17], and sonication protocol (whether it is for hyperthermia [243]-[245], thermal ablation [246], inertial cavitation [246], [247], or boiling [248]).

Numerical modeling is vital for facilitating the applications of nonlinear ultrasound. A number of numerical methods have been developed to model nonlinear ultrasound propagation [107]-[108], [12]. Some of the solvers assume that the propagating medium is homogeneous [16], [107], [12]. Though it is argued that such an assumption is reasonable for soft tissues, more accurate results can be obtained if tissue heterogeneities are taken into account. This is especially important when studying phase aberration in biological tissue [20], [179], such as body walls [249]. A summary on representative numerical solvers for modeling nonlinear wave propagation in heterogeneous media is given below. Christopher and Parker [108] solved the equivalent Westervelt equation with an operator splitting method. The diffraction part was solved with the ASA and the nonlinearity term was solved by utilizing the frequency domain solution to Burgers' equation. This method is limited to parallel layered media [108]. Varslot and Taraldsen [42] derived a one-way model permitting smooth variation for all acoustical variables. A numerical solution to this equation was implemented using the operator splitting method. The Texas time-domain code was extended by Jing and Cleveland to solve the generalized Khokhlov-Zabolotskaya-Kuznetsov (KZK) equation and it is accurate for sound propagation in weakly heterogeneous media [41]. A modified ASA is developed [139] for media with spatially varying

nonlinear parameter. A second-order wave equation describing nonlinear wave propagation in heterogeneous, attenuating media was solved with the FDTD method by Pinton *et al.* [9]. A k-space time-domain method solving the coupled nonlinear wave equations was investigated [49] for modeling wave propagation in heterogeneous media with power law absorption. Almost at the same time, a k-space time-domain method for solving the second-order nonlinear wave equation was proposed [8] for thermoviscous fluids. Most recently, a mixed domain method (MDM) for modeling nonlinear one-wave propagation in dissipative, weakly heterogeneous media (speed of sound contrast being less than 1.1) has been presented [223].

As demonstrated in [223], wave fields at a certain frequency can be produced by MDM in two ways for linear wave propagation. One is to obtain the result by applying the temporal Fourier transform to the transient simulation MDM result (denoted transient MDM, or TMDM). A more computationally efficient way is to directly implement the MDM at the frequency of interest (denoted frequency-specific MDM, or FSMDM). This carries a huge benefit especially when modeling continuous waves (CWs), which is often used in HIFU, since there is only a single frequency of interest and the latter approach could be orders of magnitude faster than the former. This benefit, however, is lost when modeling nonlinear wave propagation, since specific equations for describing harmonics are missing. In this chapter, the FSMDM is extended to modeling the second harmonic ultrasound field in heterogeneous, lossy media for weakly nonlinear cases (Mach number $\varepsilon \ll 1$). First, the frequency-domain equation that describes the second harmonic frequency is derived. For weakly nonlinear cases, the fundamental frequency wave field is independent of the second harmonics, while the second harmonic wave field is directly produced by that of the fundamental frequency. To evaluate the accuracy of the FSMDM, four cases with imaginary tissue maps are investigated: wave propagation in a homogeneous nonlinear medium, a

nonlinear medium with heterogeneous attenuation, a nonlinear medium with heterogeneous speed of sound, and a nonlinear medium with heterogeneous attenuation and speed of sound. Finally, a realistic human tissue map is used to evaluate the accuracy of the FSMDM. The FSMDM is compared with the TMDM throughout this chapter.

3.2.Theory

The governing equation reads [223]

$$\nabla^2 p - \frac{1}{c^2}\frac{\partial^2 p}{\partial t^2} + \frac{\delta}{c^4}\frac{\partial^3 p}{\partial t^3} + \frac{\beta}{\rho c^4}\frac{\partial^2 p^2}{\partial t^2} = 0, \tag{3.1}$$

where p is the acoustic pressure, c is the speed of sound, t is the time, δ is the sound diffusivity and $\delta = 2\alpha c^3/\hat{\omega}^2$, where α is the absorption coefficient, $\hat{\omega}$ is the angular frequency, and β is the nonlinearity coefficient. All acoustical parameters vary spatially. The density is assumed to be a constant for simplification. For weakly nonlinear media, a quasilinear solution $p = p_1 + p_2$ is permitted [23], where p_1 is the pressure at the fundamental frequency ω and p_2 is the pressure at the second harmonic frequency 2ω. Additionally, it is assumed that $|p_1| \gg |p_2|$. By using the notation [23]

$$p_n(x,y,z,t) = \frac{1}{2i}P_n(x,y,z)e^{in\omega t} + c.c., \quad n = 1,2, \tag{3.2}$$

where $c.c.$ denotes the complex conjugate of preceding terms [23]. The pressure p can be expressed as

$$p(x,y,z,t) = \frac{1}{2i}P_1(x,y,z)e^{i\omega t} + \frac{1}{2i}P_2(x,y,z)e^{i2\omega t} + c.c. \tag{3.3}$$

For weakly nonlinear cases, we have the approximation

$$p^2(x,y,z,t) \cong -\frac{1}{4}P_1^2(x,y,z)e^{i2\omega t}. \tag{3.4}$$

Substituting Eq. (3.3) and Eq. (3.4) into Eq. (3.1) produces

$$\nabla^2\left(\frac{1}{2i}P_1 e^{i\omega t} + \frac{1}{2i}P_2 e^{i2\omega t}\right) - \frac{1}{c^2}\frac{\partial^2}{\partial t^2}\left(\frac{1}{2i}P_1 e^{i\omega t} + \frac{1}{2i}P_2 e^{i2\omega t}\right) =$$

$$-\frac{\delta}{c^4}\frac{\partial^3}{\partial t^3}\left(\frac{1}{2i}P_1 e^{i\omega t}+\frac{1}{2i}P_2 e^{i2\omega t}\right)-\frac{\beta}{\rho c^4}\frac{\partial^2}{\partial t^2}\left(-\frac{1}{4}P_1^2 e^{i2\omega t}\right). \quad (3.5)$$

Rearranging Eq. (3.5) yields

$$\nabla^2 P_1+\frac{\omega^2}{c^2}P_1=\frac{i\omega^3\delta}{c^4}P_1, \quad (3.6)$$

and

$$\nabla^2 P_2+\frac{4\omega^2}{c^2}P_2=\frac{i8\omega^3\delta}{c^4}P_2-\frac{i2\omega^2\beta}{\rho c^4}P_1^2. \quad (3.7)$$

Equation Eq. (3.6) should be solved first to calculate P_1. The fundamental frequency pressure will serve as part of the source term in Eq. (3.7) to calculate the second harmonic pressure P_2. Applying the Fourier transform to Eq. (3.6) and Eq. (3.7) with respect to *x* and *y* yields

$$\frac{\partial^2\tilde{P}_1}{\partial z^2}+K_1^2\tilde{P}_1=F_{xy}\left[\frac{i\omega^3\delta}{c^4}P_1+\frac{\omega^2}{c_0^2}\left(1-\frac{c_0^2}{c^2}\right)P_1\right], \quad (3.8)$$

And

$$\frac{\partial^2\tilde{P}_2}{\partial z^2}+K_2^2\tilde{P}_2=F_{xy}\left[\frac{i8\omega^3\delta}{c^4}P_2+\frac{\omega^2}{c_0^2}\left(1-\frac{c_0^2}{c^2}\right)P_2-\frac{i2\omega^2\beta}{\rho c^4}P_1^2\right], \quad (3.9)$$

where $\tilde{P}_1(k_x,k_y,z)$ is the wave-vector domain pressure field at the fundamental frequency, $K_1^2=\frac{\omega^2}{c_0^2}-k_x^2-k_y^2$, where c_0 is a constant and is typically chosen as the minimum speed of sound in the medium under study, k_x and k_y are the wavenumbers in the x- and y-dimensions; $\tilde{P}_2(k_x,k_y,z)$ is the wave-vector domain pressure field at the second harmonic frequency, $K_2^2=\frac{4\omega^2}{c_0^2}-k_x^2-k_y^2$, where F_{xy} is the Fourier transform operator in the x- and y-dimensions. One-way propagation solutions to Eq. (3.8) and Eq. (3.9) can be found with the one-dimensional Greens function [223] and they are written as

$$\tilde{P}_1(z)=\tilde{P}_1(0)e^{iK_1 z}+\frac{e^{iK_1 z}}{2iK_1}\int_0^z e^{-iK_1 z'}\left\{F_{xy}\left[\frac{i\omega^3\delta}{c^4}P_1+\frac{\omega^2}{c_0^2}\left(1-\frac{c_0^2}{c^2}\right)P_1\right]\right\}dz', \quad (3.10)$$

And

$$\tilde{P}_2(z) = \tilde{P}_2(0)e^{iK_2 z} + \frac{e^{iK_2 z}}{2iK_2}\int_0^z e^{-iK_2 z'}\left\{F_{xy}\left[\frac{i8\omega^3\delta}{c^4}P_2 + \frac{\omega^2}{c_0^2}\left(1-\frac{c_0^2}{c^2}\right)P_2 - \frac{i2\omega^2\beta}{\rho c^4}P_1^2\right]\right\}dz'. \quad (3.11)$$

Equations Eq. (3.10) and Eq. (3.11) are solved with a Simpson-like scheme [223]. By applying the inverse Fourier transform to $\tilde{P}_1$ and $\tilde{P}_2$, the fundamental and second harmonic frequency pressure P_1 and P_2 can be obtained. This method, therefore, is denoted the FSMDM. Alternatively, the fundamental and second harmonic frequency wave fields can be obtained by applying the temporal Fourier transform to the transient simulation result. This is the TMDM and is described in [223].

3.3.Results

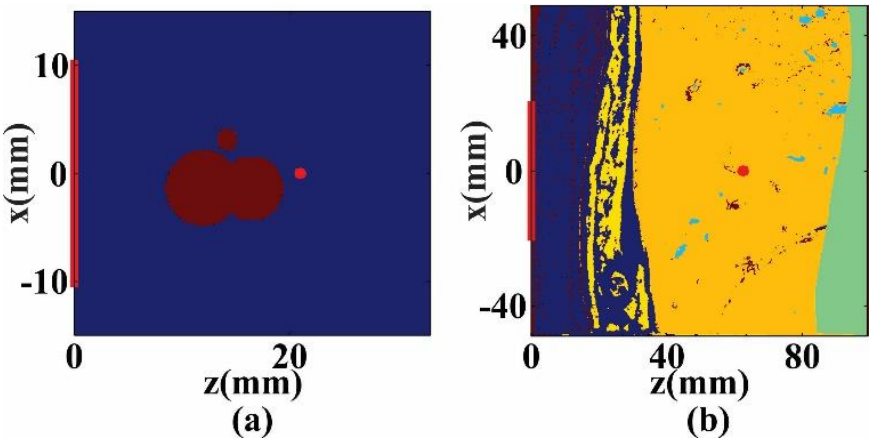

Figure 3.1 (a) *In silico* model used for the first four cases where three cylinders having identical or different acoustical properties from the background medium are considered; (b) a realistic human tissue map with nonlinearity coefficient variation, speed of sound variation, and attenuation coefficient variation. The computational domain shown here are cropped form the original domain for illustration purposes. The superficial layer is connective tissue (red), then is fat (dark blue) with embedded connective tissue (red) and muscle (yellow), followed by liver (orange) and tissue (green). Blood (light blue) is inside the liver. The red line on the left boundary indicates the array position. The red dot is the geometrical focus.

To validate the FSMDM, a case with three cylinders (two of them partially overlap) immersed in water is first studied and the corresponding acoustic medium is shown in Fig. 3.1(a). First, the cylinders are assumed to have the same acoustical properties as the water: speed of sound

is 1500 m/s, density is 1000 kg/m^3, and nonlinearity coefficient is 3.6 for the whole domain. Source plane pressure amplitude is 1 MPa and the frequency is 1 MHz A planar phased array is used to generate a focused ultrasound beam. Transducer diameter and focal length are both 14λ (λ is the wavelength in water and it is 1.5 mm). The transverse dimension of the computational domain is 100λ and the propagation distance is 22λ. The results from the TMDM are used as the benchmark and the accuracy of the TMDM has been confirmed in [223]. In the TMDM, a 40-cycle sine wave is applied as the input signal to mimic a continuous wave. For this and the next three cases involving cylinders, the spatial resolution in both the TMDM and FSMDM is 1/8λ and the temporal resolution in the TMDM is $1/(16f_c)$, where f_c is the fundamental frequency. The temporal domain size is 80 μs in the TMDM. L2 normalized errors are calculated to quantitatively analyze the accuracy of the FSMDM and they are defined as

$$L2 = \frac{\|p_{FSMDM} - p_{benchmark}\|}{\|p_{benchmark}\|}, \tag{3.12}$$

where $\|p\|$ is the L2 norm of the normalized acoustic pressure.

For the first case (homogeneous medium), the fundamental and second harmonic frequency pressure fields simulated by the TMDM and FSMDM are shown in Fig. 3.2. Figure 3.2(e) compares the fundamental and the second harmonic pressure distributions along the white dashed line (across the transducer geometrical focus). Pressures in Figs. 3.2(a)-(d) are normalized by the maximum pressure and pressures in Fig. 3.2(e) are normalized by the maximum fundamental frequency pressure. The agreement between the TMDM and FSMDM is very good. L2 norm errors are calculated with the normalized pressure for the focal region (a 16.5 mm by 3.0 mm rectangle centered around the focus) and they are 0.0044 for the fundamental frequency and 0.0112 for the second harmonics.

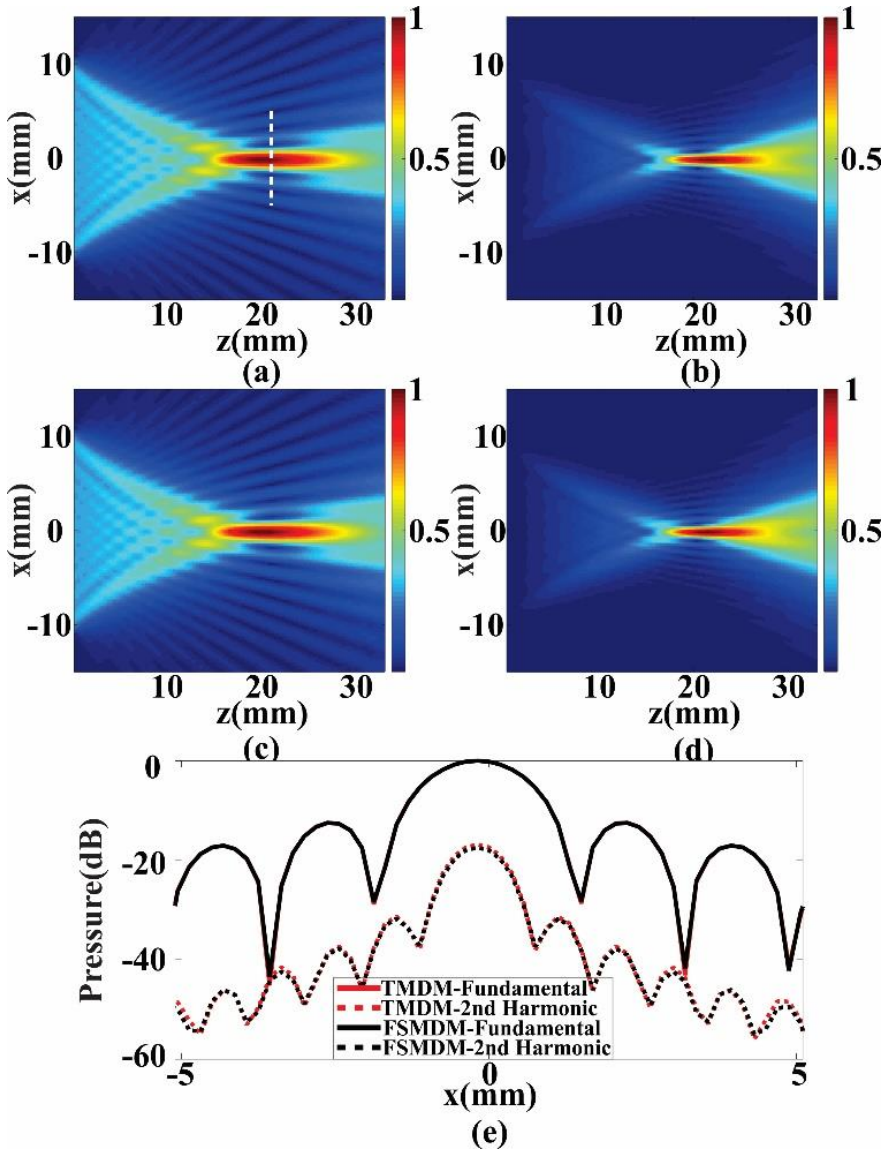

Figure 3.2 Simulation results for the homogeneous medium case. (a) Fundamental frequency field and (b) the second harmonic field simulated by the TMDM. (c) Fundamental frequency field and (d) the second harmonic field simulated by the FSMDM. (e) Comparison for the pressure distribution along the white dashed line simulated by the TMDM and FSMDM.

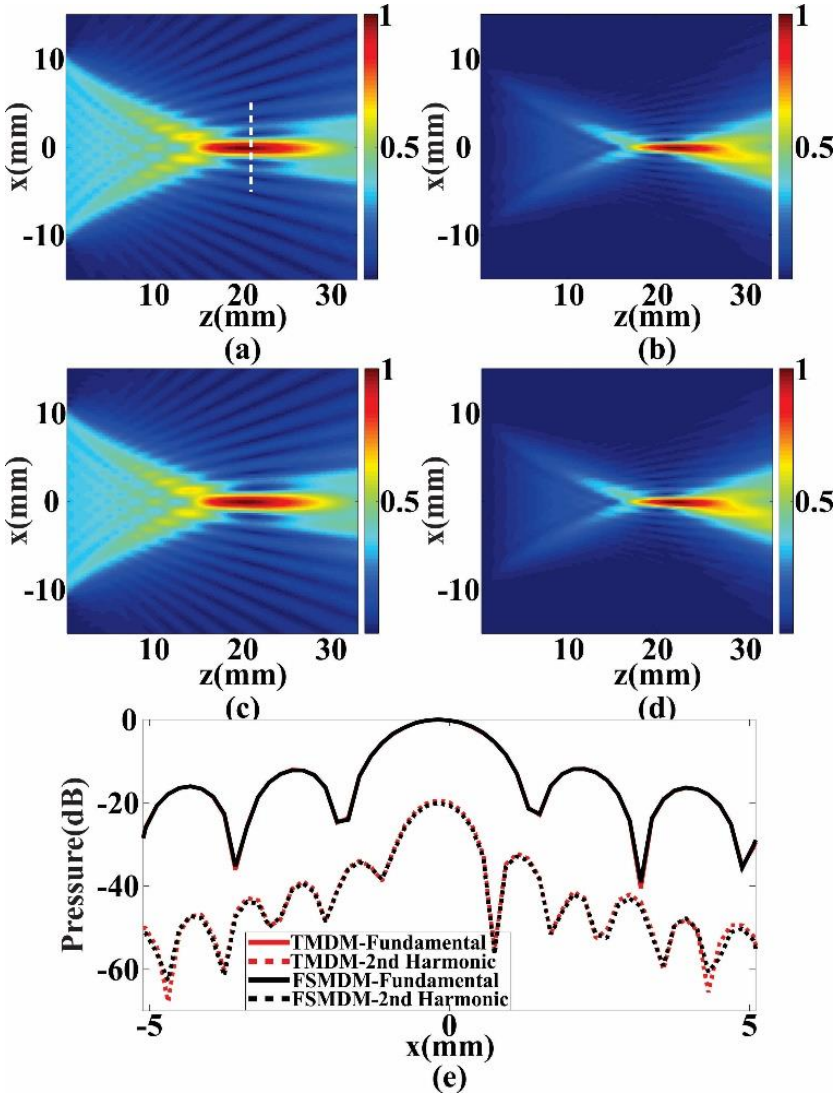

Figure 3.3 Simulation results for the case with heterogeneous attenuation. (a) Fundamental frequency field and (b) the second harmonic field simulated by the TMDM. (c) Fundamental frequency field and (d) the second harmonic field simulated by the FSMDM. (e) Comparisons for the pressure distribution along the white dashed line simulated by the TMDM and FSMDM.

Next, heterogeneous attenuations are added to the nonlinear medium. The attenuation coefficient inside the cylinders is 1.5 $dB \cdot MHz^{-y} \cdot cm^{-1}$ and is 0 outside the cylinders. The power law exponent y is equal to 2. Simulation results for the nonlinear medium with heterogeneous attenuations are plotted in Fig. 3.3. L2 norm errors (calculated for a 16.5 mm by 3.0 mm rectangle

region centered around the focus) are 0.0039 for the fundamental frequency and 0.0107 for the second harmonics.

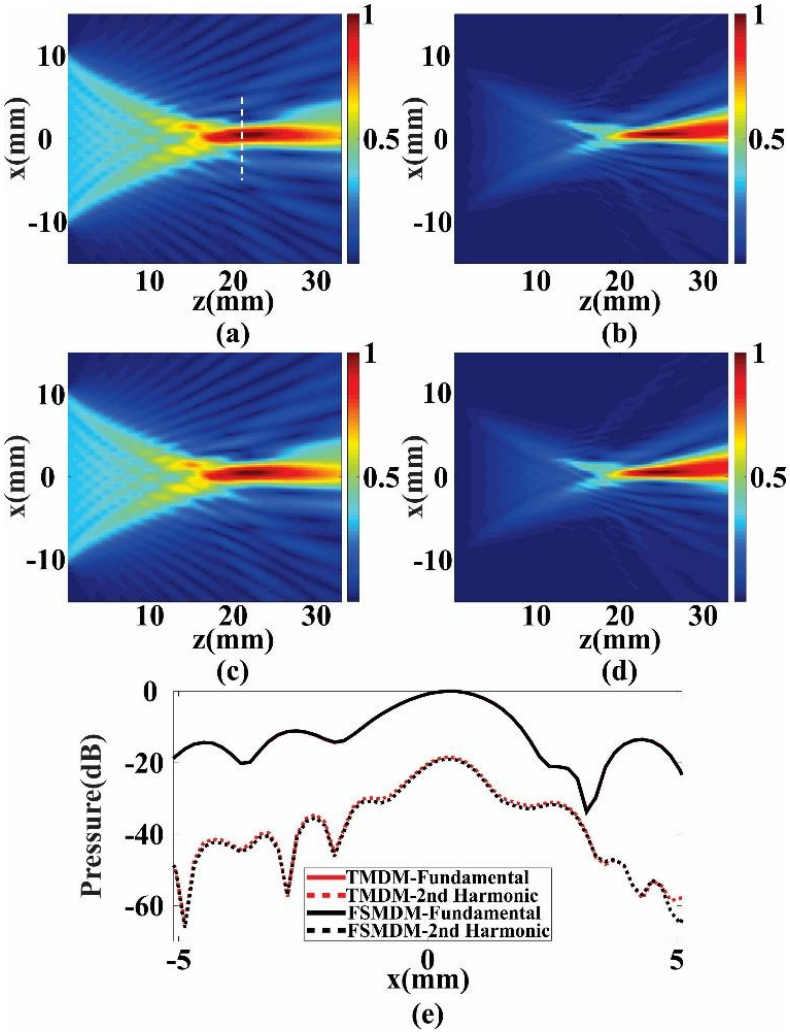

Figure 3.4 Simulation results for the case with heterogeneous speed of sound. (a) Fundamental frequency field and (b) the second harmonic field simulated by the TMDM. (c) Fundamental frequency field and (d) the second harmonic field simulated by the FSMDM. (e) Comparisons for the pressure distribution along the white dashed line simulated by the TMDM and FSMDM.

In the third case, the speed of sound variation is considered. The speed of sound inside the cylinders is 1575 m/s and is 1500 m/s outside the cylinders. Simulation results for this case are shown in Fig. 3.4. Defocusing is visible in this case due to phase aberration. Pressures are again

normalized. L2 norm errors (calculated for a 16.5 mm by 4.3 mm rectangle centered around the focus) are 0.0046 for the fundamental frequency and 0.0145 for the second harmonics.

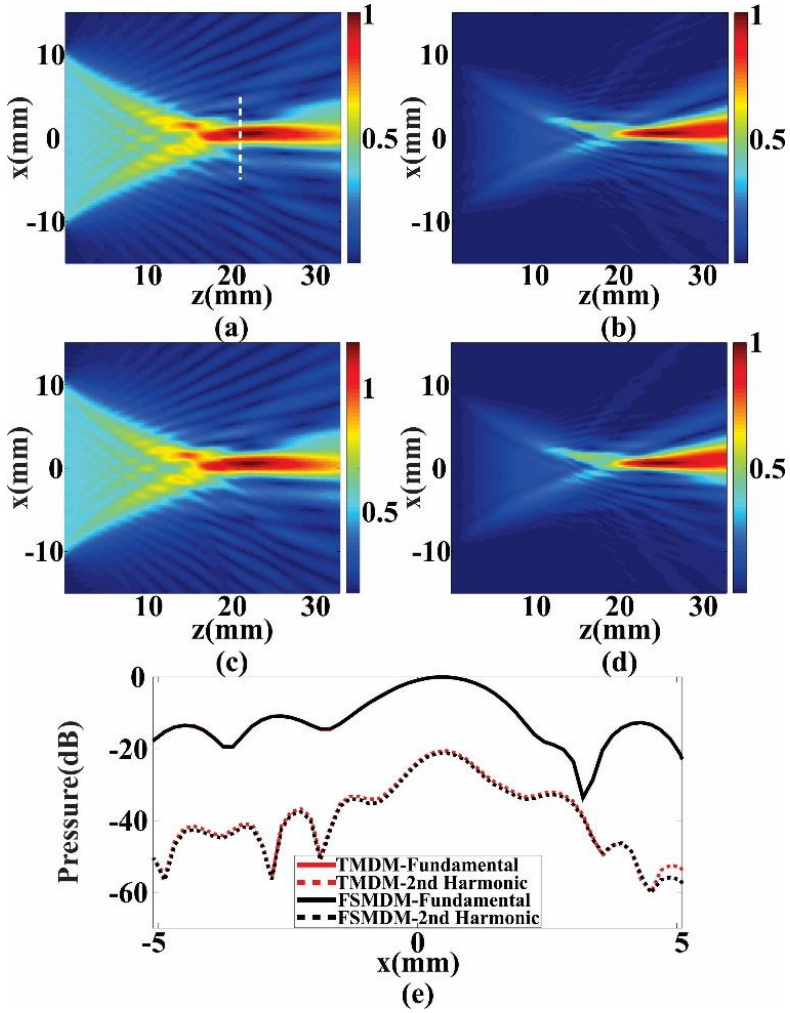

Figure 3.5 Simulation results for the case with heterogeneous attenuation and speed of sound. (a) Fundamental frequency field and (b) the second harmonic field simulated by the TMDM. (c) Fundamental frequency field and (d) the second harmonic field simulated by the FSMDM. (e) Comparisons for the pressure distribution along the white dashed line simulated by the TMDM and FSMDM.

In the fourth case, both speed of sound variation and spatially varying attenuations are included. The attenuation coefficient inside the cylinders is 1.5 $dB \cdot MHz^{-y} \cdot cm^{-1}$ and is 0 outside the cylinders. The power law exponent y is equal to 2. The speed of sound inside the cylinders is 1575

m/s and is 1500 m/s outside the cylinders. Normalized pressure fields simulated by the TMDM and FSMDM are illustrated and compared in Fig. 3.5. L2 norm errors (calculated for a 16.5 mm by 4.3 mm rectangle centered around the focus) are 0.0035 for the fundamental frequency and is 0.0119 for the second harmonics. Overall, these four cases exhibit similar levels of error.

Table 3.1. Acoustical properties of a realistic human tissue map

	Nonlin. Coef.	Speed of sound m/s	Density kg/m3	Atten. Coef. @ 1 MHz (dB/cm)	Power law exponent y
connective	5.0	1613	1120	1.57	1.1
fat	5.8	1478	950	0.48	1.1
muscle	5.5	1547	1050	1.09	1.1
liver	4.3	1595	1060	0.5	1.2
blood	4.05	1584	1060	0.2	2.0
tissue	5.5	1540	1000	0.5	1.1

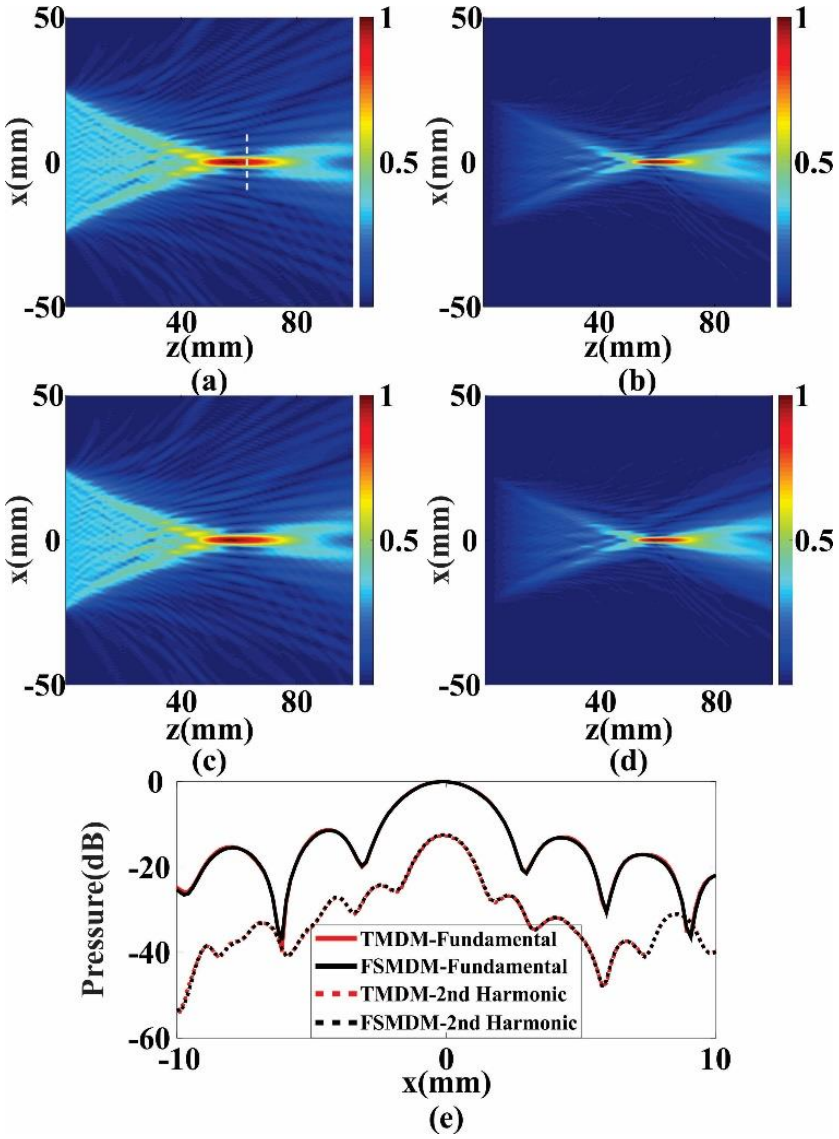

Figure 3.6 Simulation results for the case of a realistic human tissue map. (a) Fundamental frequency field and (b) the second harmonic field simulated by the TMDM. (c) Fundamental frequency field and (d) the second harmonic field simulated by the FSMDM. (e) Comparisons for the pressure distribution along the white dashed line simulated by the TMDM and FSMDM.

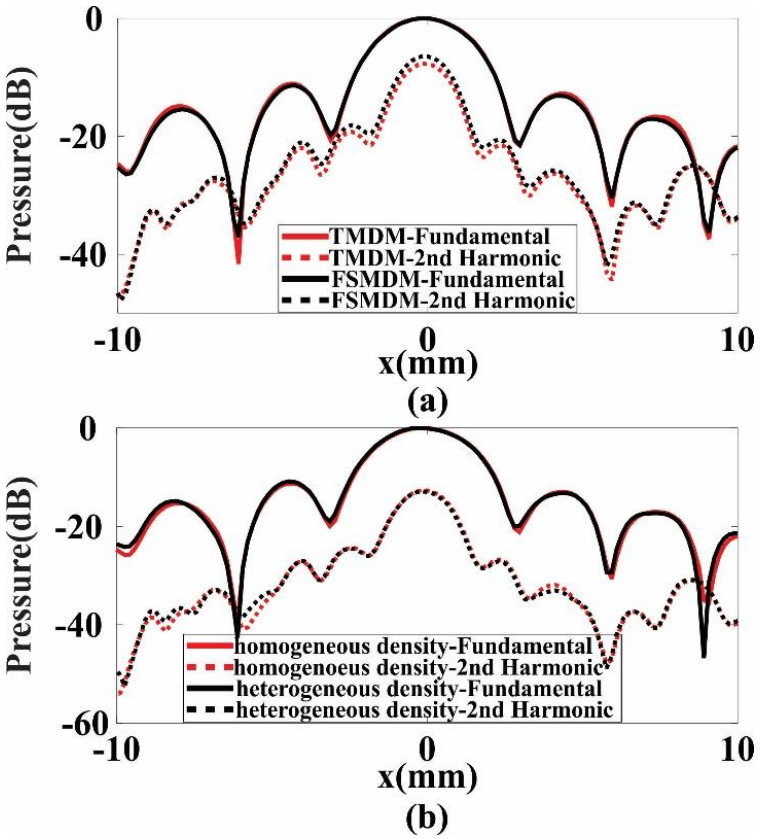

Figure 3.7 (a) Comparison for the pressure distribution along the white dashed line (illustrated in Fig. 3.6(a)) simulated by the TMDM and FSMDM. (b) Comparison for the pressure distribution along the white dashed line (illustrated in Fig. 3.6(a)) simulated by the TMDM with and without density heterogeneities.

To further validate the FSMDM, a realistic human tissue map with spatially varying speed of sound, attenuation, and nonlinearity is studied. The tissue map is illustrated in Fig. 3.1(b) and the acoustical properties for different tissue parts are listed in Table 3.1 [250]. The red line on the left boundary indicates the array position. The red dot is the geometrical focus. The temporal domain size in the TMDM is around 91 μs in this case. The spatial resolution is 0.165 mm and temporal resolution is $1/(16f_c)$. In this case, the fundamental frequency f_c is 0.7 MHz. The Kramers-Kronig dispersion relation is implemented by replacing the speed of sound c with c_p and $c_p = (1/\hat{c} + \alpha_0 \tan(\pi y/2)\hat{\omega}^{y-1})^{-1}$,where $\hat{c}$ is the sound speed at zero frequency [228], and the power

law sound absorption follows $\alpha(\hat{\omega}) = \alpha_0 \hat{\omega}^y$, where α_0 is the absorption in Np·MHz^{-y}·m^{-1}. The fundamental and second harmonic frequency pressure fields simulated by the TMDM and FSMDM are shown in Figs. 3.6(a)-(e). Figure 3.6(e) compares the pressure distributions along the white dashed line (across the transducer geometrical focus). L2 norm errors (calculated for a 24.7 mm by 2.0 mm rectangle centered around the focus) are 0.0114 and 0.0185 for the fundamental frequency and second harmonics, respectively.

3.4.Discussion

The FSMDM is an extension of the TMDM and is capable of modeling weakly nonlinear wave propagation in attenuating media with arbitrary, weak heterogeneities (in terms of the speed of sound [223]). Successive approximations have been made in deriving the equations for the fundamental frequency and second harmonics [23]. As a result, the fundamental frequency pressure is governed by the equation for linear acoustics. Using the quasilinear theory, the second harmonics can be solved by an equation where the fundamental frequency pressure is regarded as a source term on the right-hand side of the equation. In this study, five cases, including a case using a realistic human tissue map, are used to evaluate the accuracy of the FSMDM. Results from the TMDM are used as the benchmark for calculating the errors. From the transverse pressure distribution comparison, it is shown that the FSMDM fundamental frequency pressures are almost identical to those of the TMDM for all cases. The L2 norm errors for the fundamental frequency field in the focal region are small and are on the order of 0.001 for the first four cases. This suggests that it is reasonable to assume that the fundamental frequency field is decoupled from those of harmonics at least for the cases under study, where the second harmonics amplitude is about 20 dB lower than that of the fundamental frequency. On the other hand, the FSMDM and TMDM also produce similar second harmonic ultrasound fields. For example, similar wave field

distortions due to the presence of heterogeneities are observed. Though the L2 norm errors are larger when compared to the fundamental frequency, they are still reasonably small and are on the order of 0.01.

The numerical implementation throughout this study is based on MATLAB 2018a (The MathWorks Inc., Natick, MA) on a 64-bit operating system with a 12-core 3.00-GHz Intel Xeon (R) Gold 6136 CPU (Intel Corp., Santa Clara, CA) processor and 192 GB of RAM. Though TMDM and FSMDM show similar results for the same problem, the FSMDM is computationally superior. For example, to simulate the wave propagation using the human tissue map, the TMDM takes about 481.73 s while the FSMDM is two orders of magnitude faster, needing merely 2.82 s. This is because in the FSMDM, the pressure at the frequencies of interest can be directly obtained without running transient simulations.

The FSMDM suffers from several limitations and intrinsic errors though. The FSMDM uses the similar algorithm as that of the TMDM [223], and the possible sources of errors should also be similar, and they are as follows: 1) the FSMDM is only accurate for media with weakly heterogeneous speed of sound, e.g., soft tissue; 2) the FSMDM is a one-way model and reflections are not included; 3) stair-casing errors [232] occur when representing complex geometries with rectilinear grids; 4) truncation errors introduced by numerical integration [234]; and 5) spatial aliasing errors [72] due to the finite-size computational domain. The spatial aliasing error is possibly more severe for the second harmonics. For most cases above, the L2 norm error for the fundamental frequency is considerably smaller than the second harmonics. This could be attributed to how the second harmonics are calculated in the FSMDM. The spatial aliasing error is first introduced to the fundamental frequency when implementing Eq. (3.10). This error is further carried into the second harmonic field, which contains its own spatial aliasing errors when

implementing Eq. (3.11). To minimize this error, a larger domain should be considered. Alternatively, absorption layers can also be used to reduce the spatial aliasing error [73].

One limitation of the FSMDM is that the governing equations are derived with the quasilinear theory and they are only valid for weakly nonlinear cases [23], [139]. It would be interesting to examine when the quasilinear approximation would be violated. To this end, pressure amplitude can be increased from 1 MPa to 2 MPa within the human tissue map. The transverse pressure distributions are show in Fig. 3.7(a) and the L2 norm errors for the same rectangle region are 0.0216 and 0.0559 for the fundamental frequency and second harmonics, respectively. As expected, the second harmonics calculated by the TMDM is much stronger than the previous case with 1 MPa pressure amplitude. It is now about 8 dB lower than the fundamental frequency. Since the quasilinear approximation fails in this case, the FSMDM is less accurate, indicated by the greater errors. It should also be pointed out that the FSMDM would overestimate the amplitude of the fundamental frequency, since it does not consider the energy transfer from the fundamental frequency to the second harmonics. Though only the second harmonics are studied here, governing equations for higher harmonics can also be derived [251]. Similarly, it is also possible to derive the equation for the difference frequency generated from the interaction of two fundamental frequencies, which is useful for studying problems such as nonlinear coefficient tomography and parametric arrays [23], [252]. All these equations can be subsequently solved by the FSMDM.

Finally, the FSMDM studied here does not consider density heterogeneities, though there is no fundamental barrier to do this. The simplification of considering homogeneous density is made based on the assumption that density heterogeneities have a less important role in affecting the acoustic field, particularly for soft tissue. Figure 3.7(b) compares the transverse pressure

distribution in the human tissue map with and without density heterogeneities using the TMDM. Density values for the tissue map are listed in Table 3.1. Using the results with density heterogeneities as the benchmark, the L2 norm errors in the same focal region are 0.0311 and 0.0287 for the fundamental frequency and second harmonics, respectively. These results suggest that the density variation does not significantly affect the acoustic field in soft tissue and can be neglected.

3.5.Conclusion

The FSMDM is presented and evaluated in this study for the simulation of the second harmonic ultrasound field. The governing equation for the second harmonic is derived using the quasilinear theory. Attenuation, speed of sound, and nonlinear coefficient are all spatially varying functions. The FSMDM is introduced to solve the governing equation for the second harmonics. Five various cases are investigated to validate the FSMDM for weakly nonlinear and weakly heterogeneous media. Simulation results show that the FSMDM and its counterpart (TMDM) give similar results for all five cases. However, the computational speed of the FSMDM is substantially faster than the TMDM. Due to this advantage, the FSMDM could be proven useful for a variety of applications such as HIFU treatment planning and nonlinearity coefficient tomography.

3.6.Acknowledgment

The authors would like to thank Dr. Gianmarco Pinton for providing the human tissue map. This work was supported by the U.S. National Institutes of Health under Grant R01EB025205. Juanjuan Gu was supported by a fellowship from the China Scholarship Council.

CHAPTER 4

MODIFIED MIXED DOMAIN METHOD

The work presented in this chapter is submitted to The Journal of the Acoustical society of America [253]

In this chapter, phase correction and amplitude compensation are introduced to the MDM, which is only accurate for modeling wave propagation in weakly heterogeneous media. Multiple reflections are also incorporated with the one-way model to improve the accuracy. The resulting model is denoted as the modified mixed-domain method (MMDM) and is numerically evaluated for its accuracy and efficiency using two distinct cases: a layered medium and a human skull. It is found that the MMDM is significantly more accurate than the MDM for strongly heterogeneous media, especially when the phase aberrating layer is roughly perpendicular to the acoustic beam. Additionally, convergence study suggests that the second-order reflection is sufficient for wave modeling in lossy biological media. The method developed in this work could be used to facilitate therapeutic ultrasound for treating brain-related diseases and disorders.

4.1.Introduction

Numerical modeling of acoustic wave propagation in heterogeneous media is of great importance for medical ultrasound. In therapeutic ultrasound applications, for example, numerical simulations can be used to study the phase aberration in MR-guided focused ultrasound surgery [254], [187] and to improve the treatment outcome. For diagnostic ultrasound, numerical modeling has been used as an important tool for image reconstruction [178], [186], [255] as well as to understand the sources of image degradation in ultrasound imaging [20].

A myriad of wave propagation algorithms that take medium heterogeneities into account have been developed. A vast majority of these algorithms operate in the time-domain. Treeby *et al.* [49] developed the KSTD using the coupled nonlinear wave equation. Jing *et al.* [8] alternatively developed the KSTD from the Westervelt equation. Pinton *et al.* [9] studied a heterogeneous nonlinear attenuating full-wave model based on the FDTD method. Frequency-domain methods have also been investigated. For example, Clement and Hynynen [66] combined the ASA with ray theory to describe the propagation of ultrasound through randomly oriented, dissipative, layered media. Vyas and Christensen [84] modified the conventional ASA method to model linear wave propagation in inhomogeneous media. Most recently, the MDM for modeling linear/nonlinear wave propagation in dissipative, weakly heterogeneous media has been presented [223], [29].

Although there are many existing ultrasound numerical models, none can currently achieve efficient yet sufficiently accurate simulations for linear/nonlinear acoustic wave propagation in large-scale, strongly heterogeneous media. Driven by this motivation, this chapter aims to establish and validate an accuracy-efficiency balanced numerical model for simulating acoustic wave propagation in strongly heterogeneous media. Within the realm of biomedical ultrasound, this model is particularly pertinent to transcranial ultrasound, and could therefore facilitate research on HIFU for treating brain-related diseases [256], [3] as well as research on ultrasound-mediated neuromodulation [257]. This numerical model is a non-trivial extension to the previously developed MDM [223], which is a one-way model and is only accurate for weakly heterogeneous media. To extend the original MDM to modeling wave propagation in strongly heterogeneous media, phase and amplitude corrections are proposed and evaluated in this chapter. The phase correction term is first theoretically derived. As the transmission coefficient due to the variation

of sound speed is not considered in the original MDM, an amplitude compensation term is also proposed. Reflections are added to the one-way model to further improve the accuracy. The resulting method is denoted the modified mixed domain method (MMDM). Both a two-dimensional (2D) layered medium and a 2D human skull are studied to evaluate the accuracy of the MMDM. Results from the MATLAB toolbox k-Wave [199] are used as the benchmark for comparison and validation purposes. This study shows that the MMDM can markedly improve the results for strongly heterogeneous media in terms of the predicted waveform phase and amplitude, provided that the phase aberrating layer is more or less perpendicular to the ultrasound beam. While the addition of reflections can improve the accuracy of the model, it is also found that up to the second-order reflection could be sufficient for obtaining converged results when sound absorption is considered, i.e., higher order reflections do not significantly improve the result.

4.2.Theories

4.2.1. Governing Equation

We start from the generalized Westervelt equation [1] and it reads

$$\rho\nabla\cdot\left(\frac{1}{\rho}\nabla p\right)-\frac{1}{c^2}\frac{\partial^2 p}{\partial t^2}+\frac{\delta}{c^4}\frac{\partial^3 p}{\partial t^3}+\frac{\beta}{\rho c^4}\frac{\partial^2 p^2}{\partial t^2}=0, \tag{4.1}$$

where p is the acoustic pressure, ρ is the ambient density, c is the speed of sound, δ is the sound diffusivity, $\delta = 2\alpha_{NP}c^3/\omega\text{^}2$ (α_{NP} is the attenuation coefficient in Np/m and ω is the angular frequency), and β is the nonlinearity coefficient. In the original MDM, Eq. (4.1) would be first transformed by applying the normalized wave field $f = p/\sqrt{\rho}$ and the equation yields [223]

$$\nabla^2 f-\frac{1}{c^2}\frac{\partial^2 f}{\partial t^2}-f\sqrt{\rho}\nabla^2\frac{1}{\sqrt{\rho}}+\frac{\delta}{c^4}\frac{\partial^3 f}{\partial t^3}+\frac{\beta}{\sqrt{\rho}c^4}\frac{\partial^2 f^2}{\partial t^2}=0, \tag{4.2}$$

The effect of density heterogeneities is taken into account by the term $\sqrt{\rho}\nabla^2\frac{1}{\sqrt{\rho}}$. In the event that the density distribution is not sufficiently smooth, which could be the case for heterogeneous

media, the Laplacian term $\nabla^2 \frac{1}{\sqrt{\rho}}$ will lead to a δ-like function [258]. While this was not identified as a major issue for weakly heterogeneous media [223], it could render the algorithm unstable for strongly heterogeneous cases. A previous paper also discussed the adverse effect of this Laplacian term in the context of the KSTD method [101]. Consequently, the density is first assumed to be homogeneous in the governing equation. The density heterogeneity effect will be later considered via an amplitude correction term proposed in the section 4.23. To reduce the spatial aliasing error, an absorption boundary layer is added by introducing a frequency-independent absorption term $\gamma \frac{\partial p}{\partial t}$ to the governing equation [73], where $\gamma = \gamma_{max}/\cosh^2(\alpha n)$ (γ_{max} is a constant, α is a decay factor, and n denotes the distance in number of grid points from the boundary). Thus, the modified governing equation reads

$$\nabla^2 p - \frac{1}{c^2}\frac{\partial^2 p}{\partial t^2} + \frac{\delta}{c^4}\frac{\partial^3 p}{\partial t^3} + \frac{\beta}{\rho c^4}\frac{\partial^2 p^2}{\partial t^2} = \gamma \frac{\partial p}{\partial t}. \tag{4.3}$$

By performing the Fourier transform to Eq. (4.3) with respect to *x*, *y* and *t*, we have

$$\frac{\partial^2}{\partial z^2}\tilde{P} + K^2\tilde{P} = F_{xy}\left\{\left[-\frac{\omega^2}{c_0^2}\left(\frac{c_0^2}{c^2} - 1\right) + \frac{i\delta\omega^3}{c^4} + i\omega\gamma\right]F_t(p)\right\} + F_{xy}\left(\frac{\beta\omega^2}{\rho c^4}F_t(p^2)\right), \tag{4.4}$$

where $\tilde{P}$ is the Fourier transform of p, F_{xy} is the Fourier transform operator in *x*- and *y*-dimensions, F_t is the Fourier transform in the time domain, c_0 is the background sound speed and $K^2 = \omega^2/c_0^2 - k_x^2 - k_y^2$, with k_x and k_y being the wave-numbers in *x*- and *y*- dimensions. An implicit solution to Eq. (4.4) can be derived from the 1-D Green's function in an integral form [12], such that

$$\tilde{P}(z) = \tilde{P}(0)e^{iKz} + \frac{e^{iKz}}{2iK}\int_0^z e^{-iKz'}M(p(z'))dz', \tag{4.5}$$

where

$$M(p) = F_{xy}\left\{\left[-\frac{\omega^2}{c_0^2}\left(\frac{c_0^2}{c^2} - 1\right) + \frac{i\delta\omega^3}{c^4} + i\omega\gamma\right]F_t(p)\right\} + F_{xy}\left(\frac{\beta\omega^2}{\rho c^4}F_t(p^2)\right). \tag{4.6}$$

Equation (4.5) can be solved by using a Simpson-like rule [129]. In this model, wave effects such as diffraction, attenuation, dispersion and nonlinearity are all considered. Additionally, density, speed of sound, attenuation coefficient, power law exponent and nonlinear coefficient can all be spatially varying functions. The Kramers-Kronig dispersion relation is applied by directly replacing the speed of sound c with c_p and $c_p = (1/\hat{c} + \alpha_0 \tan(\pi y/2)\, \omega^{y-1})^{-1}$ [12],where $\hat{c}$ is the sound speed at zero frequency, y is the power law exponent, α_0 is the absorption in Np·MHz^{-y}·m^{-1}. This model, however, is only accurate for media with weak speed of sound contrast. As shown by our previous study [223], this model is a one-way model; it does not consider the transmission coefficient associated with the speed of sound variation. There is also an intrinsic error when computing the phase of the advancing wavefront, which grows as the speed of sound contrast increases [223]. To have a more general model that could be applied to strongly heterogeneous media, phase correction and transmission compensation will be introduced. Multiple reflections are also proposed to complement the model.

4.2.2. Phase Correction

Considering a 1D inhomogeneous medium with a speed of sound variation that is

$$\mathrm{c} = \begin{cases} c_0, when\ z \le z_0 \\ c_1, when\ z > z_0 \end{cases} \tag{4.7}$$

The analytical solution of the pressure at $\mathrm{z} + \Delta\mathrm{z}$ ($\mathrm{z} = \mathrm{z}_0$) without considering the transmission coefficient (only consider the phase change) is

$$(P_{z+\Delta z})_{analytical} = P_z e^{iK'\Delta z}, \tag{4.8}$$

where K' is the wave number and $K' = \omega/c_2$, P_z is the wave pressure at z with a frequency of ω. The original MDM solution, on the other hand, is described as [223]

$$(P_{z+\Delta z})_{MDM} = P_z e^{iK\Delta z} + \frac{e^{iK\Delta z}}{2iK} \int_0^{\Delta z} e^{-iKz'}(M) P(z')\, dz', \tag{4.9}$$

For 1D wave propagation, $K = \omega/c_0$ and $M = -\frac{\omega^2}{c_0^2}\left(\frac{c_0^2}{c^2} - 1\right)$. In this case, $c_0 = c_1$. It has been rigorously proven that this solution is only valid for weakly heterogeneous media [223]. To solve the integral equation in the form of $y(t_{n+1}) = y(t_n) + \int_{t_n}^{t_{n+1}} f(s, y(s))ds$, the Trapezoidal rule is applied and it yields

$$y_{n+1} = y_n + \frac{\Delta z}{2}[f(t_n, y_n) + f(t_{n+1}, y_{n+1})]. \tag{4.10}$$

Applying this to Eq. (4.9) yields

$$(P_{z+\Delta z})_{MDM} = P_z e^{iK\Delta z} + \frac{e^{iK\Delta z}}{2iK}\frac{\Delta z}{2}\left[M_z P_z + M_{z+\Delta z} P_{z+\Delta z} e^{-iK\Delta z}\right]. \tag{4.11}$$

By rearranging Eq. (4.11), we have

$$(P_{z+\Delta z})_{MDM} = \frac{P_z e^{iK\Delta z} + \frac{e^{iK\Delta z}}{4iK} M_z P_z \Delta z}{1 - \frac{M_{z+\Delta z}}{4iK}\Delta z}. \tag{4.12}$$

To examine the exact phase error in the MDM, Eq. (4.12) is subtracted from Eq. (4.8). Rearranging the resulting equation, the following equation is arrived at, which yields

$$(P_{z+\Delta z})_{analytical} = (P_{z+\Delta z})_{MDM} + P_z e^{iK'\Delta z}\left(1 - e^{i(K-K')\Delta z}\frac{1 + \frac{M_z}{4iK}\Delta z}{1 - \frac{M_{z+\Delta z}}{4iK}\Delta z}\right). \tag{4.13}$$

$P_z e^{iK'\Delta z}\left(1 - e^{i(K-K')\Delta z}\frac{1 + \frac{M_z}{4iK}\Delta z}{1 - \frac{M_{z+\Delta z}}{4iK}\Delta z}\right)$ is therefore the phase correction term. Although this correction is derived based on the 1D assumption, it can be applied to more general cases with sufficient accuracy as will be shown in this chapter.

4.2.3. Amplitude Compensation

The transmission coefficient due to the variation of sound speed is not considered in the original MDM, which can be a significant source of error for simulations involving a large speed of sound contrast. Although the MDM could consider the transmission coefficient due to the variation of density, as mentioned earlier, the density heterogeneity term could introduce a

singularity and render the algorithm unstable. Therefore, an amplitude compensation is introduced for addressing the density and speed of sound heterogeneities. The compensation term reads (similar to what was used in reference 83)

$$T(x,y,z) = \frac{2\rho(x,y,z+\Delta z)c(x,y,z+\Delta z)}{\rho(x,y,z)c(x,y,z)+\rho(x,y,z+\Delta z)c(x,y,z+\Delta z)}, \tag{4.14}$$

where $c(x,y,z)$ and $\rho(x,y,z)$ are the speed of sound and density at plane z, respectively; $c(x,y,z+\Delta z)$ and $\rho(x,y,z+\Delta z)$ are the speed of sound and density at plane $z+\Delta z$, respectively. Similar to Eq. (4.13), Eq. (4.14) is only exact for 1D cases [230]. To implement the phase and amplitude corrections, the second term on the right hand side of Eq. (4.13) is added to $\tilde{P}(z)$ in Eq. (4.5) during the iteration. After applying the inverse Fourier transform to $\tilde{P}(z)$, the amplitude is then corrected by multiplying $T(x,y,z)$.

4.2.4. Multiple Reflections

Reflections can be further added in the MMDM by using the following equation [230]

$$P_{reflection} = P_{incident}(T-1), \tag{4.15}$$

where $P_{incident}$ is the incident wave used for calculating the reflected wave. For example, when calculating the first-order reflection, $P_{incident}$ is the transmissive waveform at each plane, i.e., the result of the one-way MMDM. The corresponding $P_{refleciton}$ is first calculated for each layer by Eq. (4.15) and stored during the forward projection step. Subsequently, the entire first-order reflection field can be computed by considering $P_{reflection}$ as the boundary condition and having it propagate in the backward direction. When calculating the second-order reflection, $P_{incident}$ is given by the first-order reflection wave field. By propagating the resulting $P_{reflection}$ in the forward direction, the second-order reflection field can be formed. This procedure continues until the desired maximum order of reflection is reached. In general, an even-order reflection is associated with forward propagation while an odd-order reflection travels in the backward direction. The final wave

field can be obtained by superposing all solutions. It is noted that, again, Eq. (4.15) is only exact for 1D wave propagation, which is consistent with the assumption underpinning Eqs. (4.13) and (4.14). A flowchart illustrating how the corrections and reflections are implemented in the MMDM can be found in Fig. 4.1.

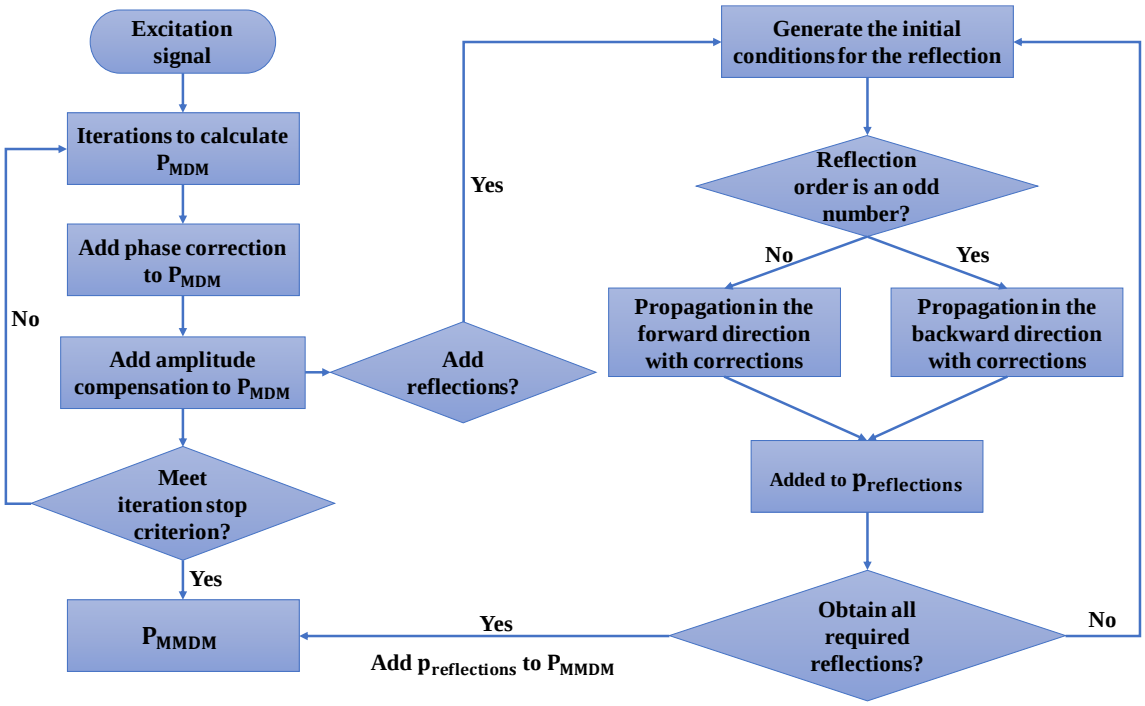

Figure. 4.1 A flowchart illustrates the scheme to add corrections and reflections to the MDM. At each iteration step, both the phase correction and amplitude compensation are added to the MDM result. For each propagation, the reflected wave field on each plane is calculated and stored. These wave fields then propagate with both phase and amplitude corrections in the forward/backward direction. The total pressure field is finally obtained by superposing the transmission and reflection wave fields.

4.3.Simulations Results

Two representative cases are first studied to evaluate the accuracy of the MMDM. In all cases, focused ultrasound beams are used and are generated with a planar phased array. For transient simulations, a Gaussian-modulated pulse is used and is expressed in Eq. (2.13). Benchmark results

are obtained by the MATLAB toolbox k-Wave [199]. Both spatial and temporal resolutions used in the benchmark simulations are sufficiently fine in order to obtain well-converged results. L2-norm errors are calculated to quantitatively analyze the accuracy of the MMDM and this error is defined in Eq. (3.12).

A layered medium shown in Fig. 4.2 (a) is first studied. In the blue region, the speed of sound is 1500 m/s and density is 1000 kg/m^3; in the red region, the speed of sound is 3000 m/s and density is 2000 kg/m^3, indicating a contrast of 2.0 for both acoustical properties. The transducer focal length is 68.6 mm and the transducer diameter is 34.3 mm, corresponding to an *F* number of 2.0. The transducer center frequency is 0.7 MHz and the pressure magnitude of the excitation p_0 is 1 Pa. The absorption layer is enabled to minimize the spatial aliasing error. For the transient simulation, γ_{max} is 0.6 and α is 0.05. For the benchmark simulation using k-Wave, the spatial step size is 1/16 λ. The time step size *dt* is 0.0022 μs, corresponding to a CFL number of 0.05.

For the MDM and MMDM simulations, the spatial step size in the *x* direction is 1/4 λ and it is 1/16 λ in the *y* direction (propagation direction). The time step size *dt* is 0.1786 μs. Additional simulations show that smaller dt does not significantly affect the result once the Nyquist sampling rate is well satisfied. Waveforms recorded at the transducer focus simulated with different methods are shown and compared in Fig. 4.2(b). The L2-norm error is 1.3689 for the simulation with MDM and is 0.0585 for the simulation with MMDM incorporating up to the fourth-order reflection (denoted as MMDM4; MMDMn stands for the MMDM incorporating up to the nth-order reflection). When the nonlinear effect is considered, the pressure magnitude is increased from 1 Pa to 1 MPa. The nonlinearity coefficient for the whole domain is 3.6. The time-domain and frequency-domain results at the focal point are plotted in Figs. 4.2(c)-(d). The L2-norm error is 1.3825 for MDM and is 0.0639 for MMDM4. In both linear and nonlinear cases, the error is reduced by

almost a factor of 20. In both Figs. 4.2(b) and 4.2(d), even-order reflections can be observed in the MMDM and k-Wave results, as anticipated.

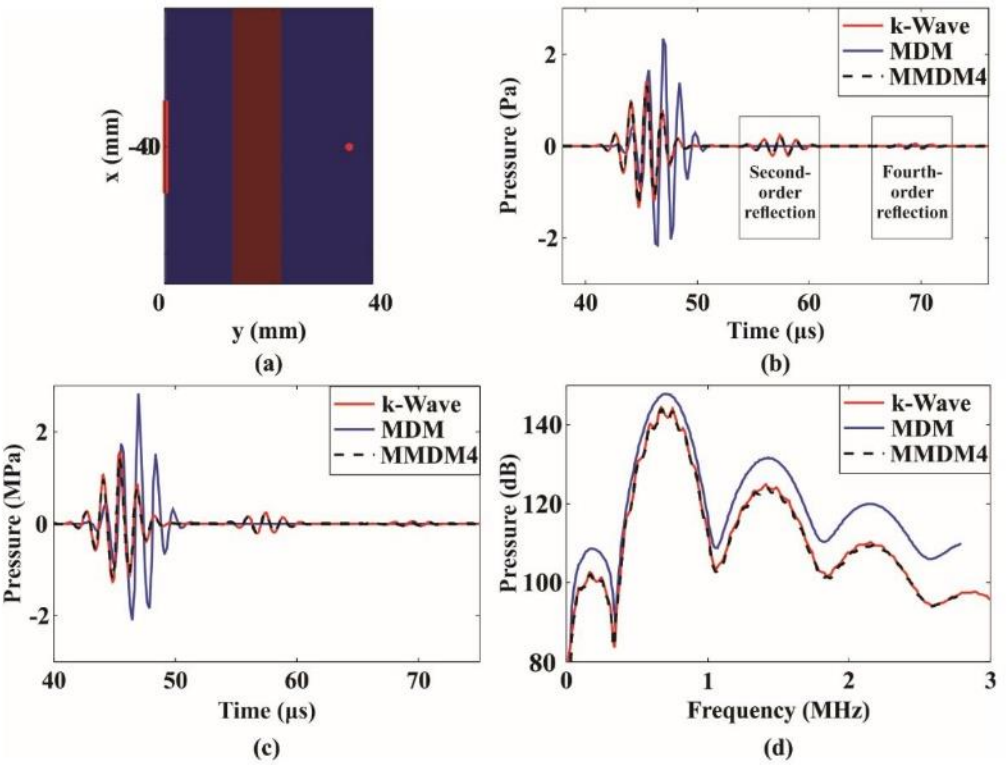

Figure. 4.2 (a) A 2D layered medium. The red line indicates the position of the phased array transducer and the red dot indicates the position of the transducer focus. (b) Waveforms recorded at the geometrical focus of the transducer. The results simulated by k-Wave, MDM and MMDM4 are compared when the medium is linear. (c) Time-domain and (d) frequency domain results at the geometrical focus of the transducer. The results simulated by k-Wave, MDM and MMDM4 are compared when the nonlinear effect is considered.

A 2D human skull is then studied to further validate the MMDM and the *in silico* model is shown in Fig. 4.3(a). The speed of sound is between 1500 m/s and 2816.1 m/s; the density is between 1000 kg/m^3 and 2588 kg/m^3. The transducer focal length is 58.6 mm and its diameter is 39.3 mm, corresponding to an F number of 1.5. The transducer center frequency is 0.7 MHz and the pressure amplitude is 1 Pa. The spatial step size in the x and y directions are both 0.1953 mm

for all simulations. The time step size in k-Wave is 0.0022 μs while it is 0.1786 μs in the MDM and MMDM. The medium is considered to be lossless. The effect of acoustic absorption will be addressed in the discussion section. We first compare the waveforms recorded at the focus of the transducer, which are plotted in Fig. 4.3 (b). The L2-norm error is 1.0721 for MDM and is 0.1128 for MMDM4. In contrast to the previous case, the even order reflections are not visible in this case as they are mixed with the primary transmissive (0^{th} order) wave. The nonlinear effect is subsequently considered. The nonlinearity coefficient is 3.6 throughout the entire domain, though in principle it can be inhomogeneous in the MDM/MMDM. The pressure magnitude is increased to 1 MPa to enhance the nonlinear effect. The time-domain and frequency-domain results at the focal point of the transducer are shown in Figs. 4.3(c)-(d). The L2-norm error is 1.0976 for MDM and is 0.1280 for MMDM4. In this case, the error is reduced by a factor of almost 10 for both linear and nonlinear simluations.

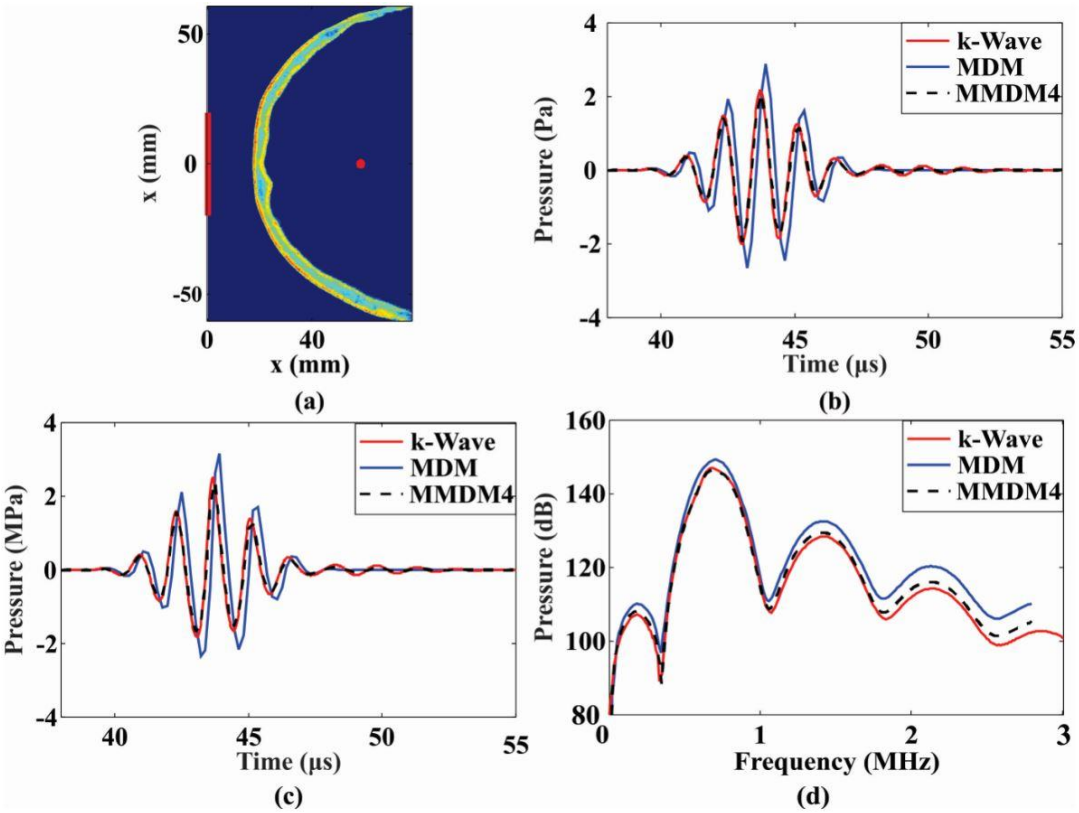

Figure. 4.3 (a) A 2D skull model. The red line on the left indicates the array position and the red dot is the geometrical focus. (b) Waveforms recorded at the geometrical focus of the transducer. The results simulated by k-Wave, MDM and MMDM4 are compared when the medium is linear. (c) Time-domain and (d) frequency domain results at the geometrical focus of the transducer. The results simulated by k-Wave, MDM and MMDM4 are compared when the nonlinear effect is considered.

The MMDM is also capable of directly modeling the acoustic field at the frequency of interest [229] since this method is intrinsically a frequency-domain method. It is shown that, compared to transient simulations, where the acoustic field of a certain frequency needs to be acquired by Fourier transform, directly operating the MDM/MMDM at the frequency of interest can be orders of magnitude more computationally efficient. This, however, has only been demonstrated for linear and weakly nonlinear cases, where the couplings between the fundamental

frequency and the harmonics are minimal [229]. In this study, linear wave propagation is assumed and the excitation signal in k-Wave is a continuous sinusoidal wave centered at 0.7 MHz. For MDM/MMDM, the absorption layer is enabled where γ_{max} is chosen as 0.5 and α is 0.03. Four sets of results, obtained by k-Wave, MDM, MMDM and MMDM4, are plotted in Figs. 4.4(a)-(d). For the region shown in Figs. 4(a)-(d) (approximately 80 mm by 80 mm), the L2-norm error is 0.3391 for MDM, 0.2863 for MMDM, and 0.1764 for MMDM4, respectively. Axial pressure distributions along $x = 0$ are also compared in Fig. 4.4(e) between different models.

4.4.Discussion

We have investigated the accuracy of the MMDM for modeling linear/nonlinear wave propagation in strongly heterogeneous media. It is found that with the phase correction, amplitude compensation, as well as the addition of reflections, the MMDM is significantly more accurate than the original MDM for the two cases tested in this study.

Some deviations in terms of the pressure amplitude between the MMDM and k-Wave results can be observed in the skull case. This is likely due to the fact that the amplitude compensation introduced in the MMDM is based on the 1D assumption, though there is also the possibility that k-Wave results are less accurate for a complicated structure like the skull [232]. This could also explain why the amplitude deviation is less visible in the layered medium case, as the layer has a more regular shape and therefore the 1D assumption is more applicable and k-Wave results are also potentially more accurate in this case. To confirm this, we investigate a case where the layer is tilted at an angle of 11° instead of being normal to the beam direction (Fig. 4.5(a)). The density and speed of sound contrast are kept at 2.0. The time domain waveforms recorded at the focal point of the transducer are compared in Fig. 4.5(b). The L2-norm error is 1.0132 for MDM and is 0.4101 for MMDM4. In this case, larger amplitude differences are observed, while the phase

correction still seems to be robust although the 1D assumption breaks down in this case. Another scenario where the 1D assumption could break down is when the wave field is strongly diverging (e.g., a spherical or cylindrical wave). This, however, is less relevant to therapeutic ultrasound and therefore is not discussed here.

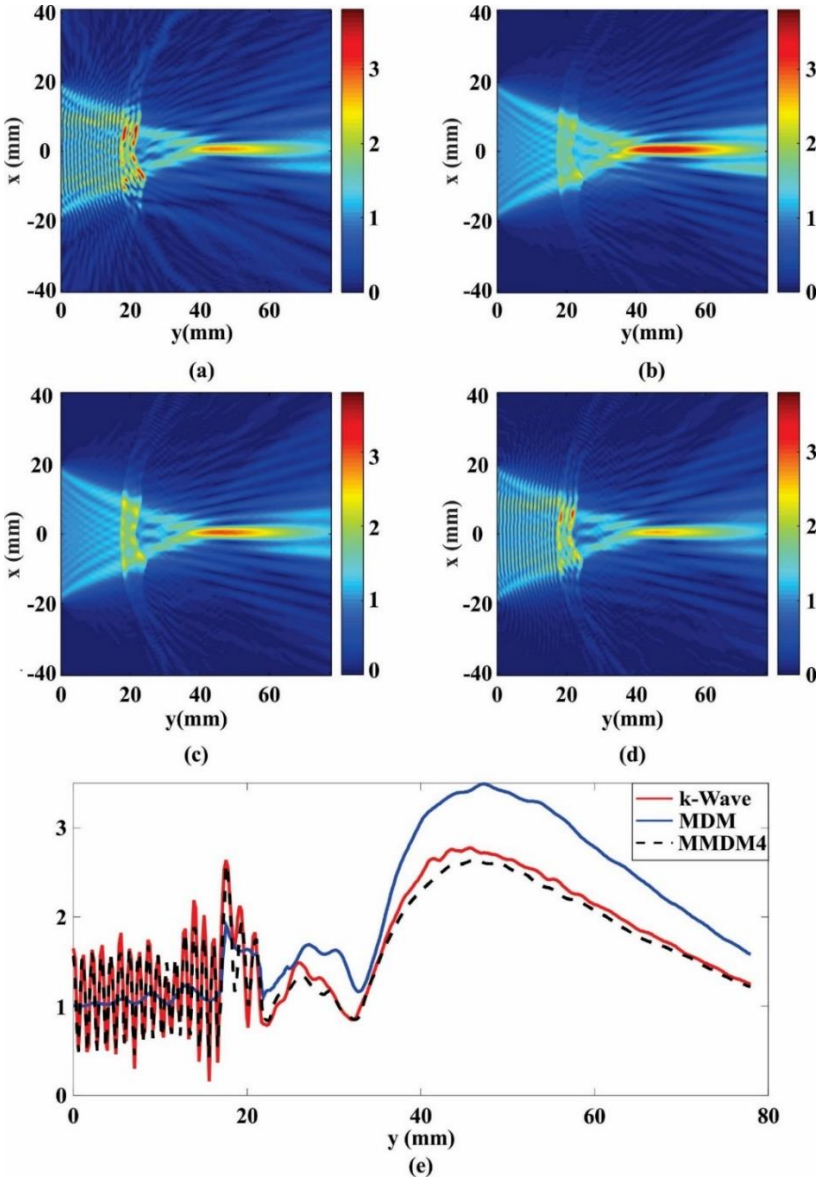

Figure. 4.4 Spatial pressure distributions for the skull case simulated with (a) k-Wave, (b) MDM, (c) MMDM and (d) MMDM4. (e) Comparison for the axial pressure distribution along x=0.

Multiple reflections have been studied as a means to improve the model. Figure 4.2(b), for example, suggests that the second-order and fourth-order reflections can be accurately modeled. Figure 4.4 compares the spatial pressure distribution for the skull case, simulated with k-Wave, MDM, MMDM and MMDM4. When reflections are included in the simulation, the accuracy is clearly improved. For example, the focal size can be more precisely predicted; the interference pattern due to waves traveling in opposite directions can be now captured.

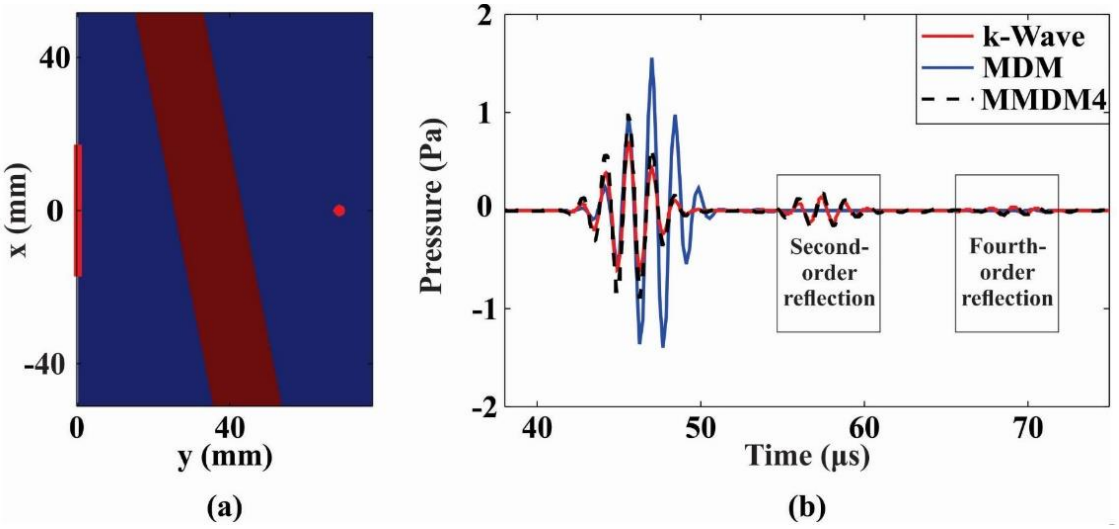

Figure. 4.5 (a) A 2D oblique-layered media. The red line indicates the position of the phased array transducer and the red dot indicates the position of the transducer focus. (b) Comparison of the waveforms at the geometrical focus of the transducer simulated with k-Wave, MDM and MMDM4.

The numerical implementation throughout this study is based on MATLAB 2018a (The MathWorks Inc., Natick, MA) on a 64-bit operating system with a 12-core 3.00-GHz Intel Xeon (R) Gold 6136 CPU (Intel Corp., Santa Clara, CA) processor and 192 GB of RAM. To simulate transient wave propagation using the 2D skull, the MMDM takes about 85 seconds and the MMDM4 takes about 345 seconds, given a computational domain that is about 120 mm by 80 mm. For generating the results shown in Fig. 4.4, however, the MMDM only takes about 1.60 seconds

and the MMDM4 takes about 5.7 seconds. Though the MMDM is computationally efficient, the computation time inevitably increases when high-order reflections are considered. Thus, it is necessary to conduct a convergence study on multiple reflections: how many reflections are necessary for achieving satisfactory results? To this end, we first examine the steady state results for the skull model with the MMDM. The L2-norm errors are calculated using MMDM50 result as the benchmark solution and the errors are plotted in Fig. 4.7. The result is considered converged when the L2-norm error is less than 0.02. It can be seen that the result is indeed converging, indicating a less significant role of higher-order reflections. The fourth-order reflection seems to be sufficient for the lossless skull simulation to attain converged results. For a more realistic simulation, absorption, which can be deduced by the density [189], is added to the skull. The absorption coefficient varies from 0.005 $\mathrm{dB}\cdot\mathrm{MHz}^{-y}\mathrm{cm}^{-1}$ to 23.45 $\mathrm{dB}\cdot\mathrm{MHz}^{-y}\mathrm{cm}^{-1}$. The power law exponent is assumed to be 2.0 in this case, as there is no well-established data on the power law exponent for skulls. The result is seen to converge faster with the consideration of absorption, and in this case, the second-order reflection is sufficient for results to converge. The results of k-Wave are not provided for the lossy skull case since k-Wave is less accurate when large absorption values are considered [259].

Two additional questions naturally arise: is it necessary to apply the corrections for soft tissue where the heterogeneities are relatively weak? Is it necessary to consider multiple reflections in soft tissue? To answer this question, a tissue map is considered as illustrated in Fig. 4.6 (a). The acoustical properties for different tissue parts are listed in Table 3.1. The excitation pressure magnitude is 1 Pa and the center frequency is 0.7 MHz. The transducer focal length is 49.5 mm and its diameter is 33.2 mm, corresponding to an *F* number of 1.5. The lossless case is first considered. The 2D pressure distributions obtained by k-Wave, MDM, and MDM2 are shown in Figs. 4.6(b)-

(d). The axial pressure distributions along x=0 are shown in Fig. 4.6 (e) for k-Wave, MDM, MMDM, and MDM2, respectively. The L2-norm error calculated using the whole domain is 0.1478 for the MDM and is 0.1444 for the MMDM (the 2D pressure distribution calculated by the MMDM is not shown in this chapter). Thus, the corrections in phase and amplitude do not significantly improve the MDM in this case. The L2-norm error, on the other hand, is 0.1182 for the MDM2, indicating that in this case the inclusion of reflections is in fact more important than the correction. While these results suggest that it may not be necessary to apply corrections or even reflections to the MDM for soft tissue, this conclusion should be further examined for problems involving considerably larger computational domains, since the phase and amplitude errors grow along the wave propagation direction in the MDM. The convergence study for the lossless soft tissue and lossy soft tissue are also carried out and the results are shown in Fig. 4.7 with the MMDM50 results as the benchmark. It can be concluded that in this soft tissue case, up to the second-order reflection could be sufficient to obtain converged results (L2-norm errors being smaller than 0.02).

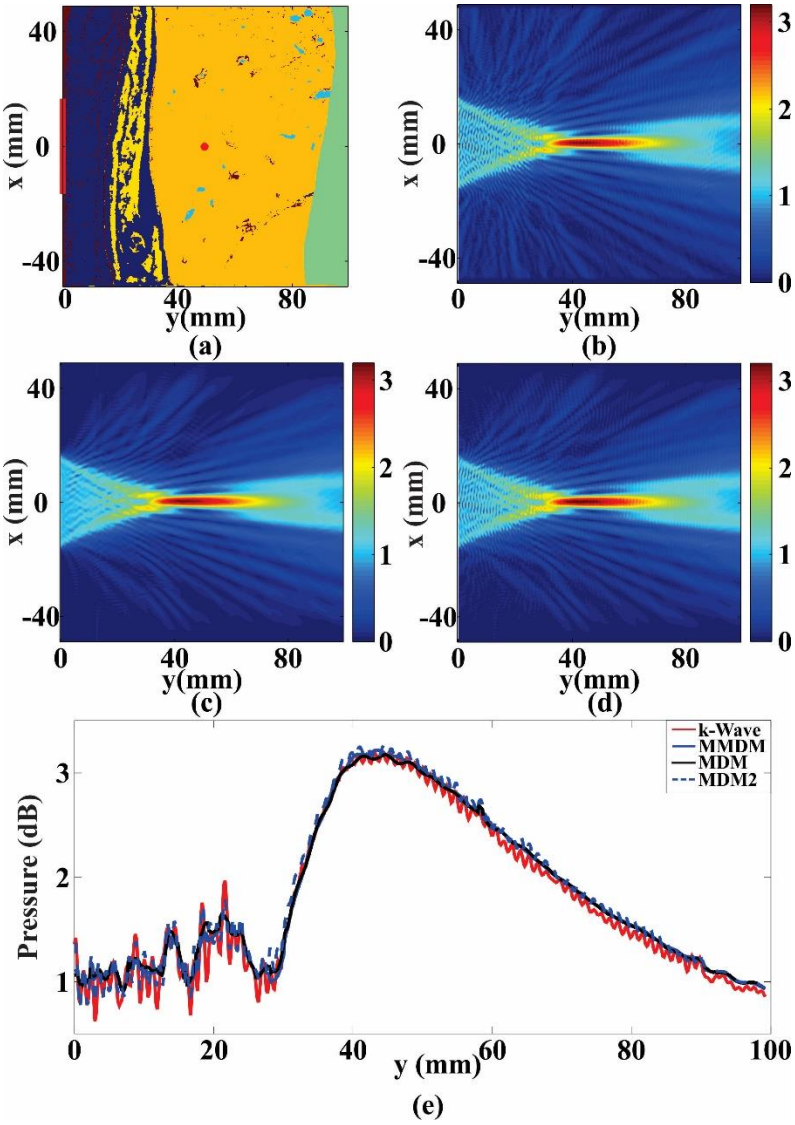

Figure. 4.6 (a) A 2D human tissue map. The superficial layers from the left to the right denote connective tissue (red), fat (dark blue) with embedded connective tissue (red), muscle (yellow), liver (orange) and tissue (green). Blood (light blue) is inside the liver. The red line on the left boundary indicates the array position. The red dot is the geometrical focus. Spatial pressure distributions simulated with (b) k-Wave, (c) MDM, and (d) MDM2 are shown. (e) Comparison of the axial pressure distributions along the beam axis.

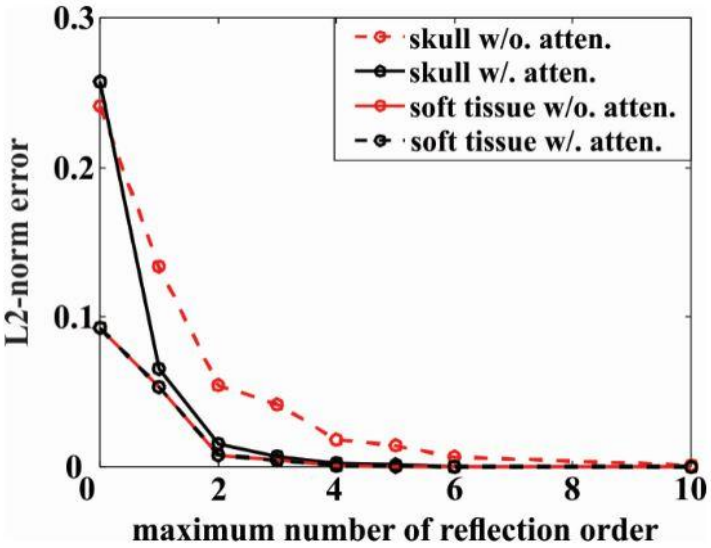

Figure. 4.7 Reflection convergence study of the MMDM for the skull and soft tissue cases with and without the attenuation.

4.5.Conclusion

In this chapter, phase correction and amplitude compensation are proposed and implemented in the MDM so that the algorithm can be more suited to modeling wave propagation in strongly heterogeneous media. The resulting model, i.e., the MMDM, is evaluated by studying two cases with strong speed of sound and density contrasts. Simulation results show that the MMDM is markedly more accurate in terms of predicting the phase and amplitude of the waveform, provided that the ultrasound beam is more or less perpendicular to the phase aberrating layer. It is also shown that reflections can be added to the MMDM to further improve the accuracy of the model. Convergence studies show that the second-order reflection is sufficient for soft tissue and lossy skull simulations. While the computation time increases with the addition of reflections, the MMDM is still computationally efficient when used to predict the wave field at specific

frequencies of interest. Though the simulations in this chapter are conducted in 2D, the algorithm can readily be extended for 3D simulations.

CHAPTER 5

mSOUND TOOLBOX

The work presented in this chapter is in preparation for IEEE Transaction on Ultrasonics, Ferroelectronics, and Frequency Control [260]

5.1.Introduction

Numerical modeling of wave propagation provides an important avenue to help understand the ultrasound-tissue interaction, innovate medical ultrasound technologies, and facilitate the characterization and design of ultrasound transducers in an efficient and cost-effective manner. For example, tissue harmonic ultrasound imaging was studied by Treeby *et al*. [177] with numerical simulations. Yin and Hynynen [261] investigated the low-frequency transcranial focused ultrasound without skull-specific aberration corrections through a numerical study. Canney *et al*. [37] combined the measurement and modeling to characterize ultrasound fields in high intensity focused ultrasound.

To date, many simulation toolboxes based on various algorithms have been made available in the public domain. Field II [262] [263] is regarded as the earliest and one of the most popular open source toolboxes for acoustic field characterization and studying ultrasound imaging approaches [264]. However, it is only capable of linear acoustic wave simulations in homogeneous media. FOCUS [63] computes the acoustic fields radiated by ultrasound transducers using the fast nearfield method (FNM) and the angular spectrum approach (ASA). Only homogeneous media or layered media are considered. In addition, the Khokhlov-Zabolotkaya-Kuznetsov (KZK) equation is used for nonlinear wave propagation in FOCUS. SimSonic [265] was developed to solve the elastodynamic equations in 2D and 3D using the finite-difference time domain (FDTD) method.

HIFU Simulator was developed by Soneson [213] [266] and it consists of a wave propagation module and a heating module. The wide-angle KZK equation is solved for the simulation of axisymmetric continuous wave beams in homogeneous or layered media. CREANUIS [140] encompasses a nonlinear wave solver based on the generalized angular spectrum method (GASM) as well as an image reconstruction scheme. The acoustic media can be considered inhomogeneous in terms of the nonlinearity coefficient. k-Wave [199] is designed for time-domain acoustic simulations in arbitrarily heterogeneous media. The coupled nonlinear first-order equations (momentum equation, mass conservation equation and the nonlinear pressure-density relation equation) are solved together with the k-space time-domain method [49]. k-Wave has been recently used for many applications, such as HIFU [267], PAT [183] and neuromodulation [232]. Moreover, k-Wave is capable of modeling elastic wave propagation [268]. However, k-Wave is based on time-domain methods and therefore can be computationally expensive. A brief summary for some of the most widely used medical ultrasound simulation toolboxes can be found in Table 5.1.

In this chapter, a new open source toolbox, mSOUND, is introduced for linear/nonlinear acoustic wave simulations in arbitrarily heterogeneous media. This toolbox is developed based on the generalized Westervelt equation. While the algorithm intrinsically models one-way propagation, users have the option to include reflections [269]. This toolbox encompasses two distinct numerical methods: the transient mixed domain method (TMDM) [223] and the frequency-specific mixed domain method (FSMDM) [229]. The TMDM generates the results in the time domain while the FSMDM generates the simulation results directly at the frequencies of interest, which are the fundamental frequency and the second harmonics, assuming sinusoidal excitations. The FSMDM should only be used if linear or weakly nonlinear wave propagation is considered.

While the TMDM is advantageous for modeling pulsed-waves and arbitrary nonlinearity (from weakly nonlinear to strongly nonlinear wave propagation), FSMDM is more suited to modeling continuous waves, and therefore is a better method to investigate conventional HIFU approaches. Backward propagation is also included in mSOUND and it operates with both the TMDM and FSMDM. With forward projection, the acoustic signal or the steady-state pressure could be recorded at a given distance from the source plane, or more generally, any point in space. With backward projection, the recorded signals can be back-projected to reconstruct the source [12] [128], in a way similar to time-reversal operation [189].

Table 5.1. Summary for contemporary medical ultrasound simulation toolboxes

Software	Solution method	Nonlinearity	Heterogeneity
Abersim [212]	Operator-splitting method and ASA	Yes(Westervelt/KZK-based)	Random phase delays
CREANUIS [140]	GASM	Yes (Westervelt-based)	Heterogeneous nonlinearity coefficients only
Field II [262]	Spatial impulse response	No	No
FOCUS [63]	FNM and ASA	Yes (KZK-based)	Layered media
HIFU Simulator [213]	Operator-splitting	Yes (wide-angle KZK)	Layered media
k-Wave [199]	k-space time-domain method	Yes (Westervelt-based)	Yes
KZK Bergen code [111]	Frequency-domain solution	Yes (KZK-based)	No
KZK Texas code[40]	Time-domain solution	Yes (KZK-based)	No
mSOUND	Mixed-domain method	Yes (Westervelt-based)	Yes
SimSonic [265]	FDTD	No	Yes

5.2.Theory

5.2.1. Forward Projection

We start from the generalized Westervelt equation which reads [1]

$$\rho\nabla\cdot\left(\frac{1}{\rho}\nabla p\right)-\frac{1}{c^2}\frac{\partial^2 p}{\partial t^2}+\frac{\delta}{c^4}\frac{\partial^3 p}{\partial t^3}+\frac{\beta}{\rho c^4}\frac{\partial^2 p^2}{\partial t^2}=0 \tag{5.1}$$

where p the acoustic pressure, ρ the ambient density, c is the speed of sound, δ is the sound diffusivity, $\delta = 2\alpha_{NP}c^3/\omega\text{^}2$ (α_{NP} is the attenuation coefficient in Np/m and ω is the angular frequency), and β is the nonlinearity coefficient. We first transform (5.1) by applying the normalized wave field $f = p/\sqrt{\rho}$ and the equation yields

$$\nabla^2 f-\frac{1}{c^2}\frac{\partial^2 f}{\partial t^2}-f\sqrt{\rho}\nabla^2\frac{1}{\sqrt{\rho}}+\frac{\delta}{c^4}\frac{\partial^3 f}{\partial t^3}+\frac{\beta}{\sqrt{\rho}c^4}\frac{\partial^2 f^2}{\partial t^2}=0. \tag{5.2}$$

By performing the Fourier transform to (5.2) with respect to *x*, *y* and *t*, we have

$$\frac{\partial^2}{\partial z^2}\tilde{F}+K^2\tilde{F}=F_{xy}\left\{\left[-\frac{\omega^2}{c_0^2}\left(\frac{c_0^2}{c^2}-1\right)+\frac{i\delta\omega^3}{c^4}+i\omega\gamma\right]F_t(f)\right\}+F_{xy}\left(\frac{\beta\omega^2}{\rho c^4}F_t(f^2)\right) \tag{5.3}$$

where $\tilde{F}$ is the Fourier transform of f, F_{xy} is the Fourier transform operator in *x*- and *y*-dimensions, F_t is the Fourier transform operator in the time domain, c_0 is the background sound speed and $K^2=\omega^2/c_0^2-k_x^2-k_y^2$, with k_x and k_y being the wavenumbers in *x*- and *y*-dimensions. An implicit one-way propagation solution to (5.3) can be derived from the one-dimensional (1D) Green's function in an integral form [12], such that

$$\tilde{F}(z)=\tilde{F}(0)e^{iKz}+\frac{e^{iKz}}{2iK}\int_0^z e^{-iKz'}M(f(z'))dz', \tag{5.4}$$

where

$$M(f)=F_{xy}\left\{\left[-\frac{\omega^2}{c_0^2}\left(\frac{c_0^2}{c^2}-1\right)+\frac{i\delta\omega^3}{c^4}+i\omega\gamma\right]F_t(f)\right\}+F_{xy}\left(\frac{\beta\omega^2}{\rho c^4}F_t(f^2)\right). \tag{5.5}$$

Equation (5.4) can be solved by using a Simpson-like rule [129]. In this algorithm, wave effects such as diffraction, attenuation, dispersion and nonlinearity are all considered. The Kramers-

Kronig dispersion relation can be applied directly by replacing the speed of sound c with c_p and $c_p = (1/\hat{c} + \alpha_0 \tan(\pi y/2)\, \omega^{y-1})^{-1}$ [12], where $\hat{c}$ is the sound speed at zero frequency, y is the power law exponent, α_0 is the absorption in Np·MHz^{-y}·m^{-1}. In mSOUND, the input attenuation coefficient is α with unit dB·MHz^{-y}·cm^{-1} and $\alpha = 868.6\alpha_0$. When modeling wave propagation in strongly heterogeneous media (e.g., skulls), phase correction (not to be confused with the correction for phase aberration) and amplitude compensation should be considered [269]. Multiple reflection at different orders can be also incorporated with the TMDM/FSMDM algorithm [269].

5.2.2. Backward Projection

Forward projection can be used to calculate the pressure field generated by acoustic sources while the backward projection can be used to obtain the source information. By changing z in (5.4) to -z [270], the backward projection algorithm can be obtained as

$$\tilde{F}(-z) = \tilde{F}(0)e^{-iKz} - \frac{e^{-iKz}}{2iK}\int_0^{-z} e^{iKz'} M\big(f(-z')\big)dz'. \tag{5.6}$$

Equation (5.6) can be again solved with the Simpson-like integral in mSOUND.

5.3.mSOUND Toolbox

5.3.1. Overview of the Toolbox

Based on the theory presented in the previous section, mSOUND is capable of simulating forward and backward wave propagation in linear/nonlinear media with arbitrary heterogeneities. This toolbox is freely available at https://m-sound.github.io/mSOUND/home. There are four main categories included in mSOUND:

- Forward projection in one/two/three-dimensional heterogeneous media using the TMDM with the functions ForwardND (`Forward1D`, `Forward2D` and `Forward3D`).
- Backward projection in one/two/three-dimensional heterogenous media using the TMDM with the functions BackwardND (`Backward1D`, `Backward2D` and `Backward3D`).

- Forward propagation in two/three-dimensional heterogeneous media using the FSMDM with the functions ForwardND_fund (`Forward2D_ fund` and `Forwad3D_fund`) and ForwardND_sec (`Forward2D_sec` and `Forward3D_sec`).
- Backward propagation in two/three-dimensional heterogenous media using the FSMDM with the functions BackwardND_fund (`Backward2D_ fund` and `Backward3D_fund`).

Simulation setups for forward and backward projections are very similar, with the only major difference being that reflections are not currently included in backward projection. In addition, backward projection for the second harmonic pressure is not implemented in mSOUND. Thus, the functions are introduced in two categories in the following parts: simulations with the TMDM and simulations with the FSMDM. Examples are given in section 5.4 to demonstrate how to conduct simulations with these functions.

5.3.2. TMDM

The functions ForwardND should be used for forward projection when transient results (waveforms) are desired. Five inputs are required when calling functions ForwardND and they are `mgrid`, `medium`, `source_p`, `sensor_mask` and `reflection_order`. `mgrid` is a structure returned by the function `set_grid` and it defines the discretized computational domain. `medium` is also a structure containing spatially distributed speed of sound, density, nonlinear coefficient, attenuation coefficient, and power law exponent. `source_p` defines the excitation signal. `sensor_mask` defines the positions where the signals are to be recorded, and it is in the Cartesian coordinate system. `reflection_order` is the maximum order of reflection to be included in the simulation. We point out here that some of the inputs share the same names as those in k-Wave (such as sensor_mask). This is to help users who are familiar with

k-Wave to more quickly learn mSOUND. The functions ForwardND are based on solving (5.4) with the Simpson-like rule. The marching is along the main propagation direction (y for 2D and z for 3D) and users have the option to record the acoustic pressure at the positions defined by `sensor_mask`. Figure 5.1 illustrates the simulation steps of the TMDM. Backward projection has the similar procedures of setting up a simulation with functions BackwardND.

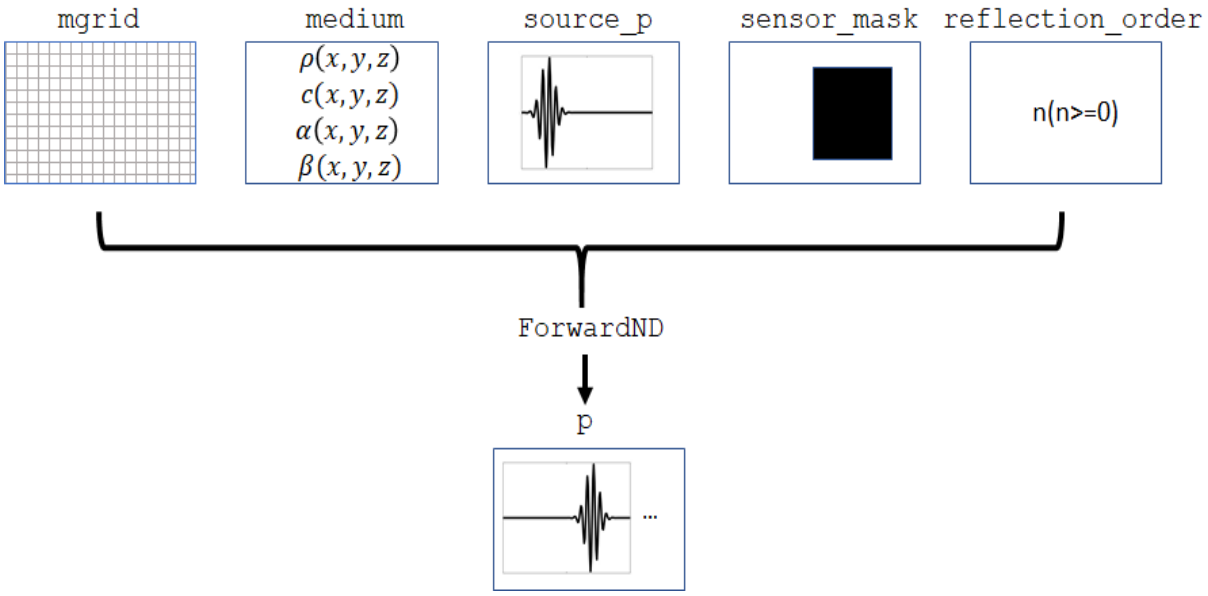

Figure 5.1 Illustration of the simulation with the TMDM for heterogeneous media.

5.3.3. FSMDM

When computing the steady-state pressure field at the fundamental frequency (`p_fundamental`) with the FSMDM, there are five required inputs for calling functions ForwardND_fund and they are: `mgrid`, `medium`, `source_p`, `omega_c` and `reflection_order`. `omega_c` is the center frequency of the sinusoidal wave. When the FSMDM is used for the simulation of the second harmonic pressure, `p_fundamental` will be used as one of the required inputs for calling the functions ForwardND_sec. Density is assumed homogeneous, though, for the simulation of the second harmonic wave field [229]. Reflections are

also not included in the second harmonic simulation. The simulation steps of FSMDM are illustrated in Figure 5.2. Backward projections are simulated with the functions BackwardND_fund.

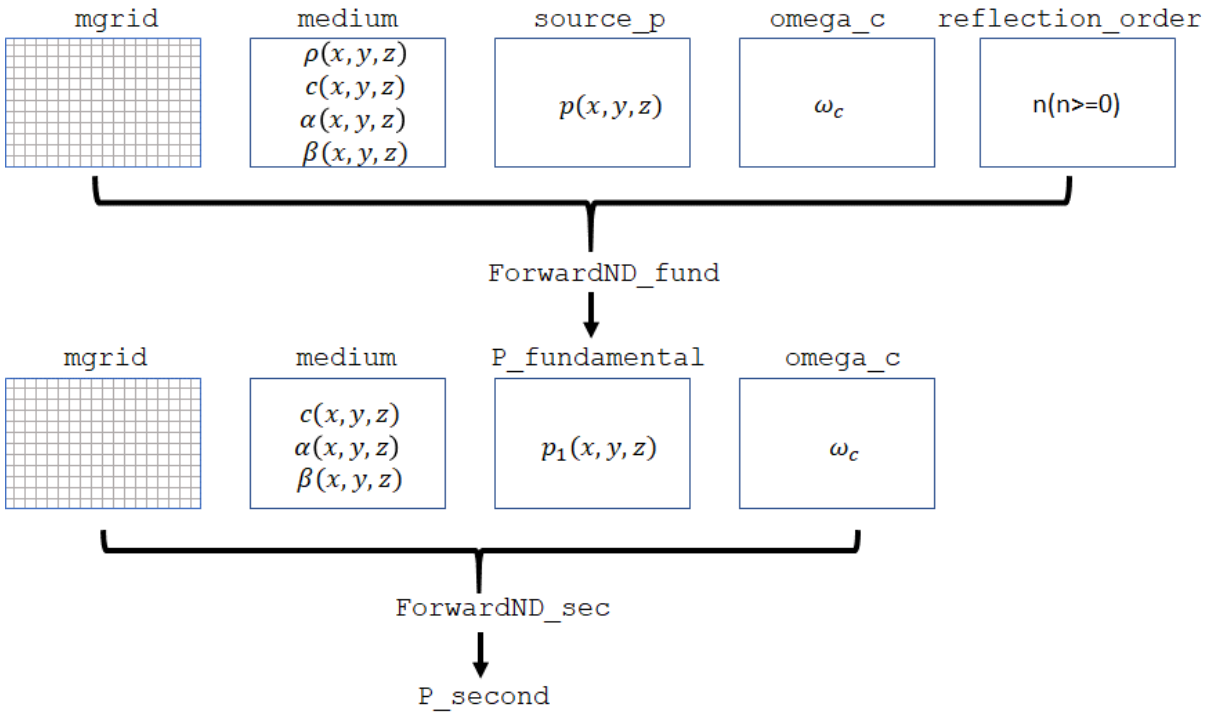

Figure 5.2 Illustration of the simulation with the FSMDM for heterogeneous media.

5.4.mSOUND Simulation Examples

5.4.1. Forward Projection with TMDM

In the first example, a 2D multiple-layered media (shown in Fig. 5.3(a)) with heterogenous density, speed of sound, attenuation coefficient and power law exponent is used to show how to set up simulations with the TMDM. A nonlinearity coefficient of 3.6 is used for the whole domain. A phased array is used to generate the focused beam. The schematic for the generation of a focused beam using a phased array can be found in Fig. 5.4(a). The MATLAB syntax is given below:

```
% define the computational domain
dx = 5.3571e-04; %[m]
dy = 1.3393e-04; %[m]
```

```
dt = 1.7857e-07; %[s]
x_length = 0.1050; %[m]
y_length = 0.0750; %[m]
t_length = 1.0286e-04; %[s]
mgrid = set_grid(dt, t_length, dx, x_length, dy, y_length);
% define the phased array
fc = 0.7e6; %center frequency [Hz]
TR_focus = 0.0686;  %focal length [m]
TR_radius = 0.0171; %transducer radius [m]
medium.c0 = 1500;   %reference speed of sound [m/s]
delay = sqrt((mgrid.x).^2 + TR_focus^2)/medium.c0; %[s]
delay = delay - min(delay);
% define the excitation waveform
p0 = 1; %[Pa]
ts = [-4/fc:dt:4/fc].';  %excitation pulse length [s]
delay = repmat(delay, length(ts), 1);
ts = repmat(ts, 1, mgrid.num_x);
source_p =
p0*sin(2*pi*fc*(ts+delay)).*exp((ts+delay).^2*fc^2/2);
source_p(:, abs(mgrid.x)>TR_radius) = 0;

% define the medium properties
load layered.mat  %the mat file can be downloaded from
https://github.com/m-
SOUND/mSOUND/blob/master/download/layered.mat
medium.c = c;      %[m/s]
medium.rho = rho;  %[kg/m^3]
medium.beta = 3.6;
medium.ca = ca;    %[dB·MHz^-y cm^-1]
medium.cb = cb;
medium.NRL_gamma = 0.6;
medium.NRL_alpha = 0.05;

% run the simulation
sensor_mask = zeros(mgrid.num_x, mgrid.num_y+1);
sensor_mask(:, 2:end) = 1;
reflection_order = 2;
p_time = Forward2D(mgrid, medium, source_p, sensor_mask,
reflection_order, 'NRL');
p_time =
reshape(p_time, mgrid.num_t, mgrid.num_x, mgrid.num_y+1);
```

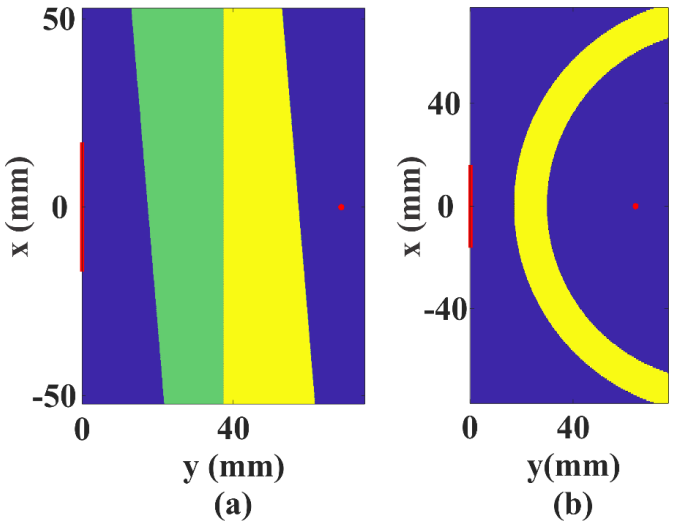

Figure 5.3 (a) A 2D heterogeneous layered media for the simulation with TMDM and (b) a 2D heterogeneous curved-layered media for the simulation with FSMDM.

The discrete computational domain is defined with the function `set_grid`. The spatial resolution (dx), temporal resolution (dt), marching step size (dy), and the computational domain size (`x_length, y_length, t_length`) are used to calculate the Cartesian coordinates and discrete wavenumbers for discrete Fourier transform (DFT). In mSOUND, a smaller time step size dt does not significantly affect the result once the Nyquist sampling rate is well satisfied. Moreover, there is no Courant-Friedrichs-Lewy (CFL) number to be satisfied in this algorithm since mSOUND is not based on time-domain methods [223]. The returned information is encapsulated in the structure `mgrid`. The excitation pressure `source_p` is indexed as (time, source_position).

Medium properties are defined within the structure `medium.` In 2D heterogeneous media, for example, `medium.c`, `medium.rho`, `medium.beta`, `medium.ca` and `medium.cb` are given as matrices with a size (`mgrid.num_x, mgrid.num_y+1`). `mgrid.num_x` and `mgrid.num_y` are the numbers of grid points in the x and y direction. In this case, wave propagates in the y direction. The row number is `mgrid.num_y+1` because the medium

properties for the source plane also need to be provided. For 3D simulations, the medium properties should be given as matrices with a size (`mgrid.num_x, mgrid.num_y, mgrid.num_z+1`). For homogeneous media, though, the medium properties can be described by a single scalar. `medium.c0` is the reference speed of sound and generally, it is chosen as the minimum value of `medium.c`.

`sensor_mask` and `reflection_order` are also required to call the function `Forward2D`. The `sensor_mask` contains the positions in Cartesian coordinate with a matrix size (`mgrid.num_x, mgrid.num_y+1`) with the recording positions marked with logical value 1 while other positions are marked with 0. If the `sensor_mask` is given as `ones(mgrid.num_x, mgrid.num_y+1)`, the pressure field will be recorded throughout the entire domain, including the source plane. `reflection_order` indicates the maximum order of reflections to be included in the simulation. This number is recommended to be 2 for lossy biological media in order to achieve the best tradeoff between accuracy and computation time.

There are optional inputs available for the users to choose. For instance, by invoking '`NRL`' (which stands for non-reflecting layer), non-reflecting layers are added to the computational domain and would minimize the spatial aliasing error [73]. If the non-reflecting layer is activated, `medium.NRL_gamma` and `medium.NRL_alpha` must be given. A large `medium.NRL_gamma` or a small `medium.NRL_alpha` implies more energy will be absorbed and thus reducing the aliasing error. On the contrary, if `medium.NRL_alpha` is too small, the acoustic filed becomes inaccurate due to excess absorption. For simulations with large speed of sound or density contrast (contrast ratio being larger than 1.05), '`correction`' is recommended. '`correction`' will correct both the phase and amplitude errors for strongly heterogeneous media using the algorithms depicted in [269]. If users would like to check the wave

field as the simulation is progressing, the '`animation`' option can be enabled, which is only allowed for the TMDM. '`record_animation`' will record the animation and save the animation file as '`animation.avi`'. '`animation`' and '`record_animation`' are not implemented for 1D simulations. For 3D simulations, the animation of the wave propagation is produced along the xz plane ($y = 0$).

When all the required inputs described above are given, the simulation commences by calling the function `Forward2D`. A wait bar will display the progress of the simulation and helps the user estimate the simulation time. The recorded pressure field will be returned as a binary grid in the MATLAB's standard column-wise linear index ordering and it is indexed as (`mgrid.num_t, sensor_mask`), where `mgrid.num_t` is the total points in time. The time-domain signal recorded at the transducer focus is shown in Fig. 5.4(b).

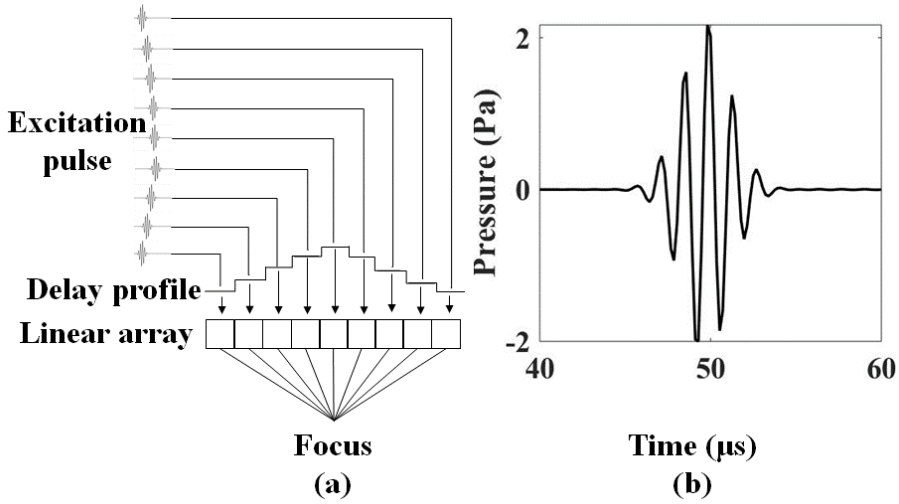

Figure 5.4 (a) Sketch of generating focused beam with phased array. (b) The time-domain signal recorded at the transducer focus. Results are simulated with the function `Forward2D` in the heterogeneously layered media shown in Fig. 5.3(a).

5.4.2. Forward Projection with FSMDM

Simulations with FSMDM can directly obtain the pressure distributions at the frequencies

of interest. A half-ring medium mimicking a skull is presented below to illustrate the simulation with the forward functions `Forward2D_fund` and `Forward2D_sec`. In this case, the density, speed of sound and nonlinearity coefficient are all heterogeneous. A phased array is again used to generate the focused beam. The MATLAB syntax shown below

```
% define the computational domain
dx = 5.3571e-04;  %[m]
dy = 1.3393e-04;  %[m]
x_length = 0.1543; %[m]
y_length = 0.0771; %[m]
mgrid = set_grid(0, 0, dx, x_length, dy, y_length);

% define the excitation signal
fc = 0.7e6; %center frequency [Hz]
p0 = 1.0e6; %excitation pulse magnitude [Pa]
TR_focus = 0.0643;  %focal length [m]
TR_radius = 0.0161; %aperture radius [m]
medium.c0 = 1500;   %reference speed of sound [m/s]
delay = sqrt((mgrid.x).^2 + TR_focus^2)/medium.c0;
delay = delay - min(delay);
source_p = p0*exp(1i*2*pi*fc*delay);
source_p(abs(mgrid.x)>TR_radius) = 0;

% define the medium
load annulus.mat  % the mat file can be download from
https://github.com/m-
SOUND/mSOUND/blob/master/download/annulus.mat.
medium.c = c;       %[m/s]
medium.rho = rho;  %[kg/m^3]
medium.beta = beta;
medium.ca = 0.0;   %[dB·MHz^-y cm^-1]
medium.cb = 2.0;
medium.NRL_gamma = 0.5;
medium.NRL_alpha = 0.03;

% run the simulation
omegac = fc*2*pi;
reflection_order = 4;
P_fundamental = Forward2D_fund(mgrid, medium, source_p, omega_c,
reflection_order, 'correction', 'NRL');
P_second = Forward2D_sec(mgrid, medium, P_fundamental, omega_c,
'correction', 'NRL');
```

For FSMDM simulations, `dt` and `t_length` are disregarded. `source_p` defines the spatially distributed pressure on the source plane. When the basic inputs: `mgrid`, `medium`, `source_p`, `omega_c` and `reflection_order` are given, `Forward2D_fund` can be called upon to generate `P_fundamental`, which is the pressure at the fundamental frequency. `P_fundamental` is then used as one of the required inputs to call the function `Forward2D_sec` for calculating the second harmonic wave field. '`correction`' and '`NRL`' are two optional inputs for both the function `Forward2D_fund` and `Forward2D_sec`. Noteworthy is that when density heterogeneity has to be considered for the simulation of the pressure at the second harmonic, '`correction`' option must be enabled. Otherwise, density will be assumed homogeneous. The pressure fields at the fundamental and second harmonic are shown in Fig. 5.5.

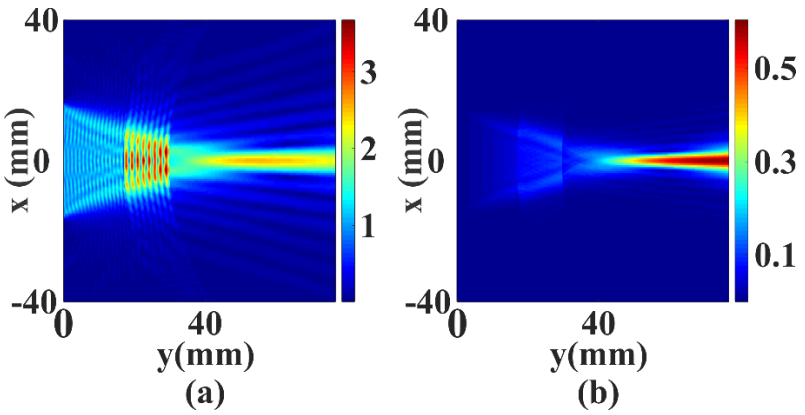

Figure 5.5 Spatially distributed pressure (a) at the fundamental frequency and (b) at the second-harmonic frequency. The computational domain shown here is cropped from the original domain for illustration purposes. Results are simulated with the `Forward2D_fund` and `Forwad2D_sec` functions respectively in the heterogeneously half annular media(shown in Fig. 5.3(b)).

5.4.3. Backward Projection with TMDM

mSOUND is also capable of propagating the pressure field backward toward the source,

which can be useful for near-field acoustical holography [271], sound focusing in heterogeneous media, and PAT. In PAT, for example, short-pulses of laser are first delivered into biological tissues, which are to be absorbed by the tissue, particularly the blood vessels. Ultrasonic waves are consequently produced via thermos-elastic expansion. By projecting the ultrasonic wave backward toward the tissue (in a way similar to time-reversal [272], [273], [183],) the initial ultrasonic pressure distribution can be recognized, rendering an image of the vessels.

To demonstrate the application for PAT, an initial source with the 'mSOUND' shape is used in this chapter for the illustration of the simulation with backward projection. The forward propagation of the emitted ultrasonic wave from the source is simulated with the k-Wave toolbox. The received signals are backward projected with the mSOUND toolbox for the initial source image reconstruction. In this case, `Backward2D` is used. The definitions of '`mgrid`', '`medium`' and '`sensor_mask`' are similar to those in the forward projection. The '`source_p`' required for the function `Backward2D` is the signals recorded at the right boundary of Fig. 5.6(a), generated by k-Wave. The details of the simulation setup for this example can be found from the mSOUND website and the syntax is not provided here to save space. Figure 5.6(b) shows the reconstructed source distribution with the time-reversal algorithm in k-Wave and Fig. 5.6(c) shows the same source distribution with the backward projection in mSOUND. The two results look virtually the same.

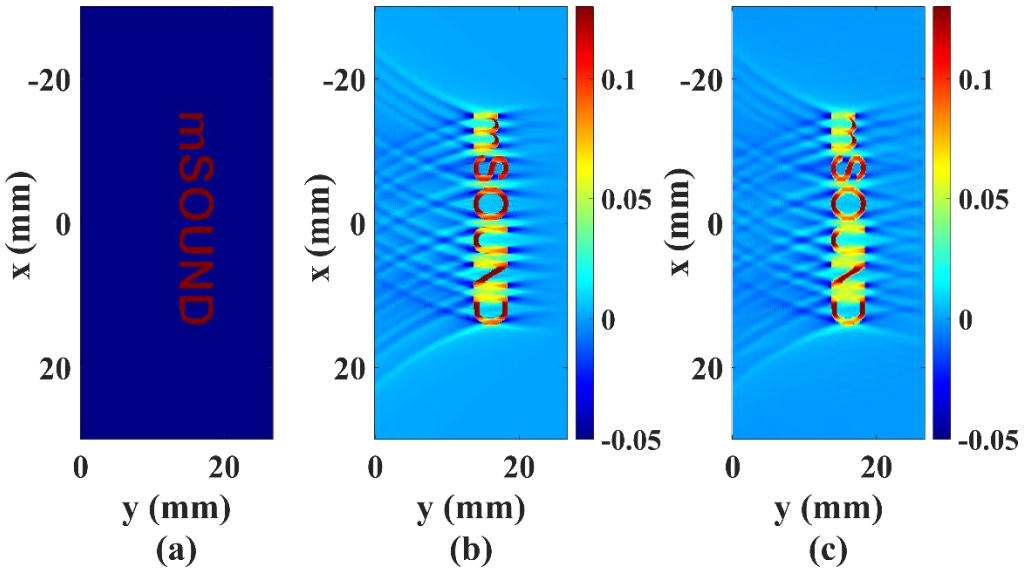

Figure 5.6 True source distribution. Source distribution reconstruction using (a) the time-reversal method in k-Wave and (c) the backward projection method in mSOUND. The computational domain shown here is cropped from the original domain for illustration purposes.

Currently, the mSOUND toolbox assumes that the transducer is planar since a source plane needs to be defined. Though phased array can be used for mimicking curved transducers in mSOUND, users have the option to first use k-Wave/FOCUS to propagate the wave from a curved transducer for a small distance, and subsequently use the pressure recorded on that plane as the input in mSOUND. One such example is provided in the example section on the mSOUND website. mSOUND currently does not have a module for solving the bio-heat transfer equation. Users can also first obtain the pressure amplitude distribution using the FSMDM at the frequency of interest, and then use that as the input for k-Wave to conduct thermal simulations. One example pertaining to this is also provided on the mSOUND website. mSOUND currently does not have a shock-wave capturing algorithm and therefore is not best suited for modeling shock waves in the context of lithotripsy or histotripsy. If shock wave modeling is still desired, artificial attenuation needs to be included to prevent the Gibbs effect [129].

5.5.Conclusion

mSOUND is a user-friendly toolbox for the simulation of acoustic wave propagation in heterogeneous media and it contains two models for both the forward and backward projection. One mode is the TMDM and it can give transient pressure distribution. The other one is the FSMDM and it can efficiently generate the steady-state pressure distribution at the frequency of interest. Three examples are used to explain how to set up simulations with this toolbox. We envision that mSOUND can be readily applied to tackle a variety of ultrasound problems: study the phase aberration in tissue [87], imaging reconstruction in PAT, ultrasound waveform tomography [235], data generation for machine learning [274], among others.

CHAPTER 6

CONCLUDING REMARKS AND FUTURE WORK

6.1.Conclusions and Contributions

Numerical modeling is being widely used in clinical applications. In this dissertation, the MDM is first developed for simulating nonlinear wave propagation in soft tissue. A couple of cases were studied to evaluate the MDM. It is demonstrated that the MDM is an efficient and accurate algorithm for modeling medical ultrasound propagating in soft tissue.

The MDM can directly calculate the pressure at the fundament frequency, and it will greatly improve the computation speed. To extend this advantage to nonlinear wave propagation, the FSMDM is developed for modeling the second harmonic pressure field. A realistic human tissue map is used to investigate the accuracy of the FSMDM. Results from the TMDM are used as the benchmark solutions. L2 norm errors calculated with the normalized pressure for the focal region is 0.0114 for the fundamental frequency and 0.0185 for the second harmonics. Thus, for weakly nonlinear cases, the FSMDM can obtain the pressure at the fundamental and the second harmonic frequency efficiently with high accuracy.

As has been theoretically analyzed in the Appendix A, the TMDM/FSMDM is valid for weakly heterogeneous media. Phase correction and amplitude compensation are introduced for modeling wave propagation in strongly heterogeneous media. Reflections are also incorporated to the MDM to further improve the accuracy of the numerical model. The new model is denoted as the modified mixed domain method (MMDM). Simulation results show that the MMDM is markedly more accurate in terms of predicting the phase and amplitude of the waveform, provided that the ultrasound beam is more or less perpendicular to the phase aberrating layer. Convergence studies show that the second-order reflection is sufficient for soft tissue and lossy skull simulations.

Moreover, the frequency-domain MMDM shows the superiority of computation speed in transcranial ultrasound simulations, even when reflections of high orders are included.

Finally, the MDM, FSMDM and MMDM are integrated to an open source toolbox mSOUND (https://m-sound.github.io/mSOUND/home), which is developed for the simulation of acoustic wave propagation in heterogeneous media. Three examples are used to explain how to set up simulations with this toolbox. The mSOUND toolbox is expected to be useful in a variety of ultrasound applications: studying the phase aberration in tissue/transcranial ultrasound, ultrasound waveform tomography, transducer characterization, data generation for machine learning, etc.

6.2.Future Work

Based on the present dissertation, some future work is suggested:

1. Improve the amplitude compensation for thermal field prediction. Currently, the amplitude correction is derived from 1D and works well when the ultrasound beam is more or less perpendicular to the phase aberrating layer.
2. Investigate shock wave modeling for both pulse-waves and continuous waves. Operator splitting method can be applied. The nonlinear effect can be solved with time-domain algorithm. Other effects (diffraction, attenuation, dispersion and density heterogeneity) can be solved with the mixed-domain method.
3. Experimentally verify the MDM/MMDM with wave propagation in the soft tissue and the human skull.
4. Integrate mSOUND with the high computational capability of graphic processing units (GPUs) to deliver fast, accurate and versatile ultrasound modeling solutions. Additionally, to improve the usability of the toolbox, the algorithms will also be written in C, and be compiled so that it can be used in both MATLAB and C.

5. More applications can be investigated with the mSOUND toolbox. For example, due to the efficient computational speed, it can be used to generate the data for deep leaning training. It can also be combined with bioheat equations for temperature estimation in HIFU applications.

REFERENCES

[1] J. Gu and Y. Jing, "Modeling of wave propagation for medical ultrasound: a review," *IEEE Transactions on Ultrasonics Ferroelectrics and Frequency Control,* vol. 62, pp. 1979-1992, 2015.

[2] M. J. Park, Y. S. Kim, B. Keserci, H. Rhim, and H. K. Lim, "Volumetric MR-guided high-intensity focused ultrasound ablation of uterine fibroids: treatment speed and factors influencing speed," *European Radiology,* vol. 23, pp. 943-950, Apr 2013.

[3] N. McDannold, G. T. Clement, P. Black, F. Jolesz, and K. Hynynen, "Transcranial Magnetic Resonance Imaging-Guided Focused Ultrasound Surgery of Brain Tumors: Initial Findings in 3 Patients," *Neurosurgery,* vol. 66, pp. 323-332, Feb 2010.

[4] P. L. M. J. van Neer, M. G. Danilouchkine, M. D. Verweij, L. Demi, M. M. Voormolen, A. F. W. van der Steen, *et al.*, "Comparison of fundamental, second harmonic, and superharmonic imaging: A simulation study," *The Journal of the Acoustical Society of America,* vol. 130, pp. 3148-3157, Nov 2011.

[5] K. Firouzi, B. T. Cox, B. E. Treeby, and N. Saffari, "A first-order k-space model for elastic wave propagation in heterogeneous media," *The Journal of the Acoustical Society of America,* vol. 132, pp. 1271-1283, Sep 2012.

[6] V. K. Kalyani, Pallavika, and S. K. Chakraborty, "Finite-difference time-domain method for modelling of seismic wave propagation in viscoelastic media," *Applied Mathematics and Computation,* vol. 237, pp. 133-145, Jun 2014.

[7] P. Moczo, J. O. A. Robertsson, and L. Eisner, "The finite-difference time-domain method for modeling of seismic wave propagation," *Advances in Geophysics, Vol 48,* vol. 48, pp. 421-516, 2007.

[8] Y. Jing, T. R. Wang, and G. T. Clement, "A k-Space Method for Moderately Nonlinear Wave Propagation," *IEEE Transactions on Ultrasonics Ferroelectrics and Frequency Control,* vol. 59, pp. 1664-1673, Aug 2012.

[9] G. F. Pinton, J. Dahl, S. Rosenzweig, and G. E. Trahey, "A Heterogeneous Nonlinear Attenuating Full-Wave Model of Ultrasound," *IEEE Transactions on Ultrasonics Ferroelectrics and Frequency Control,* vol. 56, pp. 474-488, Mar 2009.

[10] P. J. Westervelt, "Parametric Acoustic Array," *The Journal of the Acoustical Society of America,* vol. 35, pp. 535-537, 1963.

[11] P. V. Yuldashev and V. A. Khokhlova, "Simulation of three-dimensional nonlinear fields of ultrasound therapeutic arrays," *Acoustical Physics,* vol. 57, pp. 334-343, May 2011.

[12] Y. Jing, M. L. Tao, and G. T. Clement, "Evaluation of a wave-vector-frequency-domain method for nonlinear wave propagation," *The Journal of the Acoustical Society of America,* vol. 129, pp. 32-46, Jan 2011.

[13] J. Huijssen, A. Bouakaz, M. D. Verweij, and N. de Jong, "Simulations of the nonlinear acoustic pressure field without using the parabolic approximation," *2003 IEEE Ultrasonics Symposium Proceedings, Vols 1 and 2,* pp. 1851-1854, 2003.

[14] A. I. Nachman, J. F. Smith, and R. C. Waag, "An Equation for Acoustic Propagation in Inhomogeneous-Media with Relaxation Losses," *The Journal of the Acoustical Society of America,* vol. 88, pp. 1584-1595, Sep 1990.

[15] W. Kreider, P. V. Yuldashev, O. A. Sapozhnikov, N. Farr, A. Partanen, M. R. Bailey, *et al.,* "Characterization of a Multi-Element Clinical HIFU System Using Acoustic Holography and Nonlinear Modeling," *IEEE Transactions on Ultrasonics Ferroelectrics and Frequency Control,* vol. 60, pp. 1683-1698, Aug 2013.

[16] I. M. Hallaj and R. O. Cleveland, "FDTD simulation of finite-amplitude pressure and temperature fields for biomedical ultrasound," *The Journal of the Acoustical Society of America,* vol. 105, pp. L7-L12, May 1999.

[17] G. Pinton, J. F. Aubry, M. Fink, and M. Tanter, "Effects of nonlinear ultrasound propagation on high intensity brain therapy," *Medical Physics,* vol. 38, pp. 1207-1216, Mar 2011.

[18] G. F. Pinton and G. E. Trahey, "Modeling of shock wave propagation in large amplitude ultrasound," *Ultrasonic Imaging,* vol. 30, pp. 44-60, Jan 2008.

[19] E. Vlaisavljevich, A. Maxwell, M. Warnez, E. Johnsen, C. A. Cain, and Z. Xu, "Histotripsy-Induced Cavitation Cloud Initiation Thresholds in Tissues of Different Mechanical Properties," *IEEE Transactions on Ultrasonics Ferroelectrics and Frequency Control,* vol. 61, pp. 341-352, Feb 2014.

[20] G. F. Pinton, G. E. Trahey, and J. J. Dahl, "Sources of Image Degradation in Fundamental and Harmonic Ultrasound Imaging: A Nonlinear, Full-Wave, Simulation Study (vol 58, pg 754, 2011)," *IEEE Transactions on Ultrasonics Ferroelectrics and Frequency Control,* vol. 58, pp. 1272-1283, Jun 2011.

[21] J. E. Soneson and M. R. Myers, "Thresholds for Nonlinear Effects in High-Intensity Focused Ultrasound Propagation and Tissue Heating," *IEEE Transactions on Ultrasonics Ferroelectrics and Frequency Control,* vol. 57, pp. 2450-2459, Nov 2010.

[22] G. Taraldsen, "A generalized Westervelt equation for nonlinear medical ultrasound," *The Journal of the Acoustical Society of America,* vol. 109, pp. 1329-1333, Apr 2001.

[23] M. Hamilton and D. Blackstock, *Nonlinear Acoustics*. San Diego: Academic Press, 1998.

[24] Y. Jing, D. Shen, and G. T. Clement, "Verification of the Westervelt Equation for Focused Transducers," *IEEE Transactions on Ultrasonics Ferroelectrics and Frequency Control,* vol. 58, pp. 1097-1101, May 2011.

[25] B. E. Treeby and B. T. Cox, "Modeling power law absorption and dispersion for acoustic propagation using the fractional Laplacian," *The Journal of the Acoustical Society of America,* vol. 127, pp. 2741-2748, May 2010.

[26] W. Chen and S. Holm, "Modified Szabo's wave equation models for lossy media obeying frequency power law," *The Journal of the Acoustical Society of America,* vol. 114, pp. 2570-2574, Nov 2003.

[27] T. L. Szabo, "Time-domain wave-equations for lossy media obeying a frequency power-law," *The Journal of the Acoustical Society of America, vol*. 96, pp. 491–500, Jul. 1994.

[28] M. G. Wismer and R. Ludwig, "An Explicit Numerical Time-Domain Formulation to Simulate Pulsed Pressure Waves in Viscous Fluids Exhibiting Arbitrary Frequency Power-Law Attenuation," *IEEE Transactions on Ultrasonics Ferroelectrics and Frequency Control,* vol. 42, pp. 1040-1049, Nov 1995.

[29] J. F. Kelly and R. J. McGough, "Fractal ladder models and power law wave equations," *The Journal of the Acoustical Society of America,* vol. 126, pp. 2072-2081, Oct 2009.

[30] S. P. Nasholm and S. Holm, "Linking multiple relaxation, power-law attenuation, and fractional wave equations," *The Journal of the Acoustical Society of America,* vol. 130, pp. 3038-3045, Nov 2011.

[31] G. V. Norton and J. C. Novarini, "Including dispersion and attenuation directly in the time domain for wave propagation in isotropic media," *The Journal of the Acoustical Society of America,* vol. 113, pp. 3024-3031, Jun 2003.

[32] M. Ochmann and S. Makarov, "Representation of the Absorption of Nonlinear-Waves by Fractional Derivatives," *The Journal of the Acoustical Society of America,* vol. 94, pp. 3392-3399, Dec 1993.

[33] V. P. Kuznetsov, "Equations of Nonlinear Acoustics," *Soviet Physics Acoustics-Ussr,* vol. 16, pp. 467-470, 1971.

[34] P. D. Fox, A. Bouakaz, and F. Tranquart, "Computation of steered nonlinear fields using offset KZK axes," *2005 IEEE Ultrasonics Symposium, Vols 1-4,* pp. 1984-1987, 2005.

[35] G. F. Pinton and G. E. Trahey, "A comparison of time-domain solutions for the full-wave equation and the parabolic wave equation for a diagnostic ultrasound transducer," *IEEE Transactions on Ultrasonics Ferroelectrics and Frequency Control,* vol. 55, pp. 730-733, Mar 2008.

[36] J. N. Tjotta, S. Tjotta, and E. H. Vefring, "Effects of Focusing on the Nonlinear-Interaction between 2 Collinear Finite-Amplitude Sound Beams," *The Journal of the Acoustical Society of America,* vol. 89, pp. 1017-1027, Mar 1991.

[37] M. S. Canney, M. R. Bailey, L. A. Crum, V. A. Khokhlova, and O. A. Sapozhnikov, "Acoustic characterization of high intensity focused ultrasound fields: A combined measurement and modeling approach," *The Journal of the Acoustical Society of America,* vol. 124, pp. 2406-2420, Oct 2008.

[38] S. Lee and M. F. Hamilton, "Time-Domain Modeling of Pulsed Finite-Amplitude Sound Beams," *The Journal of the Acoustical Society of America,* vol. 97, pp. 906-917, Feb 1995.

[39] X. M. Yang and R. O. Cleveland, "Time domain simulation of nonlinear acoustic beams generated by rectangular pistons with application to harmonic imaging," *The Journal of the Acoustical Society of America,* vol. 117, pp. 113-123, Jan 2005.

[40] R. O. Cleveland, M. F. Hamilton, and D. T. Blackstock, "Time-domain modeling of finite-amplitude sound in relaxing fluids," *The Journal of the Acoustical Society of America,* vol. 99, pp. 3312-3318, Jun 1996.

[41] Y. Jing and R. O. Cleveland, "Modeling the propagation of nonlinear three-dimensional acoustic beams in inhomogeneous media," *The Journal of the Acoustical Society of America,* vol. 122, pp. 1352-1364, Sep 2007.

[42] T. Varslot and G. Taraldsen, "Computer simulation of forward wave propagation in soft tissue," *IEEE Transactions on Ultrasonics Ferroelectrics and Frequency Control,* vol. 52, pp. 1473-1482, Sep 2005.

[43] T. Tsuchiya and Y. Kagawa, "Finite-Element Analysis of Focusing Field in Nonlinear Acoustic-Waves," *Japanese Journal of Applied Physics Part 1-Regular Papers Short Notes & Review Papers,* vol. 30, pp. 51-53, 1991.

[44] J. E. Soneson, "A parametric study of error in the parabolic approximation of focused axisymmetric ultrasound beams," *The Journal of the Acoustical Society of America,* vol. 131, pp. El481-El486, Jun 2012.

[45] T. Kamakura, T. Ishiwata, and K. Matsuda, "Model equation for strongly focused finite-amplitude sound beams," *The Journal of the Acoustical Society of America,* vol. 107, pp. 3035-3046, Jun 2000.

[46] T. Kamakura, "Two model equations for describing nonlinear sound beams," *Japanese Journal of Applied Physics Part 1-Regular Papers Short Notes & Review Papers,* vol. 43, pp. 2808-2812, May 2004.

[47] T. B. Fan, Z. B. Liu, T. Chen, F. Q. Li, and D. Zhang, "A modeling approach to predict acoustic nonlinear field generated by a transmitter with an aluminum lens," *Medical Physics,* vol. 38, pp. 5033-5039, Sep 2011.

[48] T. Kamakura, H. Nomura, and G. T. Clement, "Application of the split-step Pade approach to nonlinear field predictions," *Ultrasonics,* vol. 53, pp. 432-438, Feb 2013.

[49] B. E. Treeby, J. Jaros, A. P. Rendell, and B. T. Cox, "Modeling nonlinear ultrasound propagation in heterogeneous media with power law absorption using a k-space pseudospectral method," *The Journal of the Acoustical Society of America,* vol. 131, pp. 4324-4336, Jun 2012.

[50] M. Tabei, T. D. Mast, and R. C. Waag, "A k-space method for coupled first-order acoustic propagation equations," *The Journal of the Acoustical Society of America,* vol. 111, pp. 53-63, Jan 2002.

[51] Q. H. Liu and J. P. Tao, "The perfectly matched layer for acoustic waves in absorptive media," *The Journal of the Acoustical Society of America,* vol. 102, pp. 2072-2082, Oct 1997.

[52] X. J. Yuan, D. Borup, J. Wiskin, P. Berggren, and S. A. Johnson, "Simulation of acoustic wave propagation in dispersive media with relaxation losses by using FDTD method with PML absorbing boundary condition," *IEEE Transactions on Ultrasonics Ferroelectrics and Frequency Control,* vol. 46, pp. 14-23, Jan 1999.

[53] V. I. Goland and L. M. Kushkuley, "Strongly focusing multielement therapeutic emitters for noninvasive ultrasonic ablation of adipose tissue," *Acoustical Physics,* vol. 55, pp. 496-509, Oct 2009.

[54] S. Tjotta, "Higher order model equations in nonlinear acoustics," *Acustica,* vol. 87, pp. 316-321, May-Jun 2001.

[55] Z. W. Qian, "Nonlinear Acoustics in Higher-Order Approximation," *Acta Physica Sinica-Overseas Edition,* vol. 4, pp. 670-675, Sep 1995.

[56] L. H. Soderholm, "A higher order acoustic equation for the slightly viscous case," *Acustica,* vol. 87, pp. 29-33, Jan-Feb 2001.

[57] J. N. Tjotta and S. Tjotta, "Finite Amplitude Ultrasound Beams," *1994 IEEE Ultrasonics Symposium Proceedings, Vols 1-3,* pp. 709-714, 1994.

[58] D. S. Ding and Z. H. Lu, "The second harmonic component in the Bessel beam," *Applied Physics Letters,* vol. 68, pp. 608-610, Jan 29 1996.

[59] J. H. Huang, D. S. Ding, and Y. S. Hsu, "Second-harmonic generation of practical Bessel beams," *Journal of Sound and Vibration,* vol. 328, pp. 148-155, Nov 27 2009.

[60] H. T. Oneil, "Theory of Focusing Radiators," *The Journal of the Acoustical Society of America,* vol. 21, pp. 516-526, 1949.

[61] M. D. Verweij, B. Treeby, and L. Demi, "Simulation of ultrasound fields," in *Comprehensive Biomedical Physics*, ed Oxford: Elsevier Science Ltd, 2014, pp. 465-499.

[62] E. G. Williams, *Fourier acoustics*. London: Academic Press, 1999.

[63] R. J. McGough, "Rapid calculations of time-harmonic nearfield pressures produced by rectangular pistons," *The Journal of the Acoustical Society of America,* vol. 115, pp. 1934-1941, May 2004.

[64] D. Chen and R. J. McGough, "A 2D fast near-field method for calculating near-field pressures generated by apodized rectangular pistons," *The Journal of the Acoustical Society of America,* vol. 124, pp. 1526-1537, Sep 2008.

[65] R. J. McGough, T. V. Samulski, and J. F. Kelly, "An efficient grid sectoring method for calculations of the near-field pressure generated by a circular piston," *The Journal of the Acoustical Society of America,* vol. 115, pp. 1942-1954, May 2004.

[66] G. T. Clement and K. Hynynen, "Field characterization of therapeutic ultrasound phased arrays through forward and backward planar projection," *The Journal of the Acoustical Society of America,* vol. 108, pp. 441-446, Jul 2000.

[67] P. R. Stepanishen and K. C. Benjamin, "Forward and Backward Projection of Acoustic Fields Using FFT Methods," *The Journal of the Acoustical Society of America,* vol. 71, pp. 803-812, 1982.

[68] X. Z. Zeng and R. McGough, "Evaluation of the angular spectrum approach for simulations of near-field pressures," *The Journal of the Acoustical Society of America,* vol. 123, pp. 68-76, Jan 2008.

[69] P. T. Christopher and K. J. Parker, "New Approaches to the Linear Propagation of Acoustic Fields," *The Journal of the Acoustical Society of America,* vol. 90, pp. 507-521, Jul 1991.

[70] G. T. Clement, R. Liu, S. V. Letcher, and P. R. Stepanishen, "Forward projection of transient signals obtained from a fiberoptic pressure sensor," *The Journal of the Acoustical Society of America,* vol. 104, pp. 1266-1273, Sep 1998.

[71] P. Wu, R. Kazys, and T. Stepinski, "Analysis of the numerically implemented angular spectrum approach based on the evaluation of two-dimensional acoustic fields .2. Characteristics as a function of angular range," *The Journal of the Acoustical Society of America,* vol. 99, pp. 1349-1359, Mar 1996.

[72] P. Wu, R. Kazys, and T. Stepinski, "Analysis of the numerically implemented angular spectrum approach based on the evaluation of two-dimensional acoustic fields .1. Errors due to the discrete Fourier transform and discretization," *The Journal of the Acoustical Society of America,* vol. 99, pp. 1339-1348, Mar 1996.

[73] Y. Jing, "On the use of an absorption layer for the angular spectrum approach (L)," *The Journal of the Acoustical Society of America,* vol. 131, pp. 999-1002, Feb 2012.

[74] M. Hlawitschka, R. J. McGough, K. W. Ferrara, and D. E. Kruse, "Fast Ultrasound Beam Prediction for Linear and Regular Two-Dimensional Arrays," *IEEE Transactions on Ultrasonics Ferroelectrics and Frequency Control,* vol. 58, pp. 2001-2012, Sep 2011.

[75] J. Koskela, E. Vahala, M. de Greef, L. P. Lafitte, and M. Ries, "Stochastic ray tracing for simulation of high intensity focal ultrasound therapy," *The Journal of the Acoustical Society of America,* vol. 136, pp. 1430-1440, Sep 2014.

[76] Stepanis.Pr, "Transient Radiation from Pistons in an Infinite Planar Baffle," *The Journal of the Acoustical Society of America,* vol. 49, pp. 1629-&, 1971.

[77] P. Wu and T. Stepinski, "Spatial impulse response method for predicting pulse-echo fields from a linear array with cylindrically concave surface," *IEEE Transactions on Ultrasonics Ferroelectrics and Frequency Control,* vol. 46, pp. 1283-1297, Sep 1999.

[78] Y. G. Du, H. Jensen, and J. A. Jensen, "Investigation of an angular spectrum approach for pulsed ultrasound fields," *Ultrasonics,* vol. 53, pp. 1185-1191, Aug 2013.

[79] G. T. Clement, R. Liu, S. V. Letcher, and P. R. Stepanishen, "Temporal backward planar projection of acoustic transients," *The Journal of the Acoustical Society of America,* vol. 103, pp. 1723-1726, Apr 1998.

[80] U. Vyas and D. A. Christensen, "Extension of the angular spectrum method to calculate pressure from a spherically curved acoustic source," *The Journal of the Acoustical Society of America,* vol. 130, pp. 2687-2693, Nov 2011.

[81] P. Wu and T. Stepinski, "Extension of the angular spectrum approach to curved radiators," *The Journal of the Acoustical Society of America,* vol. 105, pp. 2618-2627, May 1999.

[82] J. A. Jensen, D. Gandhi, and W. D. Obrien, "Ultrasound Fields in an Attenuating Medium," *IEEE 1993 Ultrasonics Symposium Proceedings, Vols 1 and 2,* pp. 943-946, 1993.

[83] G. T. Clement and K. Hynynen, "Forward planar projection through layered media," *IEEE Transactions on Ultrasonics Ferroelectrics and Frequency Control,* vol. 50, pp. 1689-1698, Dec 2003.

[84] U. Vyas and D. Christensen, "Ultrasound Beam Simulations in Inhomogeneous Tissue Geometries Using the Hybrid Angular Spectrum Method," *IEEE Transactions on Ultrasonics Ferroelectrics and Frequency Control,* vol. 59, pp. 1093-1100, Jun 2012.

[85] B. Fornberg, "Generation of Finite-Difference Formulas on Arbitrarily Spaced Grids," *Mathematics of Computation,* vol. 51, pp. 699-706, Oct 1988.

[86] V. W. Sparrow and R. Raspet, "A Numerical-Method for General Finite-Amplitude Wave-Propagation in 2 Dimensions and Its Application to Spark Pulses," *The Journal of the Acoustical Society of America,* vol. 90, pp. 2683-2691, Nov 1991.

[87] M. Tabei, T. D. Mast, and R. C. Waag, "Simulation of ultrasonic focus aberration and correction through human tissue," *The Journal of the Acoustical Society of America,* vol. 113, pp. 1166-1176, Feb 2003.

[88] T. D. Mast, L. M. Hinkelman, M. J. Orr, V. W. Sparrow, and R. C. Waag, "Simulation of ultrasonic pulse propagation through the abdominal wall," *The Journal of the Acoustical Society of America,* vol. 102, pp. 1177-1190, Aug 1997.

[89] D. Komatitsch, "Comment on "Multidomain Pseudospectral Time-Domain (PSTD) Method for Acoustic Waves in Lossy Media" by Y. Q. Zeng, Q. H. Liu and G. Zhao, Journal of Computational Acoustics, Vol. 12, No. 3, Pp. 277-299 (2004)," *Journal of Computational Acoustics,* vol. 16, pp. 465-467, Sep 2008.

[90] Q. H. Liu, "The pseudospectral time-domain (PSTD) algorithm for acoustic waves in absorptive media," *IEEE Transactions on Ultrasonics Ferroelectrics and Frequency Control,* vol. 45, pp. 1044-1055, Jul 1998.

[91] Q. H. Liu, "Large-scale simulations of electromagnetic and acoustic measurements using the pseudospectral time-domain (PSTD) algorithm," *IEEE Transactions on Geoscience and Remote Sensing,* vol. 37, pp. 917-926, Mar 1999.

[92] Y. Q. Zeng, Q. H. Liu, and G. Zhao, "Multidomain pseudospectral time-domain (PSTD) method for acoustic waves in lossy media," *Journal of Computational Acoustics,* vol. 12, pp. 277-299, Sep 2004.

[93] Y. Q. Zeng, Q. H. Liu, and G. Zhao, "Response to Comment on "Multidomain Pseudospectral Time-Domain (Pstd) Method for Acoustic Waves in Lossy Media"," *Journal of Computational Acoustics,* vol. 16, pp. 469-470, Sep 2008.

[94] B. Fornberg, *A practical guide to pseudospectral methods*. Cambridge ; New York: Cambridge University Press, 1996.

[95] G. Wojcik, B. Fornberg, R. Waag, L. Carcione, J. Mould, L. Nikodym, *et al.*, "Pseudospectral methods for large-scale bioacoustic models," *1997 IEEE Ultrasonics Symposium Proceedings, Vols 1 & 2,* pp. 1501-1506, 1997.

[96] D. Gottlieb and J. S. Hesthaven, "Spectral methods for hyperbolic problems," *Journal of Computational and Applied Mathematics,* vol. 128, pp. 83-131, Mar 1 2001.

[97] N. N. Bojarski, "The K-Space Formulation of the Scattering Problem in the Time Domain - an Improved Single Propagator Formulation," *The Journal of the Acoustical Society of America,* vol. 77, pp. 826-831, 1985.

[98] N. N. Bojarski, "The K-Space Formulation of the Scattering Problem in the Time Domain," *The Journal of the Acoustical Society of America,* vol. 72, pp. 570-584, 1982.

[99] B. T. Cox and P. C. Beard, "Fast calculation of pulsed photoacoustic fields in fluids using k-space methods," *The Journal of the Acoustical Society of America,* vol. 117, pp. 3616-3627, Jun 2005.

[100] B. T. Cox, S. Kara, S. R. Arridge, and P. C. Beard, "k-space propagation models for acoustically heterogeneous media: Application to biomedical photoacoustics," *The Journal of the Acoustical Society of America,* vol. 121, pp. 3453-3464, Jun 2007.

[101] T. D. Mast, L. P. Souriau, D. L. D. Liu, M. Tabei, A. I. Nachman, and R. C. Waag, "A k-space method for large-scale models of wave propagation in tissue," *IEEE Transactions on Ultrasonics Ferroelectrics and Frequency Control,* vol. 48, pp. 341-354, Mar 2001.

[102] J. C. Tillett, M. I. Daoud, J. C. Lacefield, and R. C. Waag, "A k-space method for acoustic propagation using coupled first-order equations in three dimensions," *The Journal of the Acoustical Society of America,* vol. 126, pp. 1231-1244, Sep 2009.

[103] B. E. Treeby and B. T. Cox, "A k-space Green's function solution for acoustic initial value problems in homogeneous media with power law absorption," *The Journal of the Acoustical Society of America,* vol. 129, pp. 3652-3660, Jun 2011.

[104] S. Qiao, G. F. Shen, J. F. Bai, and Y. Z. Chen, "Transcostal high-intensity focused ultrasound treatment using phased array with geometric correction," *The Journal of the Acoustical Society of America,* vol. 134, pp. 1503-1514, Aug 2013.

[105] S. Operto, J. Virieux, P. Amestoy, J. Y. L'Excellent, L. Giraud, and H. B. H. Ali, "3D finite-difference frequency-domain modeling of visco-acoustic wave propagation using a massively parallel direct solver: A feasibility study," *Geophysics,* vol. 72, pp. Sm195-Sm211, Sep-Oct 2007.

[106] M. G. Wismer, "Finite element analysis of broadband acoustic pulses through inhomogenous media with power law attenuation," *The Journal of the Acoustical Society of America,* vol. 120, pp. 3493-3502, Dec 2006.

[107] R. J. Zemp, J. Tavakkoli, and R. S. C. Cobbold, "Modeling of nonlinear ultrasound propagation in tissue from array transducers," *The Journal of the Acoustical Society of America,* vol. 113, pp. 139-152, Jan 2003.

[108] P. T. Christopher and K. J. Parker, "New Approaches to Nonlinear Diffractive Field Propagation," *The Journal of the Acoustical Society of America,* vol. 90, pp. 488-499, Jul 1991.

[109] J. Tavakkoli, D. Cathignol, R. Souchon, and O. A. Sapozhnikov, "Modeling of pulsed finite-amplitude focused sound beams in time domain," *The Journal of the Acoustical Society of America,* vol. 104, pp. 2061-2072, Oct 1998.

[110] V. A. Khokhlova, R. Souchon, J. Tavakkoli, O. A. Sapozhnikov, and D. Cathignol, "Numerical modeling of finite-amplitude sound beams: Shock formation in the near field of a cw plane piston source," *The Journal of the Acoustical Society of America,* vol. 110, pp. 95-108, Jul 2001.

[111] J. Berntsen, "Numerical-Calculations of Finite-Amplitude Sound Beams," *Frontiers of Nonlinear Acoustics,* pp. 191-196, 1990.

[112] M. A. Averkiou and R. O. Cleveland, "Modeling of an electrohydraulic lithotripter with the KZK equation," *The Journal of the Acoustical Society of America,* vol. 106, pp. 102-112, Jul 1999.

[113] M. A. Averkiou and M. F. Hamilton, "Nonlinear distortion of short pulses radiated by plane and focused circular pistons," *The Journal of the Acoustical Society of America,* vol. 102, pp. 2539-2548, Nov 1997.

[114] V. A. Khokhlova, A. E. Ponomarev, M. A. Averkiou, and L. A. Crum, "Nonlinear pulsed ultrasound beams radiated by rectangular focused diagnostic transducers," *Acoustical Physics,* vol. 52, pp. 481-489, Jul-Aug 2006.

[115] M. H. Hasani, S. Gharibzadeh, Y. Farjami, and J. Tavakkoli, "Unmitigated numerical solution to the diffraction term in the parabolic nonlinear ultrasound wave equation," *The Journal of the Acoustical Society of America,* vol. 134, pp. 1775-1790, Sep 2013.

[116] S. I. Aanonsen, T. Barkve, J. N. Tjotta, and S. Tjotta, "Distortion and Harmonic-Generation in the Nearfield of a Finite-Amplitude Sound Beam," *The Journal of the Acoustical Society of America,* vol. 75, pp. 749-768, 1984.

[117] T. S. Hart and M. F. Hamilton, "Nonlinear Effects in Focused Sound Beams," *The Journal of the Acoustical Society of America,* vol. 84, pp. 1488-1496, Oct 1988.

[118] T. Kamakura, N. Hamada, K. Aoki, and Y. Kumamoto, "Nonlinearly Generated Spectral Components in the Nearfield of a Directive Sound Source," *The Journal of the Acoustical Society of America,* vol. 85, pp. 2331-2337, Jun 1989.

[119] T. Kamakura, M. Tani, Y. Kumamoto, and K. Ueda, "Harmonic-Generation in Finite-Amplitude Sound Beams from a Rectangular Aperture Source," *The Journal of the Acoustical Society of America,* vol. 91, pp. 3144-3151, Jun 1992.

[120] Y. A. Pishchalnikov, O. A. Sapozhnikov, and V. A. Khokhlova, "A modification of the spectral description of nonlinear acoustic waves with discontinuities," *Acoustical Physics,* vol. 42, pp. 362-367, May-Jun 1996.

[121] F. P. Curra, P. D. Mourad, V. A. Khokhlova, R. O. Cleveland, and L. A. Crum, "Numerical simulations of heating patterns and tissue temperature response due to high-intensity focused ultrasound," *IEEE Transactions on Ultrasonics Ferroelectrics and Frequency Control,* vol. 47, pp. 1077-1089, Jul 2000.

[122] A. Bouakaz, C. T. Lancee, and N. de Jong, "Harmonic ultrasonic field of medical phased arrays: Simulations and measurements," *IEEE Transactions on Ultrasonics Ferroelectrics and Frequency Control,* vol. 50, pp. 730-735, Jun 2003.

[123] A. Kurganov and E. Tadmor, "New high-resolution central schemes for nonlinear conservation laws and convection-diffusion equations," *Journal of Computational Physics,* vol. 160, pp. 241-282, May 2000.

[124] I. M. Hallaj, R. O. Cleveland, and K. Hynynen, "Simulations of the thermo-acoustic lens effect during focused ultrasound surgery," *The Journal of the Acoustical Society of America,* vol. 109, pp. 2245-2253, May 2001.

[125] A. Doinikov, A. Novell, P. Calmon, and A. Bouakaz, "Simulations and measurements of 3-D ultrasonic fields radiated by phased-array transducers using the Westervelt equation," *IEEE Transactions on Ultrasonics, Ferroelectrics, and Frequency Control,* vol. 61, pp. 1470-1477, 2014.

[126] S. Ginter, M. Liebler, E. Steiger, T. Dreyer, and R. E. Ridelinger, "Full-wave modeling of therapeutic ultrasound: Nonlinear ultrasound propagation in ideal fluids," *The Journal of the Acoustical Society of America,* vol. 111, pp. 2049-2059, May 2002.

[127] M. Liebler, S. Ginter, T. Dreyer, and R. E. Riedlinger, "Full wave modeling of therapeutic ultrasound: Efficient time-domain implementation of the frequency power-law attenuation," *The Journal of the Acoustical Society of America,* vol. 116, pp. 2742-2750, Nov 2004.

[128] Y. Jing, J. Cannata, and T. R. Wang, "Experimental verification of transient nonlinear acoustical holography," *The Journal of the Acoustical Society of America,* vol. 133, pp. 2533-2540, May 2013.

[129] Y. Jing, M. L. Tao, and J. Cannata, "An Improved Wave-Vector Frequency-Domain Method for Nonlinear Wave Modeling," *IEEE Transactions on Ultrasonics Ferroelectrics and Frequency Control,* vol. 61, pp. 515-524, Mar 2014.

[130] F. Prieur, T. F. Johansen, S. Holm, and H. Torp, "Fast simulation of second harmonic ultrasound field using a quasi-linear method," *The Journal of the Acoustical Society of America,* vol. 131, pp. 4365-4375, Jun 2012.

[131] J. Huijssen and M. D. Verweij, "An iterative method for the computation of nonlinear, wide-angle, pulsed acoustic fields of medical diagnostic transducers," *The Journal of the Acoustical Society of America,* vol. 127, pp. 33-44, Jan 2010.

[132] M. D. Verweij and J. Huijssen, "A filtered convolution method for the computation of acoustic wave fields in very large spatiotemporal domains," *The Journal of the Acoustical Society of America,* vol. 125, pp. 1868-1878, Apr 2009.

[133] M. D. Verweij, L. Demi, and K. W. A. van Dongen, "Computation of nonlinear ultrasound fields using a linearized contrast source method," *The Journal of the Acoustical Society of America,* vol. 134, pp. 1442-1453, Aug 2013.

[134] J. Hoffelner, H. Landes, M. Kaltenbacher, and R. Lerch, "Finite element simulation of nonlinear wave propagation in thermoviscous fluids including dissipation," *IEEE Transactions on Ultrasonics Ferroelectrics and Frequency Control,* vol. 48, pp. 779-786, May 2001.

[135] T. Walsh and M. Torres, "Finite element methods for nonlinear acoustics in fluids," *Journal of Computational Acoustics,* vol. 15, pp. 353-375, Sep 2007.

[136] B. E. Treeby, "Modeling Nonlinear Wave Propagation on Nonuniform Grids Using a Mapped k-Space Pseudospectral Method," *IEEE Transactions on Ultrasonics Ferroelectrics and Frequency Control,* vol. 60, pp. 2208-2213, Oct 2013.

[137] L. Demi, M. D. Verweij, and K. W. A. van Dongen, "Modeling Three-Dimensional Nonlinear Acoustic Wave Fields in Media with Spatially Varying Coefficient of Nonlinearity, Attenuation and Speed of Sound," *2012 IEEE International Ultrasonics Symposium (Ius),* pp. 519-522, 2012.

[138] L. Demi, K. W. A. van Dongen, and M. D. Verweij, "A contrast source method for nonlinear acoustic wave fields in media with spatially inhomogeneous attenuation," *The Journal of the Acoustical Society of America,* vol. 129, pp. 1221-1230, Mar 2011.

[139] F. Varray, A. Ramalli, C. Cachard, P. Tortoli, and O. Basset, "Fundamental and Second-Harmonic Ultrasound Field Computation of Inhomogeneous Nonlinear Medium With a Generalized Angular Spectrum Method," *IEEE Transactions on Ultrasonics Ferroelectrics and Frequency Control*, vol. 58, pp. 1366-1376, Jul 2011.

[140] F. Varray, O. Basset, P. Tortoli, and C. Cachard, "Creanuis: A Non-Linear Radiofrequency Ultrasound Image Simulator," *Ultrasound in Medicine and Biology*, vol. 39, pp. 1915-1924, Oct 2013.

[141] N. Albin, O. P. Bruno, T. Y. Cheung, and R. O. Cleveland, "Fourier continuation methods for high-fidelity simulation of nonlinear acoustic beams," *The Journal of the Acoustical Society of America*, vol. 132, pp. 2371-2387, Oct 2012.

[142] L. Demi, B. Treeby, and M. D. Verweij, "Comparison between two different full-wave methods for the computation of nonlinear ultrasound fields in inhomogeneous and attenuating tissue," *presented at the Ultrasonics Symposium (IUS)*, 2014 IEEE International Chicago, IL, 2014.

[143] J. Huijssen, M. D. Verweij, and N. de Jong, "Comparison of an angular spectrum method and a Green's function method for nonlinear propagation of pulsed acoustic fields from medical phased array transducers," *2007 IEEE Ultrasonics Symposium Proceedings, Vols 1-6*, pp. 1740-1743, 2007.

[144] F. Varray, O. Basset, C. Cachard, L. Demi, K. W. A. van Dongen, and M. D. Verweij, "Nonlinear acoustic propagation simulation tools: Comparison of BBGASM and INCS up to the fifth harmonic component," *2013 IEEE International Ultrasonics Symposium (Ius)*, pp. 1025-1028, 2013.

[145] E. A. Filonenko and V. A. Khokhlova, "Effect of acoustic nonlinearity on heating of biological tissue by high-intensity focused ultrasound," *Acoustical Physics,* vol. 47, pp. 468-475, Jul-Aug 2001.

[146] O. V. Bessonova, V. A. Khokhlova, M. R. Bailey, M. S. Canney, and L. A. Crum, "Focusing of high power ultrasound beams and limiting values of shock wave parameters," *Acoustical Physics,* vol. 55, pp. 463-473, Oct 2009.

[147] O. M. Al-Bataineh, C. M. Collins, E. J. Park, H. Lee, and N. B. Smith, "MR thermometry characterization of a hyperthermia ultrasound array designed using the k-space computational method," *Biomedical Engineering Online,* vol. 5, Oct 25 2006.

[148] D. Pajek and K. Hynynen, "The design of a focused ultrasound transducer array for the treatment of stroke: a simulation study," *Physics in Medicine and Biology,* vol. 57, pp. 4951-4968, Aug 7 2012.

[149] X. Z. Zeng, J. Li, and R. J. McGough, "A waveform diversity method for optimizing 3-D power depositions generated by ultrasound phased arrays," *IEEE Transactions on Biomedical Engineering*, vol. 57, pp. 41–47, Jan. 2010.

[150] C. Baron, J. F. Aubry, M. Tanter, S. Meairs, and M. Fink, "Simulation of Intracranial Acoustic Fields in Clinical Trials of Sonothrombolysis," *Ultrasound in Medicine and Biology,* vol. 35, pp. 1148-1158, Jul 2009.

[151] P. B. Rosnitskiy, P. V. Yuldashev, and V. A. Khokhlova, "Effect of the angular aperture of medical ultrasound transducers on the parameters of nonlinear ultrasound field with shocks at the focus," *Acoustical Physics,* vol. 61, pp. 301-307, May 2015.

[152] M. Rao, T. Varghese, and J. A. Zagzebski, "Simulation of ultrasound two-dimensional array transducers using a frequency domain model," *Medical Physics,* vol. 35, pp. 3162-3169, Jul 2008.

[153] Y. N. Makov, V. J. Sanchez-Morcillo, F. Camarena, and V. Espinosa, "Nonlinear change of on-axis pressure and intensity maxima positions and its relation with the linear focal shift effect," *Ultrasonics,* vol. 48, pp. 678-686, Dec 2008.

[154] G. S. Chen, C. Y. Lin, J. S. Jeong, J. M. Cannata, W. L. Lin, H. Chang, *et al.*, "Design and Characterization of Dual-Curvature 1.5-Dimensional High-Intensity Focused Ultrasound Phased-Array Transducer," *IEEE Transactions on Ultrasonics Ferroelectrics and Frequency Control,* vol. 59, pp. 150-155, Jan 2012.

[155] K. Okita, R. Narumi, T. Azuma, S. Takagi, and Y. Matumoto, "The role of numerical simulation for the development of an advanced HIFU system," *Computational Mechanics,* vol. 54, pp. 1023-1033, Oct 2014.

[156] B. Puel, D. Lesselier, S. Chatillon, and P. Calmon, "Simulation-Based Optimization of the Design and Settings of Ultrasonic Phased-Array Transducers with an Evolutionary Algorithm," *Review of Progress in Quantitative Nondestructive Evaluation, Vols 30a and 30b,* vol. 1335, pp. 906-913, 2011.

[157] G. Bouchoux, R. Shivashankar, T. A. Abruzzo, and C. K. Holland, "In Silico Study of Low-Frequency Transcranial Ultrasound Fields in Acute Ischemic Stroke Patients," *Ultrasound in Medicine and Biology,* vol. 40, pp. 1154-1166, Jun 2014.

[158] Y. N. Makov, V. Espinosa, V. J. Sanchez-Morcillo, J. Ramis, J. Cruanes, and F. Camarena, "Strong on-axis focal shift and its nonlinear variation in low-Fresnel-number ultrasound

beams," *The ournal of the Acoustical Society of America,* vol. 119, pp. 3618-3624, Jun 2006.

[159] O. A. Sapozhnikov, Y. A. Pishchal'nikov, and A. V. Morozov, "Reconstruction of the normal velocity distribution on the surface of an ultrasonic transducer from the acoustic pressure measured on a reference surface," *Acoustical Physics,* vol. 49, pp. 354-360, May-Jun 2003.

[160] O. A. Sapozhnikov, A. E. Ponomarev, and M. A. Smagin, "Transient acoustic holography for reconstructing the particle velocity of the surface of an acoustic transducer," *Acoustical Physics,* vol. 52, pp. 324-330, May-Jun 2006.

[161] "Ultrasonics-field characterization—specification and measurement of field parameters for high intensity therapeutic ultrasound (HITU) transducers and systems," in *IEC/TS62556, ed. International Electrotechnical Commission,* Geneva, Switzerland, 2014.

[162] O. V. Bessonova and V. Wilkens, "Membrane Hydrophone Measurement and Numerical Simulation of HIFU Fields up to Developed Shock Regimes," *IEEE Transactions on Ultrasonics Ferroelectrics and Frequency Control,* vol. 60, pp. 290-300, Feb 2013.

[163] T. Chen, T. B. Fan, W. Zhang, Y. Y. Qiu, J. Tu, X. S. Guo, *et al.*, "Acoustic characterization of high intensity focused ultrasound fields generated from a transmitter with a large aperture," *Journal of Applied Physics,* vol. 115, Mar 2014.

[164] C. Perez, H. Chen, T. J. Matula, M. Karzova, and V. A. Khokhlova, "Acoustic field characterization of the Duolith: Measurements and modeling of a clinical shock wave therapy device," *The Journal of the Acoustical Society of America,* vol. 134, pp. 1663-1674, Aug 2013.

[165] X. Ji, G. F. Shen, J. F. Bai, and Y. Z. Chen, "The characterization of an ultrasound spherical phased array for the ablation of deep-seated tissue," *Applied Acoustics,* vol. 73, pp. 529-534, May 2012.

[166] G. R. Harris, "FDA Regulation of Clinical High Intensity Focused Ultrasound (HIFU) Devices," *2009 Annual International Conference of the IEEE Engineering in Medicine and Biology Society, Vols 1-20,* pp. 145-148, 2009.

[167] J. S. Jeong, "Phase-apodisation technique to extend depth of field for high-frequency ultrasound imaging," *Electronics Letters,* vol. 49, Dec 2013.

[168] J. F. Cruza, J. Camacho, L. Serrano-Iribarnegaray, and C. Fritsch, "New Method for Real-Time Dynamic Focusing Through Interfaces," *IEEE Transactions on Ultrasonics Ferroelectrics and Frequency Control,* vol. 60, pp. 739-751, Apr 2013.

[169] R. M. Jones, M. A. O'Reilly, and K. Hynynen, "Transcranial passive acoustic mapping with hemispherical sparse arrays using CT-based skull-specific aberration corrections: a simulation study," *Physics in Medicine and Biology,* vol. 58, pp. 4981-5005, Jul 2013.

[170] F. M. Hooi and P. L. Carson, "First-arrival traveltime sound speed inversion with a priori information," *Medical Physics,* vol. 41, pp. 548-561, Aug 2014.

[171] D. Hyun, G. E. Trahey, M. Jakovljevic, and J. J. Dahl, "Short-Lag Spatial Coherence Imaging on Matrix Arrays, Part I: Beamforming Methods and Simulation Studies," *IEEE Transactions on Ultrasonics Ferroelectrics and Frequency Control,* vol. 61, pp. 1101-1112, Jul 2014.

[172] L. Demi, M. D. Verweij, and K. W. A. van Dongen, "Parallel Transmit Beamforming Using Orthogonal Frequency Division Multiplexing Applied to Harmonic Imaging-A

Feasibility Study," *IEEE Transactions on Ultrasonics Ferroelectrics and Frequency Control,* vol. 59, pp. 2439-2447, Nov 2012.

[173] L. Tong, H. Gao, H. F. Choi, and J. D'hooge, "Comparison of Conventional Parallel Beamforming with Plane Wave and Diverging Wave Imaging for Cardiac Applications: A Simulation Study," *IEEE Transactions on Ultrasonics Ferroelectrics and Frequency Control,* vol. 59, pp. 1654-1663, Aug 2012.

[174] A. Karamalis, W. Wein, and N. Navab, "Fast Ultrasound Image Simulation Using the Westervelt Equation," *Medical Image Computing and Computer-Assisted Intervention - Miccai 2010, Pt I,* vol. 6361, pp. 243-250, 2010.

[175] L. A. Aguilar, R. S. C. Cobbold, and D. A. Steinman, "Fast and Mechanistic Ultrasound Simulation Using a Point Source/Receiver Approach," *IEEE Transactions on Ultrasonics Ferroelectrics and Frequency Control,* vol. 60, pp. 2335-2346, Nov 2013.

[176] Y. D. Li and J. A. Zagzebski, "Computer model for harmonic ultrasound imaging," *IEEE Transactions on Ultrasonics Ferroelectrics and Frequency Control,* vol. 47, pp. 1259-1272, Sep 2000.

[177] B. E. Treeby, M. Tumen, and B. T. Cox, "Time Domain Simulation of Harmonic Ultrasound Images and Beam Patterns in 3D Using the k-space Pseudospectral Method," *Medical Image Computing and Computer-Assisted Intervention, Miccai 2011, Pt I,* vol. 6891, pp. 363-370, 2011.

[178] T. R. Wang and Y. Jing, "Transcranial ultrasound imaging with speed of sound-based phase correction: a numerical study," *Physics in Medicine and Biology,* vol. 58, pp. 6663-6681, Oct 2013.

[179] T. Varslot, S. E. Masoy, T. F. Johansen, and B. Angelsen, "Aberration in nonlinear acoustic wave propagation," *IEEE Transactions on Ultrasonics Ferroelectrics and Frequency Control*, vol. 54, pp. 470-479, Mar 2007.

[180] L. J. Huang, Y. Z. Lin, Z. G. Zhang, Y. Labyed, S. R. Tan, N. Nguyen, *et al.*, "Breast ultrasound waveform tomography: Using both transmission and reflection data, and numerical virtual point sources," *Medical Imaging 2014: Ultrasonic Imaging and Tomography*, vol. 9040, 2014.

[181] Y. Z. Lin, L. J. Huang, and Z. G. Zhang, "Ultrasound waveform tomography with the total-variation regularization for detection of small breast tumors," *Medical Imaging 2012: Ultrasonic Imaging, Tomography, and Therapy*, vol. 8320, 2012.

[182] Z. G. Zhang and L. J. Huang, "Efficient implementation of ultrasound waveform tomography using data blending," *Medical Imaging 2014: Ultrasonic Imaging and Tomography*, vol. 9040, 2014.

[183] B. E. Treeby, E. Z. Zhang, and B. T. Cox, "Photoacoustic tomography in absorbing acoustic media using time reversal," *Inverse Problems*, vol. 26, Nov 2010.

[184] C. Huang, K. Wang, L. M. Nie, L. H. V. Wang, and M. A. Anastasio, "Full-Wave Iterative Image Reconstruction in Photoacoustic Tomography With Acoustically Inhomogeneous Media," *IEEE Transactions on Medical Imaging*, vol. 32, pp. 1097-1110, Jun 2013.

[185] B. E. Treeby, T. K. Varslot, E. Z. Zhang, J. G. Laufer, and P. C. Beard, "Automatic sound speed selection in photoacoustic image reconstruction using an autofocus approach," *Journal of Biomedical Optics*, vol. 16, Sep 2011.

[186] C. Huang, L. M. Nie, R. W. Schoonover, Z. J. Guo, C. O. Schirra, M. A. Anastasio, *et al.*, "Aberration correction for transcranial photoacoustic tomography of primates employing adjunct image data," *Journal of Biomedical Optics,* vol. 17, Jun 2012.

[187] G. T. Clement and K. Hynynen, "A non-invasive method for focusing ultrasound through the human skull," *Physics in Medicine and Biology,* vol. 47, pp. 1219-1236, Apr 21 2002.

[188] J. F. Aubry, M. Tanter, M. Pernot, J. L. Thomas, and M. Fink, "Experimental demonstration of noninvasive transskull adaptive focusing based on prior computed tomography scans," *Journal of the Acoustical Society of America,* vol. 113, pp. 84-93, Jan 2003.

[189] Y. Jing, F. C. Meral, and G. T. Clement, "Time-reversal transcranial ultrasound beam focusing using a k-space method," *Physics in Medicine and Biology,* vol. 57, pp. 901-917, Feb 2012.

[190] P. Gelat, G. ter Haar, and N. Saffari, "A comparison of methods for focusing the field of a HIFU array transducer through human ribs," *Physics in Medicine and Biology,* vol. 59, pp. 3139-3171, Jun 2014.

[191] M. A. Solovchuk, S. C. Hwang, H. Chang, M. Thiriet, and T. W. H. Sheu, "Temperature elevation by HIFU in ex vivo porcine muscle: MRI measurement and simulation study," *Medical Physics,* vol. 41, May 2014.

[192] L. S. Wu, V. Amin, R. Roberts, and T. Ryken, "An interactive HIFU therapy planning sing simulation & visualization," *6th International Symposium on Therapeutic Ultrasound,* vol. 911, pp. 150-156, 2007.

[193] M. M. Paulides, P. R. Stauffer, E. Neufeld, P. F. Maccarini, A. Kyriakou, R. A. M. Canters, *et al.*, "Simulation techniques in hyperthermia treatment planning," *International Journal of Hyperthermia*, vol. 29, pp. 346-357, 2013.

[194] Y. F. Zhou, "Generation of uniform lesions in high intensity focused ultrasound ablation," *Ultrasonics*, vol. 53, pp. 495-505, Feb 2013.

[195] P. J. White, B. Andre, N. McDannold, and G. T. Clement, "A Pre-treatment Planning Strategy for High-Intensity Focused Ultrasound (HIFU) Treatments," *2008 IEEE Ultrasonics Symposium, Vols 1-4 and Appendix*, pp. 2056-2058, 2008.

[196] J. W. Jenne, T. Preusser, and M. Gunther, "High-intensity focused ultrasound: Principles, therapy guidance, simulations and applications," *Zeitschrift Fur Medizinische Physik*, vol. 22, pp. 311-322, 2012.

[197] D. Sinden and G. t. Haar, "Dosimetry implications for correct ultrasound dose deposition: uncertainties in descriptors, planning and treatment delivery," *Translational Cancer Research*, vol. 3, pp. 459-471, 2014.

[198] T. E. Vaughan and K. Hynynen, "Effects of parameter errors in the simulation of transcranial focused ultrasound," *Physics in Medicine and Biology*, vol. 47, pp. 37-45, Jan 2002.

[199] B. E. Treeby and B. T. Cox, "k-Wave: MATLAB toolbox for the simulation and reconstruction of photoacoustic wave fields," *Journal of Biomedical Optics*, vol. 15, Mar-Apr 2010.

[200] C. Yoon, Y. Yoo, T. K. Song, and J. H. Chang, "Pixel based focusing for photoacoustic and ultrasound dual-modality imaging," *Ultrasonics*, vol. 54, pp. 2126-2133, Dec 2014.

[201] Y. Jing and G. T. Clement, "On the use of Gegenbauer reconstructions for shock wave propagation modeling," *Journal of the Acoustical Society of America,* vol. 130, pp. 1115-1124, Sep 2011.

[202] T. Huttunen, M. Malinen, J. P. Kaipio, P. J. White, and K. Hynynen, "A full-wave Helmholtz model for continuous-wave ultrasound transmission," *IEEE Transactions on Ultrasonics Ferroelectrics and Frequency Control,* vol. 52, pp. 397-409, Mar 2005.

[203] R. Mehra, N. Raghuvanshi, L. Savioja, M. C. Lin, and D. Manocha, "An efficient GPU-based time domain solver for the acoustic wave equation," *Applied Acoustics,* vol. 73, pp. 83-94, Feb 2012.

[204] N. Nandapalan, J. Jaros, A. P. Rendell, and B. Treeby, "Implementation of 3D FFTs Across Multiple GPUs in Shared Memory Environments," *2012 13th International Conference on Parallel and Distributed Computing, Applications, and Technologies (Pdcat 2012),* pp. 167-172, 2012.

[205] F. Varray, C. Cachard, A. Ramalli, P. Tortoli, and O. Basset, "Simulation of ultrasound nonlinear propagation on GPU using a generalized angular spectrum method," *Eurasip Journal on Image and Video Processing,* 2011.

[206] B. Burger, S. Bettinghausen, M. Radle, and J. Hesser, "Real-Time GPU-Based Ultrasound Simulation Using Deformable Mesh Models," *IEEE Transactions on Medical Imaging,* vol. 32, pp. 609-618, Mar 2013.

[207] Y. Tamura, N. Tsurumi, and Y. Matsumoto, "Numerical Simulation of Cavitation in Ultrasound Field," *10th International Symposium on Therapeutic Ultrasound (Istu 2010),* vol. 1359, pp. 431-436, 2011.

[208] T. Moriyama, S. Yoshizawa, and S. Umemura, "Thermal Simulation of Cavitation-Enhanced Ultrasonic Heating Verified with Tissue-Mimicking Gel," *Japanese Journal of Applied Physics*, vol. 51, Jul 2012.

[209] N. Bretz, J. Strobel, M. Kaltenbacher, and R. Lerch, "Numerical simulation of ultrasonic waves in cavitating fluids with special consideration of ultrasonic cleaning," *2005 IEEE Ultrasonics Symposium, Vols 1-4*, pp. 703-706, 2005.

[210] M. Solovchuk, T. W. H. Sheu, and M. Thiriet, "Simulation of nonlinear Westervelt equation for the investigation of acoustic streaming and nonlinear propagation effects," *Journal of the Acoustical Society of America*, vol. 134, pp. 3931-3942, Nov 2013.

[211] J. A. Jensen and S. I. Nikolov, "Fast simulation of ultrasound images," *2000 IEEE Ultrasonics Symposium Proceedings, Vols 1 and 2*, pp. 1721-1724, 2000.

[212] M. E. Frijlink, H. Kaupang, T. Varslot, and S. E. Masoy, "Abersim: a Simulation Program for 3D Nonlinear Acoustic Wave Propagation for Arbitrary Pulses and Arbitrary Transducer Geometries," *2008 IEEE Ultrasonics Symposium, Vols 1-4 and Appendix*, pp. 1282-1285, 2008.

[213] J. E. Soneson, "A User-Friendly Software Package for HIFU Simulation," *8th International Symposium on Therapeutic Ultrasound*, vol. 1113, pp. 165-169, 2009.

[214] A. H. Chan, V. Y. Fujimoto, D. E. Moore, R. W. Martin, and S. Vaezy, "An image-guided high intensity focused ultrasound device for uterine fibroids treatment," *Medical Physics*, vol. 29, pp. 2611-2620, 2002.

[215] F. Wu, Z.-B. Wang, Y.-D. Cao, W. Chen, J. Bai, J. Zou, *et al.*, "A randomised clinical trial of high-intensity focused ultrasound ablation for the treatment of patients with localised breast cancer," *British Journal of Cancer*, vol. 89, pp. 2227-2233, 2003.

[216] F. Wu, Z.-B. Wang, H. Zhu, W.-Z. Chen, J.-Z. Zou, J. Bai, *et al.*, "Extracorporeal high intensity focused ultrasound treatment for patients with breast cancer," *Breast Cancer Research and Treatment,* vol. 92, pp. 51-60, 2005.

[217] J. Jagannathan, N. K. Sanghvi, L. A. Crum, C.-P. Yen, R. Medel, A. S. Dumont, *et al.*, "High intensity focused ultrasound surgery (HIFU) of the brain: a historical perspective, with modern applications," *Neurosurgery,* vol. 64, p. 201, 2009.

[218] A. Burgess, Y. Huang, A. C. Waspe, M. Ganguly, D. E. Goertz, and K. Hynynen, "High-intensity focused ultrasound (HIFU) for dissolution of clots in a rabbit model of embolic stroke," *PloS one,* vol. 7, p. e42311, 2012.

[219] T. D. Khokhlova and J. H. Hwang, "HIFU for palliative treatment of pancreatic cancer," *Journal of Gastrointestinal Oncology,* vol. 2, pp. 175-184, 2011.

[220] H. J. Jang, J.-Y. Lee, D.-H. Lee, W.-H. Kim, and J. H. Hwang, "Current and future clinical applications of high-intensity focused ultrasound (HIFU) for pancreatic cancer," *Gut and Liver,* vol. 4, pp. S57-S61, 2010.

[221] R. J. McGough, M. Kessler, E. Ebbini, and C. Cain, "Treatment planning for hyperthermia with ultrasound phased arrays," *IEEE Transactions on Ultrasonics Ferroelectrics and Frequency Control,* vol. 43, pp. 1074-1084, 1996.

[222] F. Dagrau, M. Rénier, R. Marchiano, and F. Coulouvrat, "Acoustic shock wave propagation in a heterogeneous medium: A numerical simulation beyond the parabolic approximation," *The Journal of the Acoustical Society of America,* vol. 130, pp. 20-32, 2011.

[223] J. Gu and Y. Jing, "Numerical Modeling of Ultrasound Propagation in Weakly Heterogeneous Media Using a Mixed Domain Method," *IEEE Transactions on Ultrasonics Ferroelectrics and Frequency Control*, vol. 65, pp. 1258-1267, 2018.

[224] K. R. Waters, M. S. Hughes, J. Mobley, and J. G. Miller, "Differential forms of the Kramers-Kronig dispersion relations," *IEEE Transactions on Ultrasonics Ferroelectrics and Frequency Control*, vol. 50, pp. 68-76, 2003.

[225] K. R. Waters, J. Mobley, and J. G. Miller, "Causality-imposed (Kramers-Kronig) relationships between attenuation and dispersion," *IEEE Transactions on Ultrasonics Ferroelectrics and Frequency Control*, vol. 52, pp. 822-823, 2005.

[226] J. Mobley, K. R. Waters, and J. G. Miller, "Causal determination of acoustic group velocity and frequency derivative of attenuation with finite-bandwidth Kramers-Kronig relations," *Physical Review E*, vol. 72, p. 016604, 2005.

[227] J. F. Kelly, R. J. McGough, and M. M. Meerschaert, "Analytical time-domain Green's functions for power-law media," *The Journal of the Acoustical Society of America*, vol. 124, pp. 2861-2872, 2008.

[228] T. L. Szabo, "Causal theories and data for acoustic attenuation obeying a frequency power law," *The Journal of the Acoustical Society of America*, vol. 97, pp. 14-24, 1995.

[229] J. Gu and Y. Jing, "Simulation of the Second Harmonic Ultrasound Field in Heterogeneous Soft Tissue Using a Mixed Domain Method," *IEEE Transactions on Ultrasonics Ferroelectrics and Frequency Control*, 2019.

[230] L. E. Kinsler, A. R. Frey, A. B. Coppens, and J. V. Sanders, "Fundamentals of acoustics,", 4th ed., Hoboken, NJ, USA: Wiley, ch. 6, sec. 2, pp. 150–152, 1999.

[231] V. A. Khokhlova, P. V. Yuldashev, P. B. Rosnitskiy, A. D. Maxwell, W. Kreider, M. R. Bailey, *et al.*, "Design of HIFU transducers to generate specific nonlinear ultrasound fields," *Physics Procedia,* vol. 87, pp. 132-138, 2016.

[232] J. L. Robertson, B. T. Cox, J. Jaros, and B. E. Treeby, "Accurate simulation of transcranial ultrasound propagation for ultrasonic neuromodulation and stimulation," *The Journal of the Acoustical Society of America,* vol. 141, pp. 1726-1738, 2017.

[233] A. C. Cangellaris and D. B. Wright, "Analysis of the numerical error caused by the stair-stepped approximation of a conducting boundary in FDTD simulations of electromagnetic phenomena," *IEEE Transactions on Antennas and Propagation,* vol. 39, pp. 1518-1525, 1991.

[234] D. L. Phillips, "A technique for the numerical solution of certain integral equations of the first kind," *Journal of the ACM,* vol. 9, pp. 84-97, 1962.

[235] G. Sandhu, C. Li, O. Roy, S. Schmidt, and N. Duric, "Frequency domain ultrasound waveform tomography: breast imaging using a ring transducer," *Physics in Medicine & Biology,* vol. 60, p. 5381, 2015.

[236] M. Pérez-Liva, J. Herraiz, J. Udías, E. Miller, B. Cox, and B. Treeby, "Time domain reconstruction of sound speed and attenuation in ultrasound computed tomography using full wave inversion a," *The Journal of the Acoustical Society of America,* vol. 141, pp. 1595-1604, 2017.

[237] K. Wang, T. Matthews, F. Anis, C. Li, N. Duric, and M. A. Anastasio, "Waveform inversion with source encoding for breast sound speed reconstruction in ultrasound computed tomography," *IEEE Transactions on Ultrasonics Ferroelectrics and Frequency Control,* vol. 62, pp. 475-493, 2015.

[238] B. Ward, A. Baker, and V. Humphrey, "Nonlinear propagation applied to the improvement of resolution in diagnostic medical ultrasound," *The Journal of the Acoustical Society of America*, vol. 101, pp. 143-154, 1997.

[239] F. Tranquart, N. Grenier, V. Eder, and L. Pourcelot, "Clinical use of ultrasound tissue harmonic imaging," *Ultrasound in Medicine & Biology*, vol. 25, pp. 889-894, 1999.

[240] D. Zhang, X. Chen, and X.-f. Gong, "Acoustic nonlinearity parameter tomography for biological tissues via parametric array from a circular piston source—Theoretical analysis and computer simulations," *The Journal of the Acoustical Society of America*, vol. 109, pp. 1219-1225, 2001.

[241] A. Cai, J.-a. Sun, and G. Wade, "Imaging the acoustic nonlinear parameter with diffraction tomography," *IEEE Transactions on Ultrasonics Ferroelectrics and Frequency Control*, vol. 39, pp. 708-715, 1992.

[242] P. B. Rosnitskiy, P. V. Yuldashev, O. A. Sapozhnikov, A. D. Maxwell, W. Kreider, M. R. Bailey, et al., "Design of HIFU transducers for generating specified nonlinear ultrasound fields," *IEEE Transactions on Ultrasonics Ferroelectrics and Frequency Control*, vol. 64, pp. 374-390, 2017.

[243] K. Hynynen, "The role of nonlinear ultrasound propagation during hyperthermia treatments," *Medical Physics*, vol. 18, pp. 1156-1163, 1991.

[244] Hynynen, "Demonstration of enhanced temperature elevation due to nonlinear propagation of focussed ultrasound in dog's thigh in vivo," *Ultrasound in Medicine and Biology*, vol. 13, pp. 85-91, 1987.

[245] W. Swindell, "A theoretical study of nonlinear effects with focused ultrasound in tissues: an “Acoustic Bragg Peak”," *Ultrasound in Medicine and Biology*, vol. 11, pp. 121-130, 1985.

[246] P. V. Yuldashev, S. M. Shmeleva, S. A. Ilyin, O. A. Sapozhnikov, L. R. Gavrilov, and V. A. Khokhlova, "The role of acoustic nonlinearity in tissue heating behind a rib cage using a high-intensity focused ultrasound phased array," *Ultrasound in Medicine and Biology*, vol. 58, p. 2537, 2013.

[247] X. Zhang, G. E. Owens, H. S. Gurm, Y. Ding, C. A. Cain, and Z. Xu, "Noninvasive thrombolysis using histotripsy beyond the intrinsic threshold (microtripsy)," *IEEE Transactions on Ultrasonics Ferroelectrics and Frequency Control*, vol. 62, pp. 1342-1355, 2015.

[248] M. S. Canney, V. A. Khokhlova, O. V. Bessonova, M. R. Bailey, and L. A. Crum, "Shock-induced heating and millisecond boiling in gels and tissue due to high intensity focused ultrasound," *Ultrasound in Medicine and Biology*, vol. 36, pp. 250-267, 2010.

[249] X. Yan and M. F. Hamilton, "Angular spectrum decomposition analysis of second harmonic ultrasound propagation and its relation to tissue harmonic imaging,", in *Ultrasonic and Advanced Methods for Nondestructive Testing and Material Characterization*, N. Dartmouth, MA, pp. 155-168, 2007.

[250] T. D. Mast, “Empirical relationships between acoustic parameters in human soft tissues*,”* *Acoustics Research Letters Online*, vol. 1, no. 2, pp. 37–42, 2000.

[251] M. Pasovic, M. Danilouchkine, A. Van Der Steen, O. Basset, N. De Jong, and C. Cachard, "Extended angular spectrum method for calculation of higher harmonics," in *10ème Congrès Français d'Acoustique*, Lyon, France, 2010.

[252] W.-S. Gan, J. Yang, and T. Kamakura, "A review of parametric acoustic array in air," *Applied Acoustics,* vol. 73, pp. 1211-1219, 2012.

[253] J. Gu and Y. Jing, " A Modified Mixed Domain Method for Modeling Acoustic Wave Propagation in Strongly Heterogeneous Media," *The Journal of the Acoustical Society of America*, 2019 (Submitted).

[254] A. I. Farrer, S. Almquist, C. R. Dillon, L. A. Neumayer, D. L. Parker, D. A. Christensen, *et al.*, "Phase aberration simulation study of MRgFUS breast treatments," *Medical Physics,* vol. 43, pp. 1374-1384, 2016.

[255] C. Jia, W. C. Vogt, K. A. Wear, T. J. Pfefer, and B. S. Garra, "Two-layer heterogeneous breast phantom for photoacoustic imaging," *Journal of Biomedical Optics,* vol. 22, p. 106011, 2017.

[256] N. Lipsman, T. G. Mainprize, M. L. Schwartz, K. Hynynen, and A. M. Lozano, "Intracranial applications of magnetic resonance-guided focused ultrasound," *Neurotherapeutics,* vol. 11, pp. 593-605, 2014.

[257] J. Kubanek, "Neuromodulation with transcranial focused ultrasound," *Neurosurgical focus,* vol. 44, p. E14, 2018.

[258] S. Pourjavid and O. J. Tretiak, "Numerical solution of the direct scattering problem through the transformed acoustical wave equation," *The Journal of the Acoustical Society of America,* vol. 91, pp. 639-645, 1992.

[259] B. E. Treeby and B. Cox, "Modeling power law absorption and dispersion in viscoelastic solids using a split-field and the fractional Laplacian," *The Journal of the Acoustical Society of America,* vol. 136, pp. 1499-1510, 2014.

[260] J. Gu and Y. Jing, "mSOUND: An open source toolbox for modeling acousitc wave propagation in heterogeneous media," *IEEE Transactions on Ultrasonics Ferroelectrics and Frequency Control*, 2019 (In preparation).

[261] X. Yin and K. Hynynen, "A numerical study of transcranial focused ultrasound beam propagation at low frequency," *Physics in Medicine & Biology*, vol. 50, p. 1821, 2005.

[262] J. A. Jensen, "Field: A program for simulating ultrasound systems," in *10th Nordicbaltic conference on biomedical imaging*, vol. 4, supplemental 1, part 1:351-353, 1996.

[263] J. A. Jensen, "A multi-threaded version of Field II," in *2014 IEEE International Ultrasonics Symposium*, pp. 2229-2232, 2014.

[264] J. F. Synnevag, A. Austeng, and S. Holm, "Adaptive beamforming applied to medical ultrasound imaging," *IEEE Transactions on Ultrasonics, Ferroelectrics, and Frequency Control*, vol. 54, pp. 1606-1613, 2007.

[265] E. Bossy, M. Talmant, and P. Laugier, "Three-dimensional simulations of ultrasonic axial transmission velocity measurement on cortical bone models," *The Journal of the Acoustical Society of America*, vol. 115, pp. 2314-2324, 2004.

[266] J. E. Soneson, "Extending the utility of the parabolic approximation in medical ultrasound using wide-angle diffraction modeling," *IEEE Transactions on Ultrasonics, Ferroelectrics, and Frequency Control*, vol. 64, pp. 679-687, 2017.

[267] V. Suomi, J. Jaros, B. Treeby, and R. O. Cleveland, "Full modeling of high-intensity focused ultrasound and thermal heating in the kidney using realistic patient models," *IEEE Transactions on Biomedical Engineering*, vol. 65, pp. 969-979, 2017.

[268] B. E. Treeby and T. Saratoon, "The contribution of shear wave absorption to ultrasound heating in bones: Coupled elastic and thermal modeling," in *2015 IEEE International Ultrasonics Symposium (IUS)*, pp. 1-4, 2015.

[269] J. Gu and Y. Jing, "A Modified Mixed Domain Method for Modeling Acoustic Wave Propagation in Strongly Heterogeneous Media," *arXiv:1905.05921*,2019.

[270] G. T. Clement, "Spatial backward planar projection in absorbing media possessing an arbitrary dispersion relation," *Acoustical Science and Technology*, vol. 31, pp. 379-386, 2010.

[271] J. D. Maynard, E. G. Williams, and Y. Lee, "Nearfield acoustic holography: I. Theory of generalized holography and the development of NAH," *The Journal of the Acoustical Society of America*, vol. 78, pp. 1395-1413, 1985.

[272] P. Burgholzer, G. J. Matt, M. Haltmeier, and G. Paltauf, "Exact and approximative imaging methods for photoacoustic tomography using an arbitrary detection surface," *Physical Review E*, vol. 75, p. 046706, 2007.

[273] Y. Hristova, P. Kuchment, and L. Nguyen, "Reconstruction and time reversal in thermoacoustic tomography in acoustically homogeneous and inhomogeneous media," *Inverse Problems*, vol. 24, p. 055006, 2008.

[274] C. R. Hart, D. Wilson, C. L. Pettit, and E. T. Nykaza, "Machine-learning models for the prediction of long-range outdoor sound propagation," *The Journal of the Acoustical Society of America*, vol. 139, pp. 2069-2069, 2016.

APPENDIX

In this appendix, we will show that the MDM is valid for inhomogeneous media with weak sound speed contrast. To simplify the problem, we choose a scenario with a 1D inhomogeneous medium with speed of sound variation only and the change occurs at the boundary where $z = z_0$. The medium is defined as

$$c = \begin{cases} c_0, z \le z_0 \\ c_1, z > z_0 \end{cases}. \tag{A1}$$

For 1D wave propagation, the solution for a point in the $z > z_0$ domain obtained from (11) is:

$$\begin{aligned} P(z) = P_0 e^{ikz} + \frac{e^{ikz}}{2ik}\int_0^{z_0} e^{-ikz'}\left(-\frac{\omega^2}{c_0^2}\left(\frac{c_0^2}{c^2}-1\right)P(z')\right)dz' \\ + \frac{e^{ikz}}{2ik}\int_{z_0}^{z} e^{-ikz'}\left(-\frac{\omega^2}{c_0^2}\left(\frac{c_0^2}{c^2}-1\right)P(z')\right)dz' \end{aligned}, \tag{A2}$$

where $k = \omega/c_0$. The second term in (A2) is zero with the speed distribution described in (A1). Thus, (A2) can be simplified to

$$P(z) = P_0 e^{ikz} + \frac{e^{ikz}}{2ik}\int_{z_0}^{z} e^{-ikz'}\left(-\frac{\omega^2}{c_0^2}\left(\frac{c_0^2}{c_1^2}-1\right)P(z')\right)dz'. \tag{A3}$$

On the other hand, the analytical solution for wave propagating in 1D cases with sound speed shown in (A1) reads

$$P(z) = \begin{cases} P_0 e^{ikz}, & z \le z_0 \\ TP_0 e^{ikz_0 + ik'(z-z_0)}, & z > z_0 \end{cases}, \tag{A4}$$

where $k' = \omega/c_1$ and T is the transmission coefficient and $T = 2c_1/(c_0 + c_1)$. Now we look at the wave field when $z > z_0$. If (A3) was valid, substituting (A4) into the right-hand side of (A3) will precisely lead to $P(z)$, i.e., $TP_0 e^{ikz_0 + ik'(z-z_0)}$. Therefore, we substitute (A4) into the right-hand side of (A3), which leads to

$$
\begin{aligned}
&P_0 e^{ikz} + \frac{e^{ikz}}{2ik}\int_{z_0}^{z} e^{-ikz'}\left(-\frac{\omega^2}{c_0^2}\left(\frac{c_0^2}{c_1^2}-1\right)TP_0 e^{ikz_0+ik'(z-z_0)}\right)dz' \\
&= P_0 e^{ikz}\left(1 + T\frac{e^{i(k-k')z_0}}{2ik}\left(\frac{\omega^2}{c_0^2}-\frac{\omega^2}{c_1^2}\right)\int_{z_0}^{z} e^{i(k'-k)z'}dz'\right) \\
&= P_0 e^{ikz}\left(1 + T\frac{e^{i(k-k')z_0}}{2ik}(k^2-k'^2)\int_{z_0}^{z} e^{i(k'-k)z'}dz'\right) \quad . \qquad \text{(A5)} \\
&= P_0 e^{ikz}(1 + e^{i(k-k')z_0}\left(e^{i(k'-k)z} - e^{i(k'-k)z_0}\right)\Big) \\
&= P_0 e^{ikz}\left(1 + e^{i(k-k')(z_0-z)} - 1\right) \\
&= P_0 e^{ikz_0+ik'(z-z_0)}
\end{aligned}
$$

From (A5), we can conclude that the transmission coefficient T caused by the sound speed variation is not included in the MDM. In fact, if we multiplied (A3) with T, substituting (A4) into (A3) would precisely lead to $P(z) = TP_0 e^{ikz_0+ik'(z-z_0)}$. This is not a major issue if the contrast in the medium is weak, since phase distortion will likely dominate over amplitude change.

Next, we focus on the accuracy of the phase when modeling wave propagation using the MDM. For convenience, we use the Riemann sum as the stepping algorithm [18]. With the left-hand Riemann sum, the MDM method for the 1D case with variation of speed of sound (the same case as above) can be written as

$$
P(z+\Delta z)_{MDM} = P(z)e^{ik\Delta z} + \frac{e^{ik\Delta z}}{2ik}\left(-\frac{\omega^2}{c_0^2}\left(\frac{c_0^2}{c_1^2}-1\right)\right)P(z)\Delta z. \qquad \text{(A6)}
$$

When wave propagates a distance of $z_0 + \Delta z$, the pressure field becomes

$$
P(z_0+\Delta z)_{MDM} = P_0 e^{ik(z_0+\Delta z)}\left(1 + \frac{k^2-k'^2}{2ik}\Delta z\right). \qquad \text{(A7)}
$$

When assuming weakly inhomogeneous medium, we have $k \approx k'$. Equation (A7) can be further simplified as

$$
P(z_0+\Delta z)_{MDM} \cong P_0 e^{ik(z_0+\Delta z)}[1 + i(k'-k)\Delta z]. \qquad \text{(A8)}
$$

When the wave travels a distance of $z_0 + \Delta z$, the analytical solution is

$$
P(z_0+\Delta z)_{Analytical} = TP_0 e^{ikz_0+ik'\Delta z}. \qquad \text{(A9)}
$$

By using the Euler's formula, (A9) becomes

$$P(z_0 + \Delta z)_{Analytical} = TP_0 e^{ik(z_0+\Delta z)}[\cos(k'\Delta z - k\Delta z) + \ isin(k'\Delta z - k\Delta z)]. \quad \text{(A10)}$$

When taking a rather small spatial step size Δz and considering that $k \approx k'$, we have $(k' - k)\Delta z \approx 0$. Equation (A10) becomes

$$P(z_0 + \Delta z)_{Analytical} = TP_0 e^{ik(z_0+\Delta z)}[1 + i(k' - k)\Delta z]. \quad \text{(A11)}$$

Comparing (A11) and (A8), it is seen that the phase difference between MDM and the analytical solution is 0 when certain assumptions are made. Thus, the MDM is accurate in weekly heterogeneous media.